FINITE DIFFERENCE SOLUTIONS OF STEADY LAMINAR FLOW THROUGH A PIPE ORIFICE

by
Theo Gordon Keith, Jr.

Dissertation submitted to the Faculty of the Graduate School
of the University of Maryland in partial fulfillment
of the requirements for the degree of
Doctor of Philosophy
1971

APPROVAL SHEET

Title of Thesis: Finite Difference Solutions of Steady Laminar Flow Through a Pipe Orifice

Name of Candidate: Theo Gordon Keith, Jr.
Doctor of Philosophy, 1971

Thesis and Abstract Approved: James E A John

James E. A. John
Professor
Mechanical Engineering

Date Approved: 8/6/71

ABSTRACT

Title of Thesis: Finite Difference Solutions of Steady Laminar Flow Through a Pipe Orifice

Theo G. Keith, Jr., Doctor of Philosophy 1971

Thesis Directed By: Professor James E. A. John

In this thesis, numerical solutions of the axisymmetric form of the Navier-Stokes equations are obtained for the steady, laminar flow of an imcompressible fluid through a circular pipe orifice plate. The method of solution employs the widely used two field method of Thom which consists of solving two coupled second order partial differential equations for stream function and vorticity. Finite difference solutions of the governing equations are obtained in a rectangular graded mesh. All derivatives are approximated by five point, unevenly spaced, differences which reduce the truncation error involved with the finite difference approximation. In order to reduce round off error, double precision arithmetic is employed throughout the calculations. Both of these features have been found essential in obtaining accurate results in reasonable lengths of computing time. In the study, a typical solution consumed approximately 15 minutes of UNIVAC 1108 time. However, computer times increased with increasing Reynolds number and decreasing orifice to pipe diameter ratio.

Two types of orifice plate profiles are considered: square edge and sharp edge. The latter type is beveled at 45° in the downstream direction. Orifice to pipe diameter ratios of .3, .4, .5, .6 and .7 have been examined for the square-edged plate. In the case of the sharp-edged orifice, a single orifice diameter ratio of .5 was studied.

Solutions were obtained for Reynolds numbers (based on the pipe radius and average fluid velocity in the pipe) from 0 to 12.5. Streamline patterns and vorticity contours are presented as functions of the Reynolds number. Distributions of velocity, axial pressure drop and wall shear stress are given. Details of recirculations regions, found in front and behind the orifice plate, are shown. Numerically obtained orifice discharge coefficients are found to compare favorably with existing experimental values (within 5% of each other). Generally, the square-edged orifice discharge coefficients are predicted slightly lower than the experimental values while the predicted sharp-edged plate coefficients are slightly larger. Differences in the orifice plate geometry are thought to account for these discrepancies.

ACKNOWLEDGMENTS

The author wishes first to express his sincere appreciation to Professor James E. A. John for allotting a great deal of his time for the guidance of this work. The many helpful suggestions of Dr. William Haberman during the preparation of the manuscript are also gratefully acknowledged.

Preliminary investigations were funded by the Independent Research program at the Naval Ship Research and Development Laboratory, Annapolis, Maryland. The required computer time for this thesis was supported in full through the facilities of the Computer Science Center of the University of Maryland.

Thanks are also due to Mrs. M. Benda for her accurate typing of the dissertation.

It should be noted that this work could never have been completed had it not been for the countless sacrifices willingly made by my wife Sandy and for these I am eternally thankful.

Finally I wish to dedicate this thesis to my parents.

TABLE OF CONTENTS

LIST OF FIGURES

LIST OF TABLES

LIST OF SYMBOLS

A_i (i = 1,..., 5)	Coefficients of first difference in radial direction
A_p	Cross-sectional pipe area
B (r, z)	Bernoulli Sum at the point (r, z)
B_i (i = 1,..., 5)	Coefficients of second difference in radial direction
C_D	Discharge coefficient
C_i (i = 1,..., 5)	Coefficients of first difference in axial direction
d	Diameter of orifice
D	Diameter of pipe
D_i (i = 1,..., 5)	Coefficients of second difference in axial direction
$\|F_i^F\|$(i = 1,..., 5)	Matrix of coefficients for forward first differences
$\|F_i^C\|$(i, 1,..., 5)	Matrix of coefficients for central first differences
$\|F_i^B\|$(i, 1,..., 5)	Matrix of coefficients for backward first differences
h	Width of spacing of grid
h_i (i = 1, 2, 3)	Scale factors
$\dot{m}$	Mass flow rate
P	Pressure
ΔP	Pressure drop - in plots reference value is taken at one pipe diameter upstream of orifice face
r	Radial dimension
R	Radius of pipe
Re	Reynolds number based on average fluid velocity in pipe and pipe radius

Re_d	Reynolds number based on average fluid velocity in pipe orifice and orifice diameter: $Re_d = 2\ Re/(d/D)$
$\|\|S_i^F\|\|$ $(i = 1,\ldots, 5)$	Matrix of coefficients for forward second differences
$\|\|S_i^C\|\|$ $(i = 1,\ldots, 5)$	Matrix of coefficients for central second differences
$\|\|S_i^B\|\|$ $(i = 1,\ldots, 5)$	Matrix of coefficients for backward second differences
S	Arc length
t	Thickness of orifice plate
u	Radial velocity component
v_i $(i = 1, 2, 3)$	Velocity components in the X_i direction
W	Axial velocity component
$\overline{W}_p$	Average fluid velocity in the pipe
X_i $(i = 1, 2, 3)$	Space coordinates in a general coordinate system
z	Axial dimension
β	Orifice to pipe diameter ratio (d/D)
ζ	Vorticity
ζ^*	Vorticity times a scale factor $(= \zeta h_2)$
λ	Ratio of grid sizes at outer intervals of a five point spread of node points
λ_r	Radial ratio of grid sizes: h_t/h_b
λ_z	Axial ratio of grid sizes: h_ℓ/h_r
ν	Kinematic Viscosity
ρ	Density
τ	Shear stress
ϕ_ψ , ϕ_ζ	Under-relaxation factors

ψ	Stream function

Subscripts

$( )_b$ $( )_B$ $( )_\beta$	Designates the value of a variable at a grid point on a radial grid line below node point "o"
$( )_\ell$ $( )_L$	Designates the value of a variable at a grid point on an axial grid line left of node point "o"
$( )_o$	Designates the value of a variable at node point "o" and also used to denote value of a solid surface
$( )_r$ $( )_R$	Designates the value of a variable at a grid point on an axial grid line to the right of node point "o"
$( )_t$ $( )_T$ $( )_\tau$	Designates the value of a variable at a grid point on a radial grid line above node point "o"

Superscripts

$( )^K$	Iteration number
$( )'$	Dimensional quantity

CHAPTER I

INTRODUCTION

The difficulties associated with the integration of the Navier-Stokes equations in their complete form has stimulated extensive efforts towards the development of methods capable of producing approximate solutions. Until recently, success in obtaining such solutions has been restricted to the limiting situations of very high and very low Reynolds number flow. In the last decade, the advent of the high-speed digital computer has profoundly changed this picture however and a considerable amount of progress has been achieved in obtaining finite difference solutions for situations where the limiting flow approximations are unacceptable.

In this thesis, the steady laminar flow of an incompressible fluid through a circular pipe orifice plate is numerically investigated. The orifice shape is circular and two separate corner profiles are considered. Figure 1-1 is a sketch of these edge profiles.

In order to obtain finite difference solutions to the complete form of the axisymmetric Navier-Stokes equations for the described flow conditions, a numerical method was used which employed a rectangular graded mesh. Although the concept of mesh grading is not new, little work has been reported on its use in the numerical solutions of the Navier-Stokes equations. Moreover, these works typically require long computing times and have experienced problems with the numerical stability.

It was felt that insufficient calculation accuracy due to round

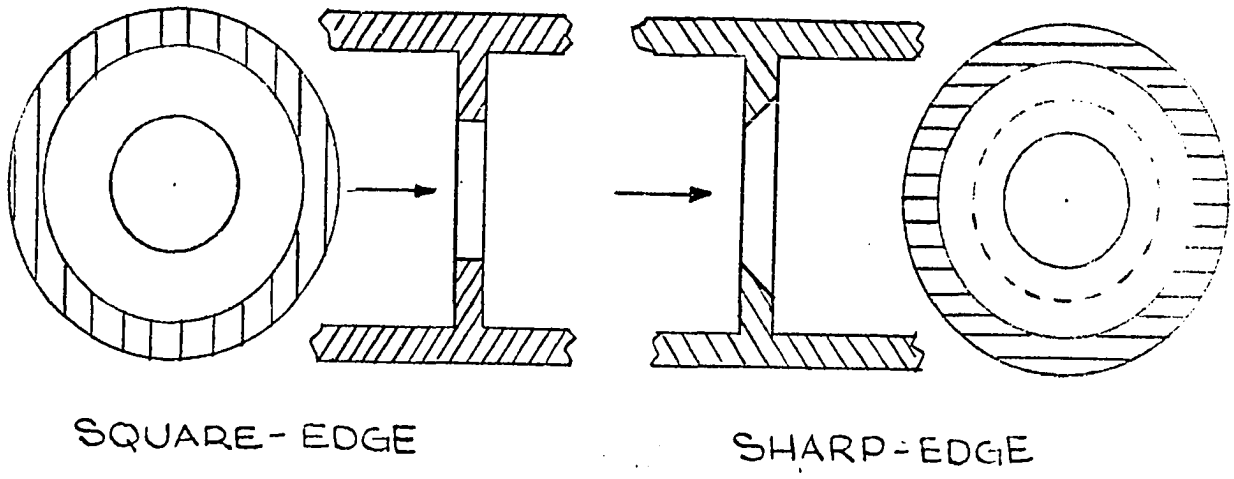

Figure 1-1

Orifice Plate Edge Profiles

off and truncation errors was intimately connected with the difficulties encountered in the earlier investigations which used the graded mesh concept. The truncation error, caused by the cutting off of the infinite term Taylor series involved in the development of the difference operator at a finite stage, can be reduced in two ways. In the more popular method, the mesh width is made as small as practical. However, such a specification places a burden upon the storage capacity of the computer and it enhances the possibility of incurring large round off error. Alternately, the truncation error may be decreased by retaining higher order terms in the Taylor series expansion. But, in order to describe the higher order terms, more information about the variable at a particular point in the flow field is required. In this study, the latter method of lowering the truncation error is employed and a finite

difference operator which uses field data from five mesh points (four points along a mesh line plus the node point at which the differencing is being performed) instead of the customary three was utilized. For simplicity, only two mesh sizes were permitted within the spread of the five node points. Even for this simplified situation, four different distributions of grid spacings were possible. To lower the round off error, extra place accuracy (double precision) for each variable was specified. This is a key consideration for it was found that accurate results could not be obtained without this additional accuracy. It must be borne in mind however that double precision is a rather expensive commodity since the total computing time is lengthened and the double place accuracy virtually cuts the available computer storage in half and therefore the total number of grid points which may be considered is reduced. This however is consistent with the concept of mesh grading which tends to optimize the grid structure.

In the next chapter, a brief account of previous investigations concerned with the numerical solutions of the Navier-Stokes equations is presented. The chapter is highlighted by aspects which are pertinent to the current study. In particular, the work of Mills (1), who obtained finite difference solutions of flow through a square-edged orifice plate for a single orifice to pipe diameter ratio of .5 is reviewed as is the experimental work of Johansen (2), who obtained orifice discharge coefficients for low Reynolds number flow.

In Chapter 3, the governing equations are introduced in terms of stream function (Ψ) and vorticity (Ω). The equations are nondimensionalized in terms of the pipe radius and the average pipe velocity. Next,

these equations are cast into finite difference form using a 5-point difference operator which does not require evenly spaced field data. The boundary conditions are imposed and the handling of the wall vorticity, especially at the intruding corners is indicated. The orifice plate graded mesh considerations are described. Finally, equations for obtaining the velocity, pressure differences and shear stress are presented.

The structure of the computer program is presented in Chapter 4. A brief discussion of under-relaxation is given and a calculation stability criteria is established.

The heart of this dissertation is contained in the fifth chapter. The results of the study along with a discussion of these results is given. Numerical solutions in the form of streamline patterns and vorticity contours are presented for the square-edged orifice plate flows for orifice to pipe diameter ratios (d/D) of .3,.4,.5,.6,.7 for Reynolds numbers up to 12.5. Similar results for the sharp-edged orifice for a single d/D of .5 are presented for Reynolds numbers up to 10. Distributions of wall vorticity (wall shear stress), velocity and pressure drop are given as functions of the Reynolds number. The details of the front and rear back-flow regions are presented. Of special interest in this chapter is the comparison of existing experimental data for the orifice discharge coefficient with the predicted values. Good agreement between the two is found.

The last chapter of this thesis summarizes the key findings and conclusions.

CHAPTER II

PREVIOUS WORK

The quantity of published work concerning finite difference solutions of the Navier-Stokes equations is so impressive that a review of that literature can not be undertaken here. However, in order to obtain some understanding of the "state of the art", a chronological index of much of the previously advanced work is presented as an appendix to this thesis.

A total of 195 entries is included in the appended list of references. Figure 2-1 is a bar graph of the yearly output of these papers. It can be seen that after a very slow start, prior to 1963, the number of articles appearing in the literature takes a very sharp turn upwards and continues to rise. The reason for this increased activity is obviously due to the increased availability of the high-speed digital computer and to the efforts of many devoted researchers. Most noteworthy of these workers is Thom. For his pioneering efforts in this area of research, he is often referred to as the "father of numerical fluid dynamics." Prior to 1960, he was involved in nearly one half of all of the literature reported. This fact is even more significant when it is realized that before 1960 most of the work was carried out by hand on desk top computers. Nevertheless, techniques originated by Thom years ago are still employed on present day digital computers.

The two dimensional version of the Navier-Stokes equations forms a set of three coupled nonlinear partial differential equations (the continuity equation and two momentum equations) with three unknowns. The unknowns are the two components of velocity and the pressure.

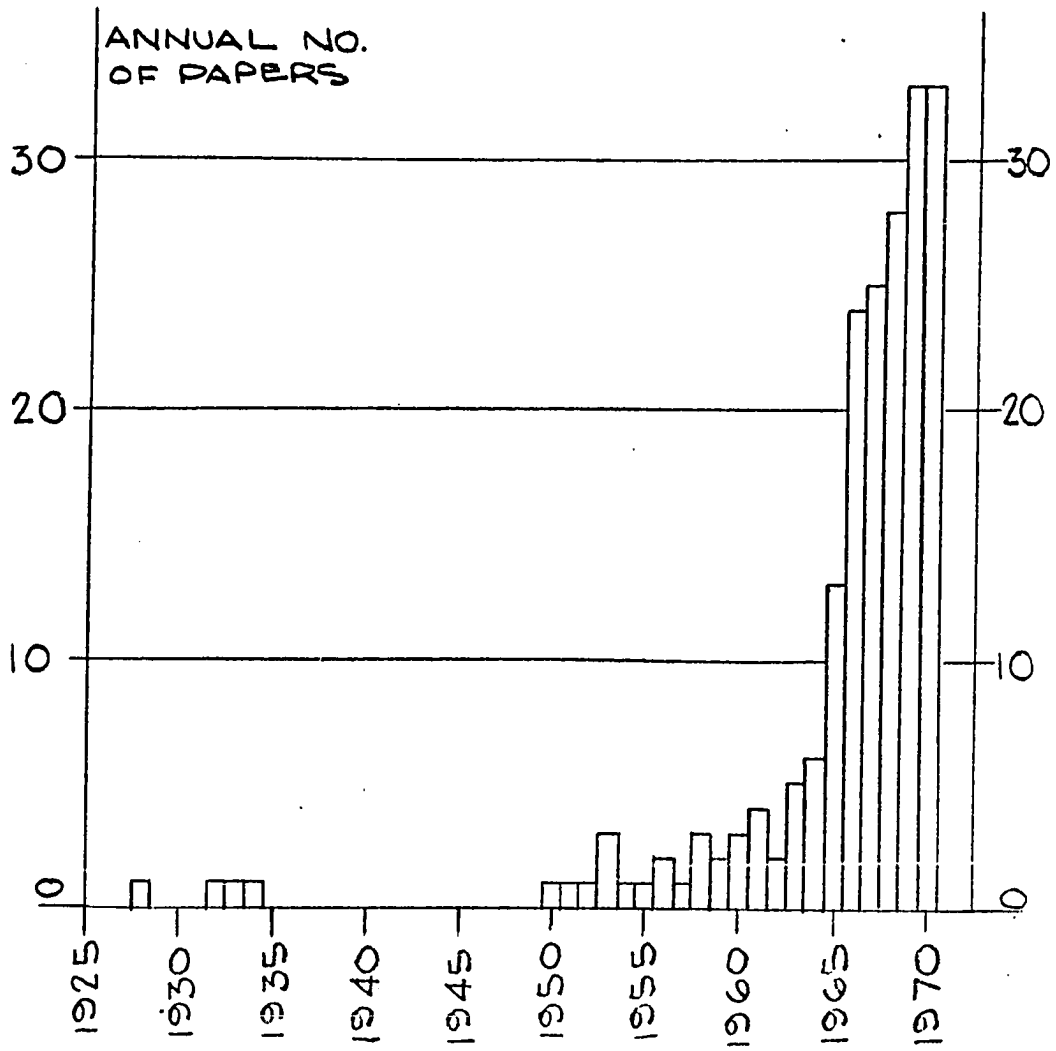

Figure 2-1

Annual Output of Papers Concerned with Finite Difference Solutions of the Navier-Stokes Equations

Success in obtaining finite difference solutions of the equations in this form is very limited. Two exceptions are Donovan (3) and Putre (4). If the pressure is eliminated from the two momentum equations and if the stream function is introduced, which results in an automatic satisfaction of the continuity equation, a single fourth order nonlinear partial differential equation containing only the stream function is obtained. While the possibility of working in terms of a single

variable is very attractive, this equation yields solutions which do not possess good convergence properties and in as much its use has also been very limited. However, it has been used by Gillis and Brandt (5) and by Truesdell and Adler (6).

Thom (7) proposed an equation form which may be regarded as a compromise of the above two formulations. In this scheme, the pressure is first eliminated and the stream function and vorticity are next introduced. This results in two second order coupled partial differential equations which contain two unknowns. This so-called two field method is widely used because it yields solutions with good convergence and it is therefore employed in this thesis.

The usual method of solving the finite difference form of the governing equations on a uniformly spaced net is not followed in the present investigation. Instead, the flow field is covered with a net which can provide a fine mesh in localized high gradient areas. To avoid difficulties associated with changes of the mesh size, the technique of mesh grading used retains a given mesh size distribution throughout the field, i.e. radial net spacing is fixed over the entire length of the field and the axial mesh spacing is the same at any radius. Further details concerned with the mesh structure will be brought forward in a later section.

As mentioned earlier, few studies involved with the finite difference solution of the Navier-Stokes equations have attempted to use the technique of rectangular mesh grading. Micheal in (8), probably was the first to employ such a grid structuring in a viscous flow situation. Numerical solutions for axisymmetric, incompressible flow

broadside to a circular disk for Reynolds numbers (based on disk diameter) between 1.5 and 50 were given. The convergence rate was very slow and in as much very long computing times were required (a typical run called for 10^4 iterations and consumed 5 hours of IBM 7094 time). Because of the handling of the boundary condition at the sharp edge of the disk the results have received criticism by Rimon and Lugt in (9) and (10). About the same time as Micheal's work, Thoman and Szewczyk (11) attempted to use a rectangular graded mesh in their study of transient flow around a circular cylinder, but they discovered that this mesh structuring was not adequate to handle the problem and it was abandoned in favor of a hybrid net. In this mixed mesh, an outer rectangular net was united with an inner circular grid and the combination proved to be very satisfactory. Here again, solution times were very long (3 to 13 hours of UNIVAC 1107 time). No other works using this mesh structuring in viscous flow calculations are known to the writer.

To reduce the size of the truncation error involved with the finite difference approximation, a five point difference operator was utilized. Others have previously used such an operator, for evenly spaced grid data, to obtain more accuracy in their calculations. Lee and Fung, in (12), used this operator for calculating flow in locally constricted tubes. Friedman and Gillis likewise employed one in a study of viscous flow in a pipe with absorbing walls, (13). Friedman also used the five point form in an investigation of flow in a circular pipe with recessed walls (14).

A Previous Numerical Study

Since the subject of this thesis is an outgrowth of a previous investigation reported by Mills in (1), it is of considerable value to detail the contents of that work so as to place the current study in clearer perspective.

Mills obtained numerical solutions of the Navier-Stokes equations for steady, axisymmetric, viscous, incompressible flow through an orifice in a circular pipe with a fixed orifice to pipe diameter ratio of one half. Streamline patterns and vorticity contours were presented for five Reynolds numbers (based on pipe diameter and average pipe velocity) of 0, 1.25, 2.5, 5., and 12.5. Also presented were the axial pressure distributions and the orifice discharge coefficients. The calculated discharge coefficients were in good agreement (although slightly higher) with existing experimental values of Johansen (2) even though there was not complete similarity in regards to orifice geometry and the location of the pressure taps. Mills' study considered a square-edged orifice with a thickness of 1/16th of the pipe radius, whereas the experimental orifice had a sharp-edge beveled by 45° on its downstream side and the thickness at the particular d/D of .5 was 1/12th of the pipe radius. Mills therefore concluded that orifice geometry was probably not an important consideration at low Reynolds numbers. Details of the orifice wake regions were not presented nor were any velocity profiles described.

Mills used the two field method on a square grid. The finite difference operator was the usual central three point form. The numerical method was tested to see how well it could reproduce the exact

Poiseuille flow distribution starting with all field values set at zero. Second and third place accuracy was all that could be obtained in 100 iterations because of the magnitude of the truncation errors involved with the finite difference operator used.

Existing Experimental Data

Because of its importance in flow metering, the orifice plate has received considerable experimental attention. Generally this experimentation has been conducted at high Reynolds numbers for fully developed turbulent flow where the orifice discharge coefficient is nearly independent of the Reynolds number. On the other hand, the situation of low Reynolds number, where there is a substantial variation in orifice discharge coefficient, has received comparatively little consideration.

Johansen (2), in a early and detailed investigation, conducted experiments in the low Reynolds number range for flow through a beveled circular orifice. The orifice plate had an edge profile with an upstream-facing square edge followed by a 45° bevel on the downstream side. The orifice thickness was made approximately 1/12th of the orifice diameter. Tests were carried out using castor oil, mineral lubricating oil, and water. Four orifice diameter ratios (d/D = .209, .401, .595, and .794) were studied. The tests revealed that there is a linear relation between discharge coefficient and square root of the Reynolds number for the range of $0 < Re_d < 10$.

Tuve and Sprenkle (15) published a comprehensive survey of all the existing orifice data then available, 1933, which applied to the low Reynolds number range. In addition, they conducted tests of their

own. Their investigation confirmed Johansen's discharge coefficient data.

Besides obtaining orifice discharge coefficient data, Johansen also carried out some visual experiments. Water was allowed to flow through a glass tube of 2.7 cm bore. A dye injection station located about 14 diameters upstream of the orifice, axially introduced a 2% methol blue in water solution enriched with a trace of bismark brown in order to trace the flow streamlines. The apparatus was vertically supported. Photographs of the flow were taken. Johansen claimed that no orifice wake region was observed below a Re_d of 30 and he did not present any photos of the flow below this value. Too great of a reliance should not be placed upon these visual studies, for water flowing at an Re_d of 10 in a .1 ft pipe has an average velocity of about .001 fps and in as much, the slightest disturbance can cause appreciable changes in the flow pattern.

Johansen's tests also indicated that vortex shedding from the edge of the orifice plate did not occur below a Re_d of 200 which is well above the largest value considered in the current study.

CHAPTER III

GOVERNING EQUATIONS

In this chapter the equations which govern the steady axisymmetric flow of an incompressible, homogeneous fluid of constant viscosity are presented in terms of the stream function and vorticity (the so-called two field approach). The equations are nondimensionalized using the pipe radius and the average fluid velocity in the pipe as the respective characteristic length and velocity. The governing equations are cast into finite difference form using 5-point difference operators. The form of the equations shows that the stream function and vorticity require boundary values on all four sides of the flow field. The vorticity boundary condition at the pipe wall and on the orifice surfaces requires a special development. The tailoring of the field mesh by grading is discussed and the net structure for the various orifice to pipe diameter ratios is presented.

Basic Equations

The equations which govern the steady, axisymmetric motion of an incompressible, Newtonian fluid in the absence of any extraneous field of force are written in nondimensional form as (16):

$$u\frac{\partial u}{\partial r} + w\frac{\partial u}{\partial z} = -\frac{\partial p}{\partial r} + \frac{1}{Re}\left(\frac{\partial^2 u}{\partial r^2} + \frac{1}{r}\frac{\partial u}{\partial r} + \frac{\partial^2 u}{\partial z^2}\right) \quad \ldots\ldots[3\text{-}1]$$

$$u\frac{\partial w}{\partial r} + w\frac{\partial w}{\partial z} = -\frac{\partial p}{\partial z} + \frac{1}{Re}\left(\frac{\partial^2 w}{\partial r^2} + \frac{1}{r}\frac{\partial w}{\partial r} + \frac{\partial^2 w}{\partial z^2}\right) \quad \ldots\ldots[3\text{-}2]$$

The continuity equation is:

$$\frac{\partial u}{\partial r} + \frac{u}{r} + \frac{1}{r}\frac{\partial w}{\partial z} = 0 \qquad \text{.....[3-3]}$$

All the parameters involved in the above expressions have been made dimensionless through introduction of the pipe radius (R) as the characteristic length and the average fluid velocity in the pipe ($\bar{W}_p$) as the characteristic velocity. Thus:

$$r = \frac{r'}{R}, \quad z = \frac{z'}{R}, \quad u = \frac{u'}{\bar{W}_p}, \quad w = \frac{w'}{\bar{W}_p},$$

$$Re = \frac{\bar{W}_p R}{\nu}, \quad P = \frac{p'}{\rho \bar{W}_p^2}$$

where the primes indicate dimensional quantities.

Elimination of the pressure from equations (3-1) and (3-2) and, the introduction of the dimensionless vorticity:

$$\zeta = \frac{\partial u}{\partial z} - \frac{\partial w}{\partial r} \qquad \text{.....[3-4]}$$

where: $\zeta = \frac{\zeta' R}{\bar{W}_p}$

produces the vorticity transport equation:

$$u\frac{\partial \zeta}{\partial r} + w\frac{\partial \zeta}{\partial z} - \frac{u\zeta}{r} = \frac{1}{Re}\left(\frac{\partial^2 \zeta}{\partial r^2} + \frac{1}{r}\frac{\partial \zeta}{\partial r} + \frac{\partial^2 \zeta}{\partial z^2} - \frac{\zeta}{r^2}\right)$$

.....[3-5]

The continuity equation is automatically satisfied by use of the dimensionless stream function which is defined as:

$$u = \frac{1}{r}\frac{\partial \psi}{\partial z}, \qquad w = -\frac{1}{r}\frac{\partial \psi}{\partial r} \qquad \ldots\ldots[3\text{-}6]$$

where: $\psi = \dfrac{\psi'}{\bar{w}_p R^2}$

Substitution of (3-6) into equations (3-4) and (3-5) results in:

$$\zeta = \frac{1}{r}\left(\frac{\partial^2 \psi}{\partial r^2} - \frac{1}{r}\frac{\partial \psi}{\partial r} + \frac{\partial^2 \psi}{\partial z^2}\right) \qquad \ldots\ldots[3\text{-}7]$$

$$\frac{\partial^2 \zeta}{\partial r^2} + \frac{1}{r}\frac{\partial \zeta}{\partial r} + \frac{\partial^2 \zeta}{\partial z^2} - \frac{\zeta}{r^2} = \frac{Re}{r}\left(\frac{\partial \psi}{\partial z}\frac{\partial \zeta}{\partial r} - \frac{\partial \psi}{\partial r}\frac{\partial \zeta}{\partial z} - \frac{\zeta}{r}\frac{\partial \psi}{\partial z}\right) \qquad \ldots\ldots[3\text{-}8]$$

Finite Differencing

In this section the governing equations (3-7) and (3-8) are put into a finite difference form. For the notation of the grid system shown in Figure 3-1, the first and second derivatives of the stream

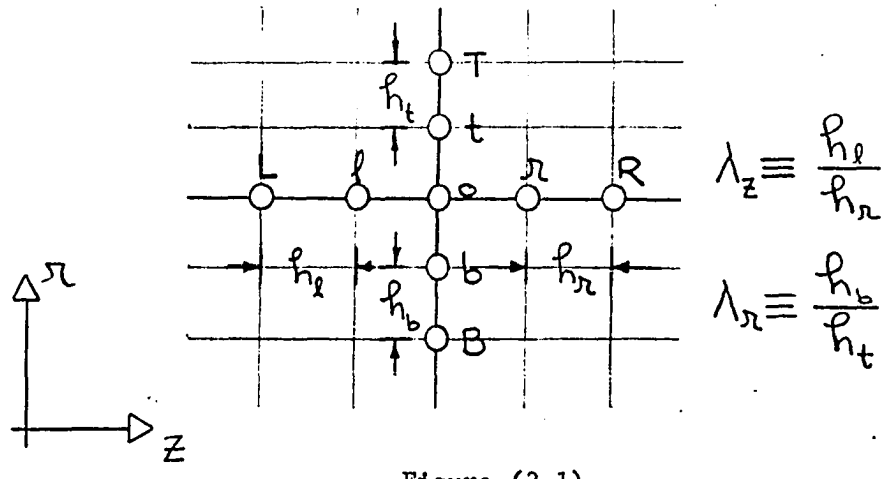

Figure (3-1)

Local Grid Structure

function can be written as:

$$\left(\frac{\partial \psi}{\partial \mathcal{R}}\right)_0 = \frac{A_1\psi_T + A_2\psi_t + A_3\psi_0 + A_4\psi_b + A_5\psi_B}{h_t} \qquad \text{.....[3-9]}$$

$$\left(\frac{\partial^2 \psi}{\partial \mathcal{R}^2}\right)_0 = \frac{B_1\psi_T + B_2\psi_t + B_3\psi_0 + B_4\psi_b + B_5\psi_B}{h_t^2} \qquad \text{.....[3-10]}$$

$$\left(\frac{\partial \psi}{\partial Z}\right)_0 = \frac{C_1\psi_R + C_2\psi_{\mathcal{R}} + C_3\psi_0 + C_4\psi_\ell + C_5\psi_L}{h_{\mathcal{R}}} \qquad \text{.....[3-11]}$$

$$\left(\frac{\partial^2 \psi}{\partial Z^2}\right)_0 = \frac{D_1\psi_R + D_2\psi_{\mathcal{R}} + D_3\psi_0 + D_4\psi_\ell + D_5\psi_L}{h_{\mathcal{R}}^2} \qquad \text{.....[3-12]}$$

Particular values of the coefficients in the above difference equations depend upon the local grid width distribution within the five point span of node points and upon the local grid width ratio (see Appendix A for details). For ease of computation, the numerical values of the coefficients are arranged into a matrix form. Details concerning these matrices will be given in the next chapter.

When equation (3-9), (3-10) and (3-12) are substituted into equation (3-7), the general 5-point form for the stream function is obtained:

$$\psi_0 = \frac{\dfrac{B_1\psi_T + B_2\psi_t + B_4\psi_b + B_5\psi_B}{h_t^2} + \dfrac{D_1\psi_R + D_2\psi_{\mathcal{R}} + D_4\psi_\ell + D_5\psi_L}{h_{\mathcal{R}}^2} - \dfrac{A_1\psi_T + A_2\psi_t + A_4\psi_b + A_5\psi_B}{\mathcal{R}_0 h_t} - \mathcal{R}_0 \int_0}{\left(\dfrac{A_3}{\mathcal{R}_0 h_t} - \dfrac{B_3}{h_t^2} - \dfrac{D_3}{h_{\mathcal{R}}^2}\right)} \qquad \text{.....[3-13]}$$

Equations for the derivatives of the vorticity may be written as in the above. Substituting these, along with the stream function derivatives given in equations (3-9) through (3-12) into equation (3-8) and solving

for ζ_0 produces:

$$\zeta_0 = \frac{\frac{B_1\zeta_T + B_2\zeta_t + B_4\zeta_b + B_5\zeta_B}{h_t^2} + \frac{D_1\zeta_R + D_2\zeta_{\Omega} + D_4\zeta_\ell + D_5\zeta_L}{h_{\Omega}^2} + \frac{A_1\zeta_t + A_2\zeta_t + A_4\zeta_b + A_5\zeta_B}{\Omega_0 h_t} + \frac{RE}{\Omega_0 h_t h_{\Omega}}(\Delta)}{\frac{1}{\Omega_0^2} - \frac{A_3}{\Omega_0 h_t} - \frac{B_3}{h_t^2} - \frac{D_3}{h_{\Omega}^2} + \frac{RE}{\Omega_0}\left[\frac{(C_1\psi_R + C_2\psi_{\Omega} + C_4\psi_\ell + C_5\psi_L)A_3 - (A_1\psi_T + A_2\psi_t + A_4\psi_b + A_5\psi_B)C_3}{h_{\Omega} h_t} - \frac{C_1\psi_R + C_2\psi_{\Omega} + C_3\psi_0 + C_4\psi_\ell + C_5\psi_L}{\Omega_0 h_{\Omega}}\right]}$$

.....[3-14]

where:

$$\Delta = (A_1\psi_T + A_2\psi_t + A_3\psi_0 + A_4\psi_b + A_5\psi_B)(C_1\zeta_R + C_2\zeta_{\Omega} + C_4\zeta_\ell + C_5\zeta_L) -$$

$$(C_1\psi_R + C_2\psi_{\Omega} + C_3\psi_0 + C_4\psi_\ell + C_5\psi_L)(A_1\zeta_T + A_2\zeta_t + A_4\zeta_b + A_5\zeta_B)$$

Although the above set of equations appears quite formidable, they may be written in a less complicated form by employment of the following definitions:

$$\xi_A \equiv A_1\zeta_T^{K-1} + A_2\zeta_t^{K-1} + A_4\zeta_b^{K} + A_5\zeta_B^{K}$$

$$\xi_B \equiv B_1\zeta_T^{K-1} + B_2\zeta_t^{K-1} + B_4\zeta_b^{K} + B_5\zeta_B^{K}$$

$$\xi_C \equiv C_1\zeta_R^{K-1} + C_2\zeta_{\Omega}^{K-1} + C_4\zeta_\ell^{K} + C_5\zeta_L^{K}$$

$$\xi_D \equiv D_1\zeta_R^{K-1} + D_2\zeta_{\Omega}^{K-1} + D_4\zeta_\ell^{K} + D_5\zeta_L^{K}$$

$$\eta_A \equiv A_1 \psi_T^{k-1} + A_2 \psi_t^{k-1} + A_4 \psi_b^{k} + A_5 \psi_B^{k} + A_3 \psi_0^{k-1}$$

$$\eta_B \equiv B_1 \psi_T^{k-1} + B_2 \psi_t^{k-1} + B_4 \psi_b^{k} + B_5 \psi_B^{k} + B_3 \psi_0^{k-1}$$

$$\eta_C \equiv C_1 \psi_R^{k-1} + C_2 \psi_\Omega^{k-1} + C_4 \psi_\ell^{k} + C_5 \psi_L^{k} + C_3 \psi_0^{k-1}$$

$$\eta_D \equiv D_1 \psi_R^{k-1} + D_2 \psi_\Omega^{k-1} + D_4 \psi_\ell^{k} + D_5 \psi_L^{k} + D_3 \psi_0^{k-1}$$

$$\alpha \equiv h_\Omega / h_t \quad , \quad \beta \equiv h_\Omega / \Omega_0$$

$$\gamma \equiv R_E / \Omega_0 \quad , \quad \delta \equiv h_\Omega^2 \Omega_0$$

The superscript, k, indicates the iteration number. Examination of this superscript in the above definitions reveals that the direction that the calculation takes is from the bottom to the top of the star shown in Figure 3-1 and from the left to the right. Substitution of the definitions into equation (3-13) and rearranging yields:

$$\psi_0^{k} = \psi_0^{k-1} + \frac{\alpha^2 \eta_B + \eta_D - \alpha\beta \eta_A - \delta \zeta_0^{k}}{\alpha\beta A_3 - \alpha^2 B_3 - D_3} \qquad \text{.....[3-15]}$$

In the same way, equation (3-14) can be written as:

$$\zeta_0^K = \frac{\alpha^2\xi_B + \xi_D + \alpha\beta\xi_A + \alpha\gamma(\eta_A\xi_C - \eta_C\xi_A)}{\beta^2 - \alpha\beta A_3 - \alpha^2 B_3 - D_3 + \alpha\gamma(\eta_C A_3 - \eta_A C_3) - \beta\gamma\eta_C} \quad \text{.....[3-16]}$$

It is not as convenient to express the vorticity as the sum of the preceding pass value and a correction term as was done for ψ in equation (3-15). This can be seen by comparing such an expression with equation (3-16);

$$\zeta_0^K = \zeta_0^{K-1} + \left\{\alpha^2(\xi_B + B_3\zeta_0^{K-1}) + (\xi_D + D_3\zeta_0^{K-1}) + \alpha\gamma\left[\eta_A(\xi_C + C_3\zeta_0^{K-1}) - \eta_C(\xi_A + A_3\zeta_0^{K-1})\right] - (\beta^2 - \beta\gamma\eta_C)\zeta_0^{K-1}\right\} \Big/ \left[\beta^2 - \alpha\beta A_3 - \alpha^2 B_3 - D_3 + \alpha\gamma(\eta_C A_3 - \eta_A C_3) - \beta\gamma\eta_C\right]$$

Boundary Conditions

From equations (3-7) and (3-8), it can be seen that ψ and ζ each require four boundary conditions: two in r and two in z. Thus values must be assigned to those variables at the inflow and outflow boundaries, along the pipe centerline and on the pipe and orifice surfaces.

Inflow and outflow boundaries: At large distances upstream of the orifice plate the fluid flows parallel to the z axis (u = 0) under a constant pressure gradient and the velocity distribution is parabolic and invarient in the axial dimension i.e., w = w(r). After passing through the orifice, the flow asympotically regains its earlier state of

the so-called Poiseuille parallel pipe flow. It therefore would appear natural to specify the classical Poiseuille flow distributions of ψ and $\mathcal{J}$ on the inflow and outflow boundaries of the flow field. The problem however is in deciding how far upstream and downstream from the orifice that these distributions should be imposed. Strictly speaking, these conditions should be specified at $\pm\infty$. But this is not possible in a numerical treatment and ways to circumvent these difficulties are desirable.

Wang and Longwell have suggested a transformation from the z to a new independent variable so as to make the boundaries finite (17); others have employed extrapolation techniques e.g. Hung (18) and Greenspan (19). In the most popular technique (and the one adopted in this thesis) finite distances are used instead of the $\pm\infty$. There is no general method available at present which defines how far the inflow and outflow boundaries should be located from a disturbing obstacle so as not to introduce any appreciable boundary disturbances into the flow field. In lieu of this, the accepted practice is: establish a set of boundary distances, find a solution using these field dimensions, increase the boundary lengths, find a second solution, compare it to the original results, continue this process until the increasing of boundary distances produces flow field changes smaller than some prescribed amount.

From previous internal flow studies, one finds two facts which are helpful in the inflow and outflow boundary establishment:

i. The upstream boundary distance can generally be made smaller than the downstream boundary length with the exception of the Re = 0

case for which the field is generally symmetrical about the mid-plane of the orifice.

ii. As the Re is increased, the upstream distance can be made smaller (although one may just as well retain the original distance) and the downstream length must be increased.

The present work benefits from the work originated by Mills in (1) and therefore a clue as to realistic boundary lengths can be obtained by consulting that paper.

In this thesis, the inflow boundary was located at a distance slightly greater than one pipe diameter from the upstream face of the orifice plate for all the flows investigated. The distance to the outflow boundary varied from one to three and one half pipe diameters, measured from the downstream side of the orifice plate, depending upon the Reynolds number of the flow and the orifice to pipe diameter ratio under consideration.

After having defined the inflow and outflow boundaries, the Poiseuille distributions of ψ and ζ are prescribed on them. The distributions are very well known and they are therefore presented here without derivation:

$$\psi = (r^4 - 2r^2)/2 \qquad \text{.....[3-17]}$$

$$\zeta = 4r \qquad \text{.....[3-18]}$$

Centerline: The boundary conditions on the pipe axis are easily written from symmetry considerations. Clearly:

$$u(0,z) = 0 \qquad \text{.....[3-19]}$$

$$\left(\frac{\partial w}{\partial r}\right)_{r=0} = 0$$

Incorporation of these into equations (3-4) and (3-6) yields respectively:

$$f(0,z) = 0 \qquad \text{.....[3-20]}$$

$$\psi(0,z) = 0$$

Pipe Walls and Orifice Surfaces: The stream function boundary condition is readily established because there is no slip on any of the solid surfaces i.e.,

$$\left.\begin{aligned} (u)_o &= \frac{1}{r_o}\left(\frac{\partial \psi}{\partial z}\right)_o = 0 \\ (w)_o &= -\frac{1}{r_o}\left(\frac{\partial \psi}{\partial r}\right)_o = 0 \end{aligned}\right\} \Rightarrow \psi = \psi_o \text{ (CONSTANT)} \qquad \text{.....[3-21]}$$

On the other hand, specification of the boundary vorticity presents difficulties because the values of f_o must generally be computed from the flow field pattern in the vicinity of the boundary surface. The method used for this calculation has been the subject of several papers (20), (21), (22). The justification of this emphasis rests in the fact that the vorticity generated at the boundary surface is the source of the flow disturbance and without accurate calculation of f_o, the numerical solution canot hope to yield meaningful results.

A comprehensive discussion of the method of calculation is given by Rimon and Lugt (22). A simplified version of their general develop-

ment is given in Appendix C. The result of the derivation is the following expression:

$$\zeta_0 = \frac{\frac{6}{r_0\delta^2}(\psi_1 - \psi_0) - \left(1 + \frac{\delta\cos\phi}{r_0}\right)\zeta_1}{2 + \frac{\delta\cos\phi}{r_0} - \frac{1}{4}\left(\frac{\delta\cos\phi}{r_0}\right)^2} + O[\delta^3] \quad \ldots\ldots [3\text{-}22]$$

where the definition of the parameters involved will be clarified in what follows. It should be mentioned that equation (3-22) was originally derived by Lester in (20) and has been used in several subsequent studies e.g., (12), (23).

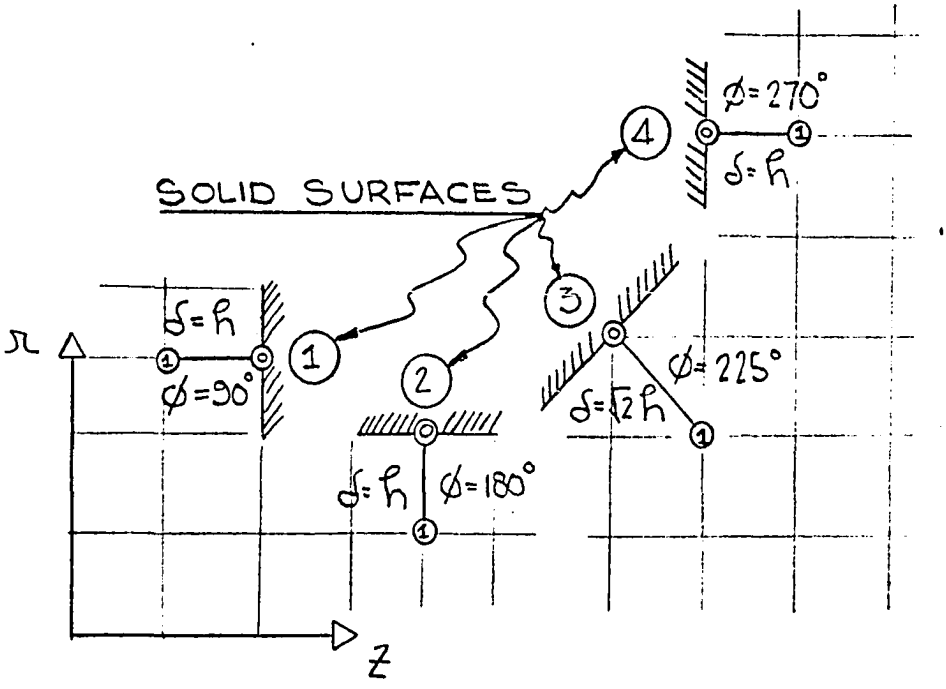

Figure (3-2)

Notation Used in Evaluation of Surface Vorticity

In this thesis, ζ_0 is calculated on solid surfaces with faces

like 1, 2, 3 and 4 of Figure 3-2. Substitution of the corresponding ϕ and δ (shown in the figure) for each face into equation (3-22) results in the following:

FACE 1 (FRONT FACE OF ORIFICE PLATE):

$$\zeta_0 = \frac{3}{\pi_0 h^2}(\psi_1 - \psi_0) - \frac{\zeta_1}{2} \qquad \text{.....[3-23]}$$

FACE 2 (PIPE WALL, TOP OF ORIFICE PLATE):

$$\zeta_0 = \frac{\frac{6}{\pi_0 h^2}(\psi_1 - \psi_0) - \left(1 - \frac{h}{\pi_0}\right)\zeta_1}{2 - \frac{h}{\pi_0} - \frac{h^2}{4\pi_0^2}} \qquad \text{.....[3-24]}$$

FACE 3 (SLANTED TOP OF SHARP-EDGED ORIFICE PLATE):

$$\zeta_0 = \frac{\frac{3}{\pi_0 h^2}(\psi_1 - \psi_0) - \left(1 - \frac{h}{\pi_0}\right)\zeta_1}{2 - \frac{h}{\pi_0} - \frac{h^2}{4\pi_0^2}} \qquad \text{.....[3-25]}$$

FACE 4 (REAR FACE OF ORIFICE PLATE):

$$\zeta_0 = \frac{3}{\pi_0 h^2}(\psi_1 - \psi_0) - \frac{\zeta_1}{2} \qquad \text{.....[3-26]}$$

Intruding Corners: The vorticity and stream function on the boundaries may be obtained using the above equations. The sharp intruding corners of the orifice plate however present a serious problem, for it was implicitly assumed in the derivation of the wall vorticity that computation was to be made on a flat boundary. In addition, a normal direction to the boundary at the point of interest was always clear.

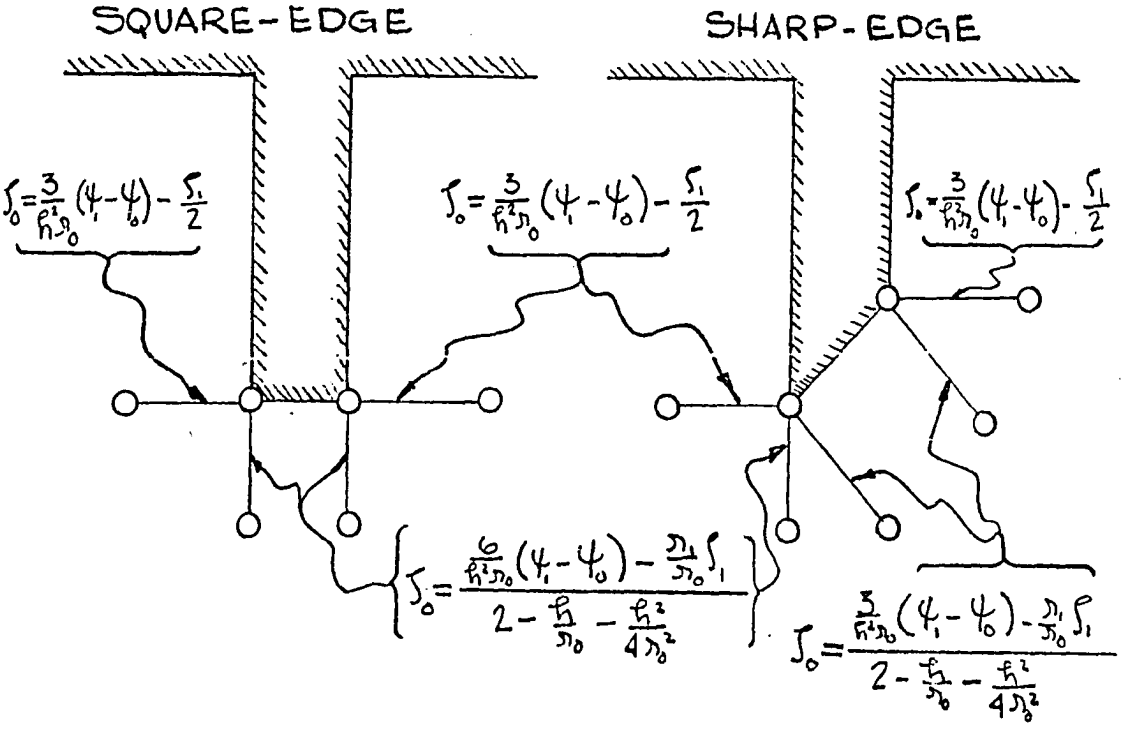

Figure (3-3)

Corner Vorticity Calculation for Square and Sharp-Edged Orifice

Because intruding corners are such large sources of vorticity generation, they have received considerable attention. For the sake of continuity of presentation, the details of the variety of ways in which they have been handled in previous studies are not presented here, but are included in this thesis as Appendix D.

It should be mentioned that virtually every method of corner vorticity computation has received criticism for one reason or another. The consensus of opinion however indicates that the method proposed long ago by Thom in (24) is preferred. Briefly, Thom's method allows the corner vorticity to be multi valued. For a square-edged orifice, the vorticity at the corner is double valued. One value comes from a calculation in the axial direction using equation (3-23) and the other from an expansion in the radial direction, equation (3-24). During the main flow calculations, the appropriate value is used. Moreover, these calculations may be improved by requiring that a very fine mesh surround the corner. The approach is ideally suited to the graded mesh concept since a small mesh size can be readily specified in the neighborhood of the corner.

Figure (3-3) graphically shows how each corner vorticity is calculated. Notice that in the case of the sharp-edged orifice, a triple valued corner is specified at the orifice tip as would occur in the situation when the thickness of a square-edged orifice was diminished to zero.

Grid Considerations

The rectangular grid, with the square grid being a special form of it, is by far the most popular form of mesh structuring used in numerical fluid flow computations. The dimension thought to contain the larger changes in the flow variables is assigned the finer of the two mesh widths. In problems where large gradients in the flow variables exist in both directions, a square mesh of necessity is used.

Specification of a sufficiently fine uniform mesh over the entire flow field is essential to assure convergence. However, such requirements can often lead to serious computational difficulties, for they:

- tax the computer storage capability
- increase the computer running time
- require extra place accuracy
- increase likelihood of computer round off error.

A more reasonable approach would allow a fine grid structure in regions where the largest changes in flow variables are expected and would permit the less dynamic portions of the field to be covered with a coarser net. A graded mesh structuring of the flow field offers several attractive features since it:

- diminishes the total number of grid points required and therefore does need as much computer storage space
- gives better flow field resolution in areas of principle concern e.g., the wake region or the intruding sharp corners
- gives the boundaries more definition by allowing more node points to occur on them.

Tailoring of the flow field mesh structure by grading has not been widely used in previous investigations concerning finite difference solutions of the Navier-Stokes equations. However, in numerical studies involving flows about cylinders or spheres e.g., (25) or (26), a transformation of the radial dimension using an exponential term so as to have a finer mesh near the surface of the body is generally used. And, as was mentioned earlier, Micheal (8) and Thoman and Szewczyk (11) have

reported using graded mesh schemes to obtain numerical solutions of viscous flow around a disk and a cylinder respectively.

For reasons of simplicity, only three grid ratios (defined as the ratio of grid widths occurring at the extremities of a spread of five node points - refer to Figure (3-1) 2, 1, and 1/2 were used in this thesis. It should also be mentioned that the analysis allows only two different grid spacings within a spread of five node points. The reason for this again is simplicity, for it was thought that if the calculations became too complicated then the entire study might be jeopardized from the standpoint of excessive computing time. Because two grid sizes are permitted within the five point span, special precautions have to be exercised when going from one grid size to another. To illustrate this matter consider Figure (3-4) which shows a change in mesh size from h_1 to h_2.

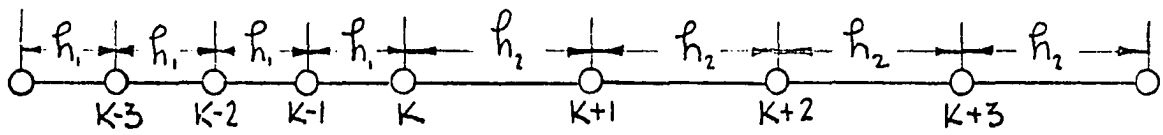

Figure (3-4)

Illustrative Grid Size Change

Table 3-1 shows the distribution of grid spacings at each node point.

Grid Point	Distribution of Grid Sizes Within 5 Point Spread	
	h_1	h_2
K-2	4	0
K-1	3	1
K	2	2
K+1	1	3
K+2	0	4

Table 3-1

Distribution of Grid Spacings for Illustrative Gride Size Change

For the problem investigated within this study only one axial distribution of grid spaces was used (the total number of axial grid points did however vary with Reynolds number and orifice to pipe diameter ratio). The radial distribution could not be fixed since five d/D ratios were considered. Both the axial and radial arrangements of grid widths are separately shown in Figure (3-5). A view of the overall grid structure for the case where d/D = .5 is given in Figure (3-6).

Miscellaneous Flow Quantities

After obtaining the stream function and vorticity distributions, several other flow quantities can be readily calculated.

Velocity components: Combining equations (3-6), (3-9) and (3-11) yields:

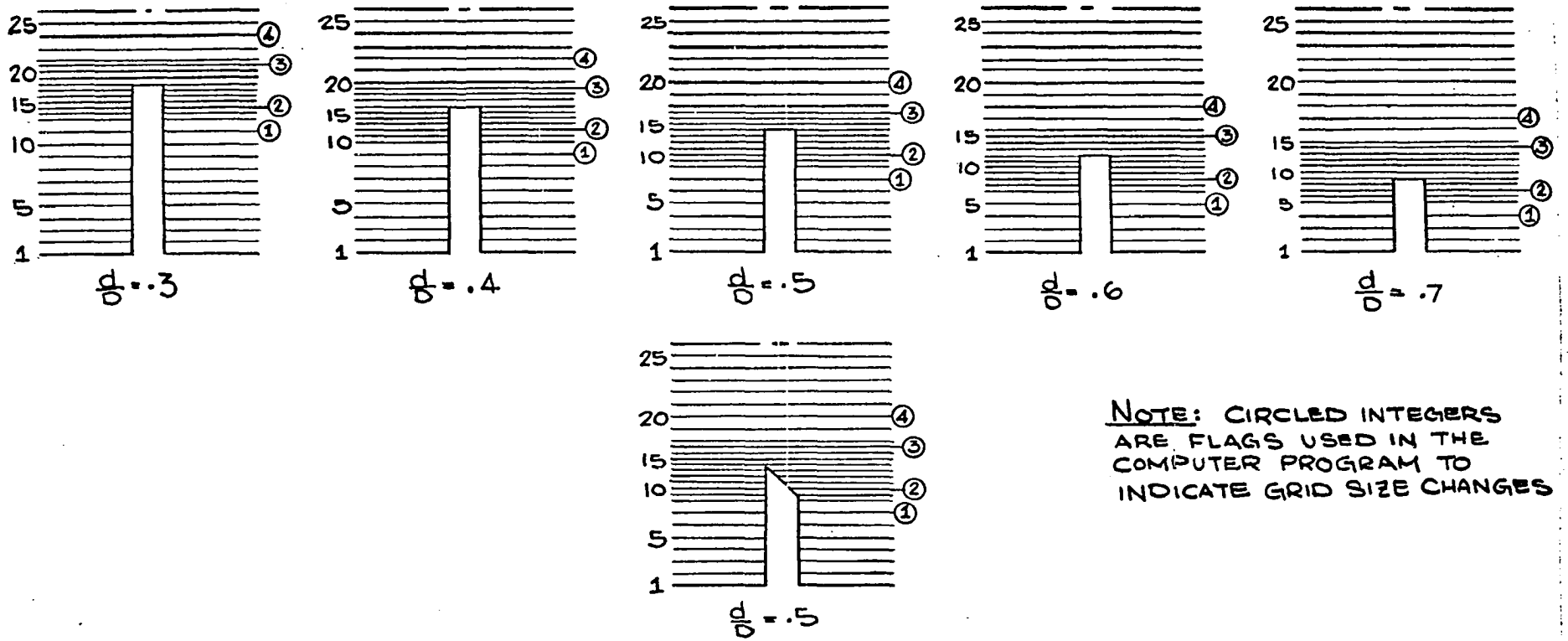

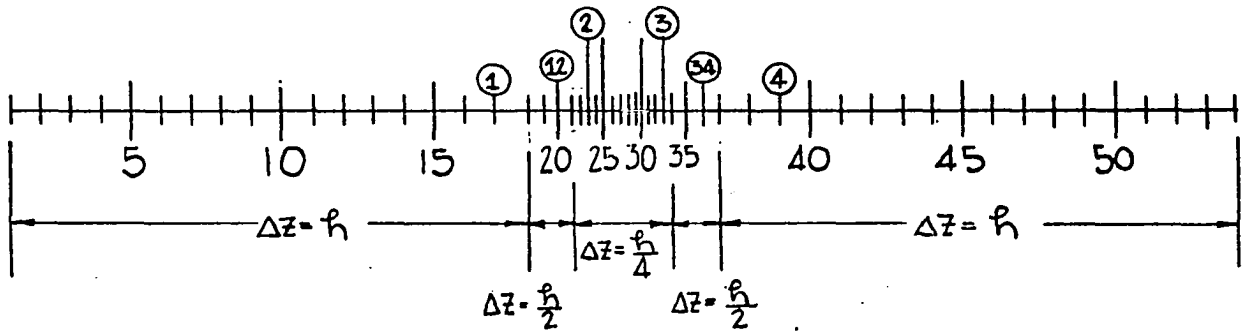

Figure 3-5

Radial and Axial Grid Structures Used in This Study

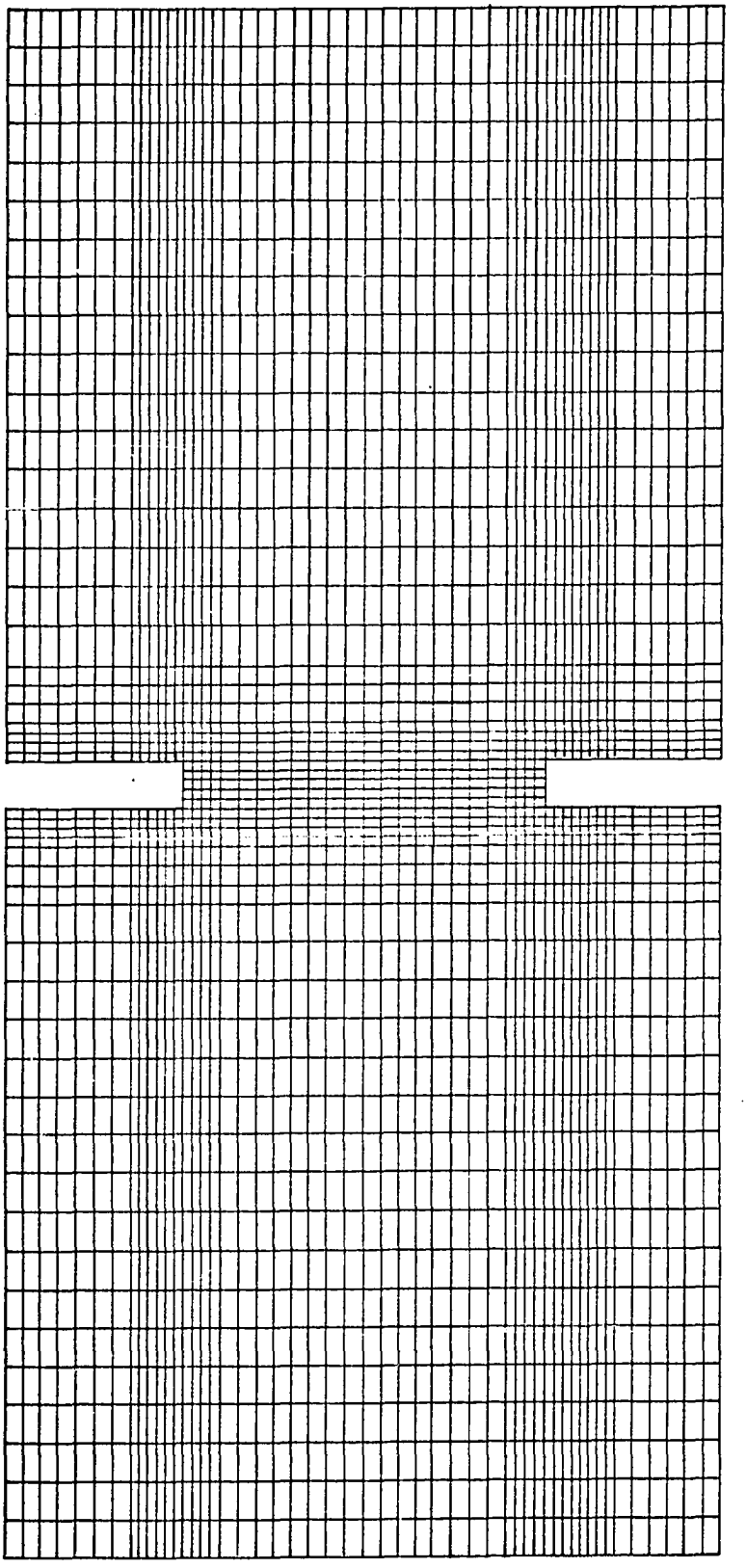

Figure 3-6

Overall Grid Structure for a Square-Edged Orifice
With d/D = .5

$$u_o = \frac{C_1\psi_R + C_2\psi_{\mathcal{R}} + C_3\psi_o + C_4\psi_\ell + C_5\psi_L}{\mathcal{R}_o h_{\mathcal{R}}} = \frac{\mathcal{D}_c}{\mathcal{R}_o h_{\mathcal{R}}} \quad \text{.....[3-27]}$$

$$W_o = -\frac{A_1\psi_T + A_2\psi_t + A_3\psi_o + A_4\psi_b + A_5\psi_B}{\mathcal{R}_o h_t} = -\frac{\mathcal{D}_A}{\mathcal{R}_o h_t} \quad \text{.....[3-28]}$$

$$|V_o| = \sqrt{W_o^2 + u_o^2} = \frac{1}{\mathcal{R}_o}\sqrt{\left(\frac{\mathcal{D}_A}{h_t}\right)^2 + \left(\frac{\mathcal{D}_c}{h_{\mathcal{R}}}\right)^2} \quad \text{.....[3-29]}$$

The above equations are written assuming that a central differencing is possible. In the vicinity of the boundaries, such a differencing cannot be taken and appropriate forward or backward differences must be used. This type of calculation will be given more detail in the next chapter. It should be mentioned that the 5-point differencing allows the velocities to be determined to an accuracy of the order of h^4 compared with a 3-point differencing accuracy of h^2.

Pressure differences: The pressure differences may be computed from the following integral form of the Navier-Stokes equations (refer to (20) or (27) for further details):

$$R_E\left[B(\mathcal{R},z_2) - B(\mathcal{R},z_1)\right] = \int_{z_1}^{z_2}\left[u\zeta R_E - \left(\frac{\partial\zeta}{\partial\mathcal{R}} + \frac{\zeta}{\mathcal{R}}\right)\right]dz \quad \text{.....[3-30]}$$

$$R_E\left[B(\mathcal{R}_2,z) - B(\mathcal{R}_1,z)\right] = \int_{\mathcal{R}_1}^{\mathcal{R}_2}\left[-w\zeta R_E + \left(\frac{\partial\zeta}{\partial z}\right)\right]d\mathcal{R} \quad \text{.....[3-31]}$$

where: $B\,(\text{BERNOULLI SUM}) \equiv P + \frac{u^2+w^2}{2}$

Inserting equations for the first differences along with equations (3-27) and (3-28) into the above two expressions, allows the arguments of the integrals to be written as:

$$\left[u\zeta R_E - \left(\frac{\partial \zeta}{\partial r} + \frac{\zeta}{r}\right)\right]_o = \left(1 - \frac{r_o}{h_t} A_3 + \frac{\eta_c}{h_r} R_E\right)\frac{\zeta_o}{r_o} - \frac{\xi_A}{h_t}$$

$$\left[-w\zeta R_E + \left(\frac{\partial \zeta}{\partial z}\right)\right]_o = \left(\frac{r_o}{h_r} C_3 + \frac{\eta_A}{h_t} R_E\right)\frac{\zeta_o}{r_o} + \frac{\xi_c}{h_r}$$

The integration was carried out numerically using Simpson's rule (28) when integrating over an even number of spaces:

$$\int_{x_1}^{x_3} f(x)dx = \frac{h}{3}\left[f(x_1) + 4f(x_2) + f(x_3)\right]$$

and:

$$\int_{x_1}^{x_4} f(x)dx = \frac{3h}{8}\left[f(x_1) + 3f(x_2) + 3f(x_3) + f(x_4)\right]$$

for integration over an odd number of grid widths. Both integral forms provide accuracy to an order of h^5.

Shearing stress: The dimensionless shear stress is written:

$$\tau = \frac{1}{R_E}\left(\frac{\partial u}{\partial z} + \frac{\partial w}{\partial r}\right) \qquad \text{.....[3-32]}$$

but: $$\zeta = \frac{\partial u}{\partial z} - \frac{\partial w}{\partial r}$$

hence:

$$\tau = \frac{\zeta + 2\left(\frac{\partial w}{\partial r}\right)}{R_E} = \frac{2\left(\frac{\partial u}{\partial z}\right) - \zeta}{R_E} \qquad \text{.....[3-33]}$$

CHAPTER IV

COMPUTER PROGRAM DETAILS

In this chapter several details necessary to the construction of the digital computer program utilized in this thesis are indicated. The use of the matrices which contain the values of the finite difference operator coefficients are described. Forward and backwards differencing, necessary in the calculation procedure is discussed. The role of under-relaxation in the stabilization of the computations is briefly mentioned and a numerical stability criteria in terms of the Reynolds number, mesh size and d/D ratio, based on the previous work of Hung (18), is established. A block diagram is used to describe the digital computer program. A test problem for the trivial case of d/D = 1 (Poiseuille flow) is solved by starting with a net initially filled with zero values of ψ and ζ. Convergence to 7 place agreement with the classical Poiseuillean values is found.

Finite Difference Details

In the preceding chapter, the general form of a five point difference operator was used to obtain the finite difference equivalents of the governing equations. The coefficients of these operators were not specified at the time because it was felt that they would upset the continuity of the presentation.

It is clear that the values of the coefficients depend upon the grid sizes and the distribution of these sizes within a five point spread of nodes. In this thesis, only two grid sizes are allowed to occur within the span of any five points and only three distributions of

these sizes are permitted. The width of the grid is characterized by the grid ratio λ which is defined in Figure 3-1 as being the ratio of the grid widths existing at the extremities of the five point span, i.e., h(bottom)/h(top) or h(left)/h(right). In this study, only three particular grid ratios are considered: $\lambda = 1/2$, 1, and 2. The distributions of grid widths over the range of five node points is conveniently expressed as: kh(left) - (4-k)h(right) or kh(bottom) - (4-k)h(top), where k = 1, 2, or 3.

The first central difference operator has 7 sets of coefficients corresponding to the different grid ratios and distributions. Likewise, there are 7 possible sets of coefficients for the second central difference operator. Rather than write out each individual operator as was done in Appendix A, the coefficients are assembled into a matrix form. These matrices have proved to be helpful in streamlining the calculation procedure in the computer program. The matrix $\|F_1^c\|$ contains the coefficients of the first central difference operator and therefore provides the values of A_1 and C_1 of equations (3-9) and (3-11). A similar matrix is used for the second central difference coefficients which correspond to the B_i and the D_i of equations (3-10) and (3-12). The matrices are:

$$\|F_1^c\| = 1/420 \begin{array}{c} \begin{matrix} \leftarrow\lambda \\ 1/2 \quad 1 \quad 2 \end{matrix} \\ \begin{Vmatrix} -14 & -35 & -64 \\ -14 & -35 & -10 \\ -30 & -35 & -42 \end{Vmatrix} \end{array} \begin{matrix} \kappa\downarrow \\ 3 \\ 2 \\ 1 \end{matrix}$$

$$\|S_1^c\| = 1/420 \begin{Vmatrix} -28 & -35 & -32 \\ -14 & -35 & 35 \\ -40 & -35 & -28 \end{Vmatrix}$$

$$\|F_2^c\| = 1/60 \begin{Vmatrix} 60 & 40 & 30 \\ 20 & 40 & 64 \\ 36 & 40 & 45 \end{Vmatrix}$$

$$\|S_2^c\| = 1/60 \begin{Vmatrix} 280 & 80 & 25 \\ 25 & 80 & 32 \\ 84 & 80 & 75 \end{Vmatrix}$$

$$\|F_3^c\| = 1/60 \begin{Vmatrix} 20 & 0 & -5 \\ 90 & 0 & -45 \\ 10 & 0 & -10 \end{Vmatrix} \qquad \|S_3^c\| = 1/60 \begin{Vmatrix} -560 & -150 & -40 \\ -60 & -150 & -60 \\ -160 & -150 & -140 \end{Vmatrix}$$

$$\|F_4^c\| = 1/60 \begin{Vmatrix} -90 & -40 & -18 \\ -128 & -40 & -10 \\ -60 & -40 & -30 \end{Vmatrix} \qquad \|S_4^c\| = 1/60 \begin{Vmatrix} 300 & 80 & 21 \\ 32 & 80 & 75 \\ 100 & 80 & 70 \end{Vmatrix}$$

$$\|F_5^c\| = 1/420 \begin{Vmatrix} 84 & 35 & 15 \\ 140 & 35 & 7 \\ 128 & 35 & 7 \end{Vmatrix} \qquad \|S_5^c\| = 1/420 \begin{Vmatrix} -112 & -35 & -10 \\ 35 & -35 & -14 \\ -128 & -35 & -7 \end{Vmatrix}$$

As an example, suppose the derivative $(\partial\psi/\partial n)_o$ is desired at the point "o" of Figure 4-1. The matrices $\|F_i^c\|$ are

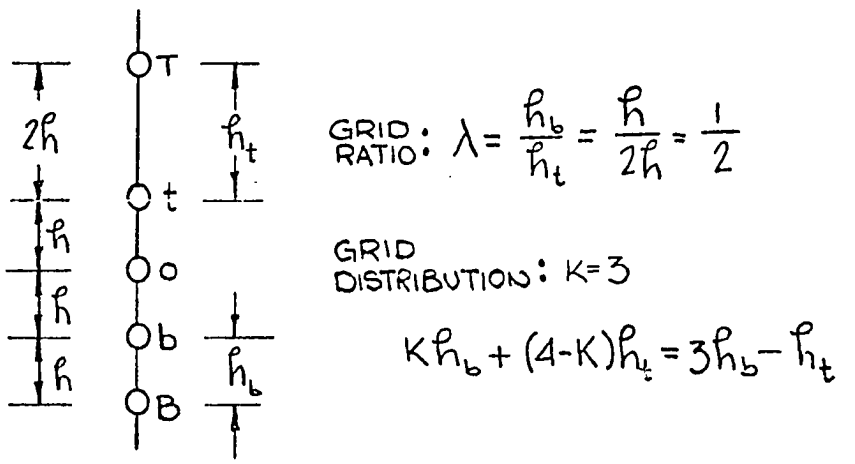

Figure (4-1)

An Example Grid Structure

entered at the point where $\lambda = 1/2$ and $k = 3$ and the following coefficients are obtained: $A_1 = -14/420$, $A_2 = 60/60$, $A_3 = 20/60$, $A_4 = -90/60$, and $A_5 = 84/420$. The derivative is therefore:

$$\left(\frac{\partial\psi}{\partial n}\right)_o = \frac{-2\psi_T + 60\psi_t + 20\psi_o - 90\psi_b + 12\psi_B}{60\,h_t}$$

It is obvious that as the boundary surfaces of the flow field are approached, a variation of the central differencing scheme is required.

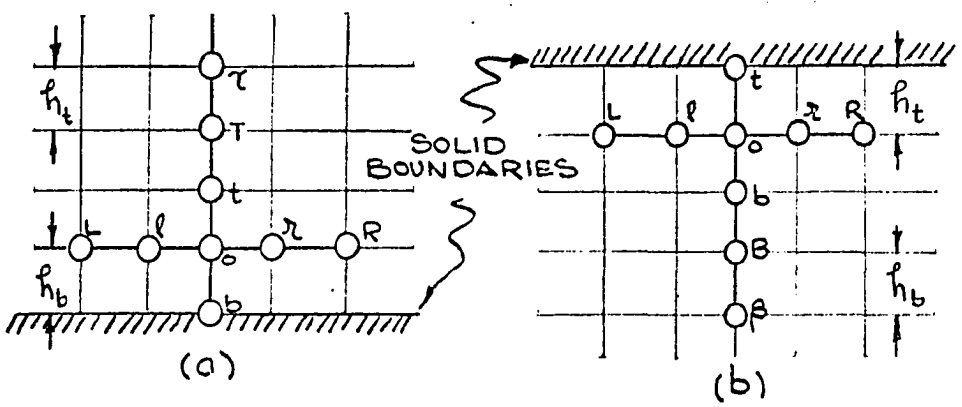

Figure (4-2)

Grid Structure Near Boundaries

If the interference with the differencing is such as to necessitate the use of a forward difference, as in Figure 4-2a, then the radial differences are computed from:

$$\left(\frac{\partial \psi}{\partial \Omega}\right)_0 = \frac{A_1\psi_\tau + A_2\psi_T + A_3\psi_0 + A_4\psi_t + A_5\psi_b}{h_t} \quad \text{.....[4-1]}$$

$$\left(\frac{\partial^2 \psi}{\partial \Omega^2}\right)_0 = \frac{B_1\psi_\tau + B_2\psi_T + B_3\psi_0 + B_4\psi_t + B_5\psi_b}{h_t^2} \quad \text{.....[4-2]}$$

Similarly, if the situation requires a backward differencing as in Figure 4-2b, then the derivatives are computed from:

$$\left(\frac{\partial \psi}{\partial \Omega}\right)_0 = \frac{A_1\psi_t + A_2\psi_b + A_3\psi_0 + A_4\psi_B + A_5\psi_\beta}{h_t} \quad \text{.....[4-3]}$$

$$\left(\frac{\partial^2 \psi}{\partial \Omega^2}\right)_0 = \frac{B_1\psi_t + B_2\psi_b + B_3\psi_0 + B_4\psi_B + B_5\psi_\beta}{h_t^2} \quad \text{.....[4-4]}$$

Values of the above coefficients different from those already

given for the central differences are required to reflect the distinction in the differencing. The off-center difference operators are presented in Appendix A and again the numerical values of the coefficients are arranged into matrix form. The superscripts "F" and "B" denote the forward and backward values respectively.

$$\|F_1^F\| = 1/420 \begin{Vmatrix} 14 & 35 & 64 \\ 21/2 & 35 & 105 \\ 20 & 35 & 56 \end{Vmatrix} \quad \|S_1^F\| = 1/420 \begin{Vmatrix} -28 & -35 & -32 \\ -14 & -35 & -70 \\ 20 & -35 & -102 \end{Vmatrix}$$

$$\|F_2^F\| = 1/60 \begin{Vmatrix} 160 & 90 & 50 \\ 225/2 & 90 & 90 \\ 60 & 90 & 120 \end{Vmatrix} \quad \|S_2^F\| = 1/60 \begin{Vmatrix} 160 & 30 & 5 \\ 210 & 30 & -15 \\ 140 & 30 & -80 \end{Vmatrix}$$

$$\|F_3^F\| = 1/60 \begin{Vmatrix} -40 & -30 & -25 \\ -25/2 & -30 & -64 \\ -18 & -30 & -45 \end{Vmatrix} \quad \|S_3^F\| = 1/60 \begin{Vmatrix} 40 & 20 & 10 \\ 10 & 20 & 32 \\ -24 & 20 & 75 \end{Vmatrix}$$

$$\|F_4^F\| = 1/60 \begin{Vmatrix} -90 & -50 & -27 \\ -64 & -50 & -35 \\ 10 & -50 & -80 \end{Vmatrix} \quad \|S_4^F\| = 1/60 \begin{Vmatrix} -420 & -100 & -24 \\ -448 & -100 & -20 \\ -320 & -100 & 10 \end{Vmatrix}$$

$$\|F_5^F\| = 1/420 \begin{Vmatrix} -32 & -105 & -50 \\ -75/2 & -105 & -42 \\ -384 & -105 & -21 \end{Vmatrix} \quad \|S_5^F\| = 1/420 \begin{Vmatrix} 1568 & 385 & 95 \\ 1610 & 385 & 91 \\ 1408 & 385 & 77 \end{Vmatrix}$$

$$\|F_1^B\| = 1/420 \begin{Vmatrix} 42 & 105 & 192 \\ 84 & 105 & 525/4 \\ 100 & 105 & 102 \end{Vmatrix} \quad \|S_1^B\| = 1/420 \begin{Vmatrix} 308 & 385 & 352 \\ 364 & 385 & 805/2 \\ 380 & 385 & 392 \end{Vmatrix}$$

$$\|F_2^B\| = 1/60 \begin{Vmatrix} -240 & -90 & -30 \\ -180 & -90 & -225/4 \\ -100 & -90 & -80 \end{Vmatrix} \quad \|S_2^B\| = 1/60 \begin{Vmatrix} -320 & 30 & 35 \\ -60 & 30 & 105/2 \\ 20 & 30 & 40 \end{Vmatrix}$$

$$\|F_3^B\| = 1/60 \begin{Vmatrix} 160 & 50 & -5 \\ 70 & 50 & 32 \\ 54 & 50 & 45 \end{Vmatrix} \quad \|S_3^B\| = 1/60 \begin{Vmatrix} 40 & -100 & -80 \\ -80 & -100 & -112 \\ -96 & -100 & -105 \end{Vmatrix}$$

$$\|F_4^B\| = 1/60 \begin{Vmatrix} 90 & 30 & 9 \\ 128 & 30 & 25/4 \\ 50 & 30 & 20 \end{Vmatrix} \quad \|S_4^B\| = 1/60 \begin{Vmatrix} 300 & 20 & -6 \\ 128 & 20 & 5/2 \\ 40 & 20 & 10 \end{Vmatrix}$$

$$\|F_5^B\| = 1/420 \begin{Vmatrix} -112 & -35 & -10 \\ -210 & -35 & -21/4 \\ -128 & -35 & -7 \end{Vmatrix} \quad \|S_5^B\| = 1/420 \begin{Vmatrix} -448 & -35 & 5 \\ -280 & -35 & -7/2 \\ -128 & -35 & -7 \end{Vmatrix}$$

Stability Considerations

In many of the existing numerical studies, it is found that there is a critical value of Reynolds number for a given grid structure which will not permit the successive correction of the node point values of the variables. In fact, correction attempts at this Reynolds number and at any other higher value will result in a divergence of the solution. To prevent this instability of the calculations, only a portion of the full correction is allowed during any one pass in the iteration process and in as much one writes that:

$$\psi_o^K = \psi_o^{K-1} + \phi_\psi (\psi_o^K - \psi_o^{K-1}) \qquad \text{.....[4-5]}$$

$$\zeta_o^K = \zeta_o^{K-1} + \phi_\zeta (\zeta_o^K - \zeta_o^{K-1}) \qquad \text{.....[4-6]}$$

where the ψ_o^K and ζ_o^K on the right side of these equations are computed from equations (3-15) and (3-16) respectively. The ϕ's are the so-called under-relaxation factors since their range of values is: $0 \leq \phi \leq 1$. From the above expressions, it is obvious that when the under-relaxation factors equal unity that a complete correction is allowed. It is further noticed that as the Reynolds number increases a greater suppression of the corrective term is required and smaller ϕ's are therefore necessary to maintain stability of the calculations. Although some theory is available for the prediction of optimum values of ϕ, in practice, their selection is still largely empirical.

Under-relaxation is not the only way to suppress the divergence, for it is known that the Reynolds number limit of the numerical stabil-

ity is intimately connected to the grid size. A reduction of the mesh spacing can also stabilize the calculations. It should be clear that the mesh cannot however be continually reduced since the number of grid points soon reaches the storage limits of even the largest of computers. Then too, smaller mesh sizes require more computing precision and double precision may not be sufficient accuracy. It is therefore worthwhile to have a relation (even if only approximate) between tolerable Reynolds number and grid spacing.

Because of the equation form, it does not appear possible to analytically derive an expression for axisymmetric flow numerical stability like those previously obtained for the situation of plane flow as in Thom and Apelt (29) and Lester (30). Hung, (18), apparently recognized this and therefore attempted a numerical solution. In that study, the grid size was fixed in the situation of pipe flow and the Re was continually increased until divergence was produced. Hung obtained a linear curve of the limiting Reynolds number against the reciprocal of the grid spacing. To utilize his work in the present situation of orifice flow, a linear equation for Hung's curve was written and after converting it into variables of the present problem, the following inequality, which must be satisfied (approximately) in order to realize convergence, is obtained:

$$R_E \leq \left(4 + \frac{2\,d/D}{h}\right) d/D \qquad \ldots\ldots[4\text{-}7]$$

Figure (4-3), is a plot of this linear relation for various d/D. The conditions under which the above was obtained must be emphasized, for

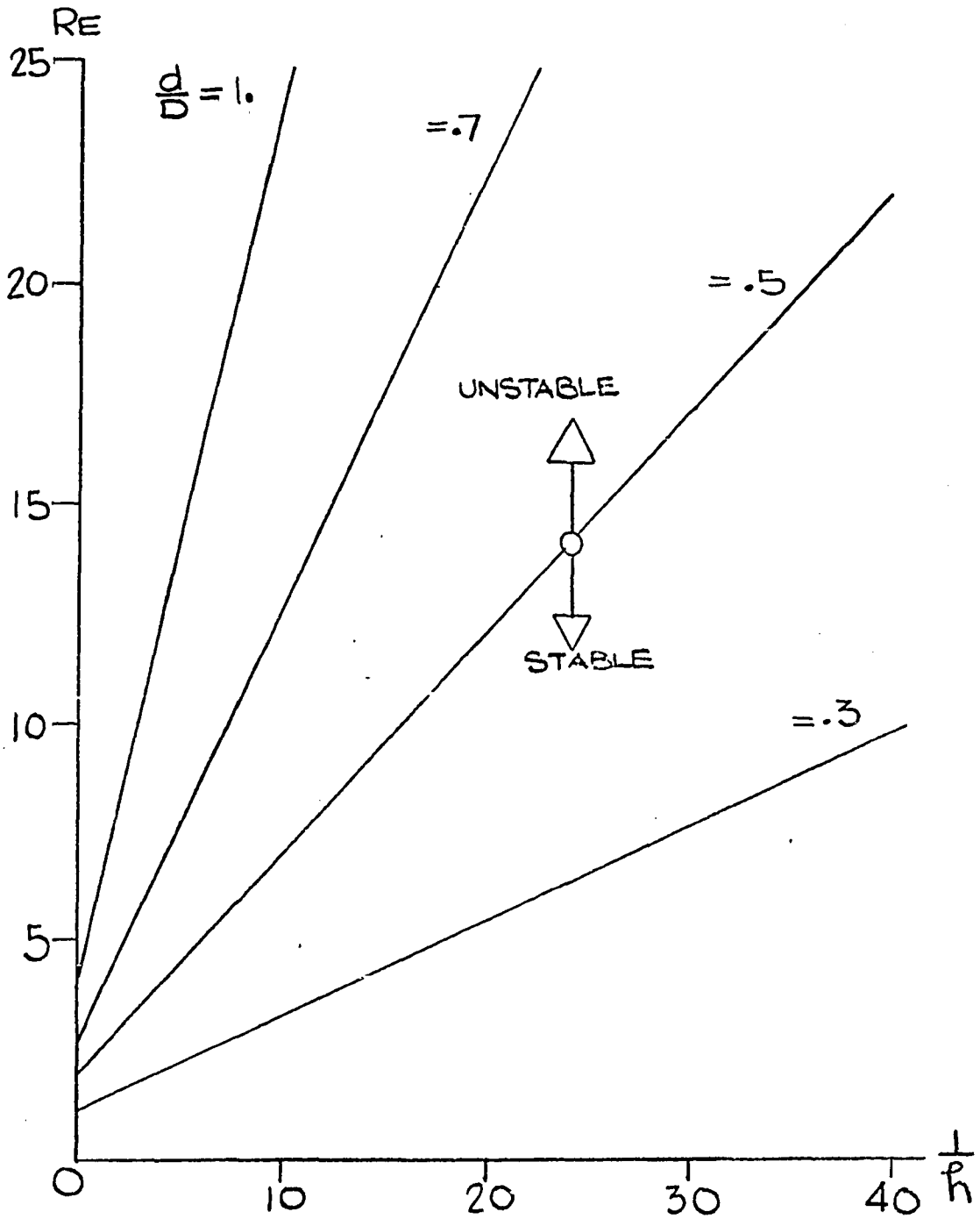

Figure 4-3

Numerical Stability Curves for
Various Orifice to Pipe Diameter Ratios

Hung's study was carried out with d/D = 1., in a uniform square grid, using a 3-point finite difference operator which has not yielded especially accurate results to the known Poiseuille solution (see section below. Thus, the curves really provide an indication as to when stability problems might be encountered. Nevertheless, these curves have been found in very good agreement with the actual computation limits both in the present study and in studies reported in the literature, e.g., Lee and Fung in (12).

Program Details

A digital computer program was written to perform the calculations described above. The program listing is presented as Appendix E and the discussion here will not be lengthy as only the most important details of that program will be brought forward.

To facilitate this discussion as well as to indicate the order of the calculations, a block diagram of the program is shown as Figure 4-4. From this diagram, it can be seen that after the input data has been read into the computer and the grid structure has been established, each node point is assigned an initial value for the ψ_{ij} and J_{ij} . These initial nodal values can be designated in different ways depending upon which input option is chosen. In one option, the variables at the nodes are assigned zeros. In another, Poiseuillean values are specified at each mesh point. In yet another option, node values are set from a previous runs distribution of ψ and J which have been preserved on magnetic tape. This latter method is an especially useful one particularly in situations where the Reynolds number is changed from one run to the next while the orifice diameter ratio remains fixed.

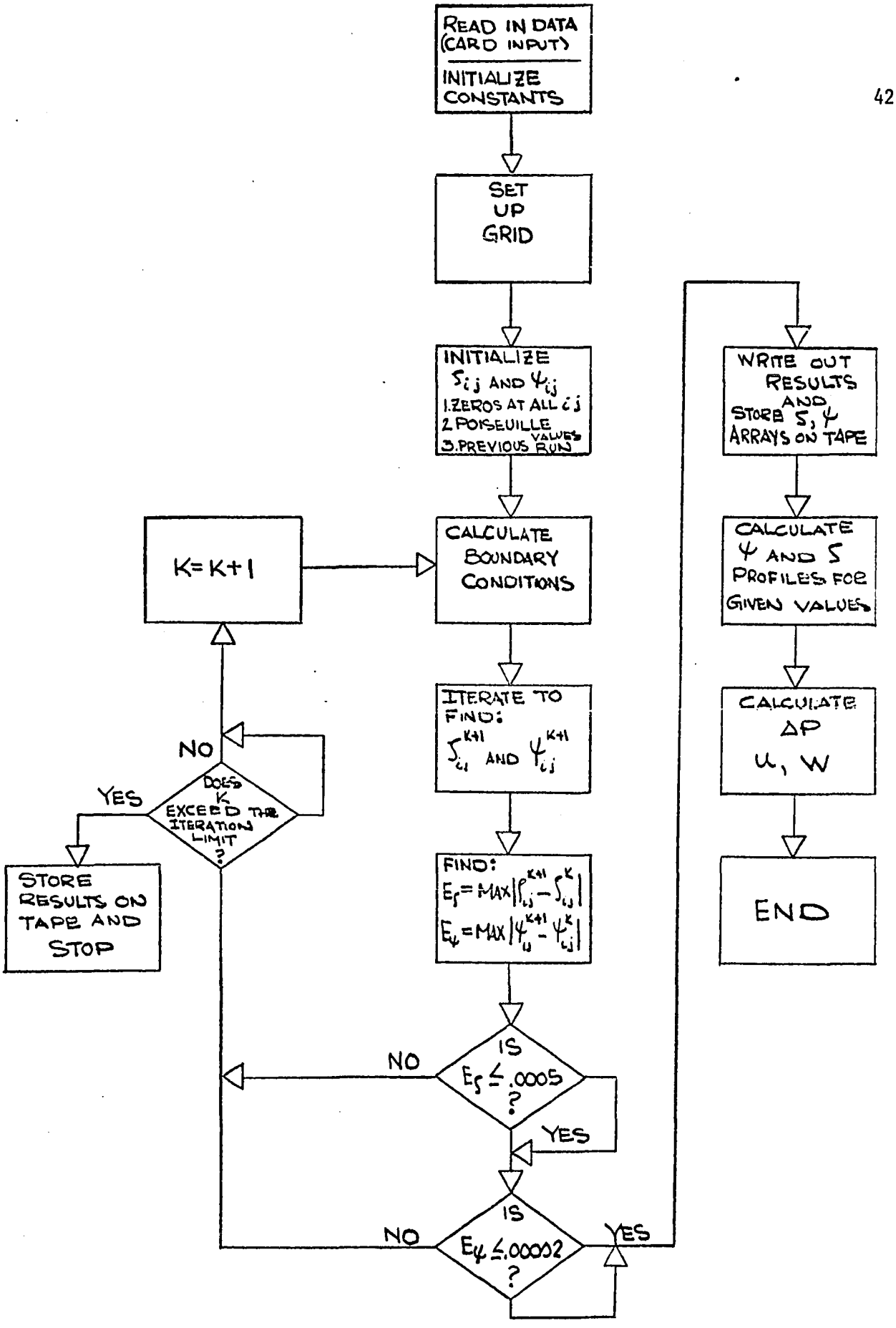

Figure 4-4

Block Diagram of Computer Program

After the boundary conditions have been calculated, the field is given a complete sweep proceeding radially from the pipe wall towards the center line and moving from left to right in the axial direction. Throughout this sweep of the field, the node equations (4-5) and (4-6) are solved at each mesh point. In addition, the absolute values of the change in each variable in successive passes is retained. If the maximum value of these differences diminishes to or below some small tolerance, then the solution is said to be converged and the calculations are allowed to go forward. If, on the other hand, the largest differences exceed these tolerance values, then the entire calculation process must be repeated, provided that the iteration limit is not surpassed. The conditions used in this study which must be satisfied in order to successfully terminate the iteration process are:

$$\left| \zeta_{ij}^{K} - \zeta_{ij}^{K-1} \right| \leq .00050 \qquad \text{.....[4-8]}$$

$$\left| \psi_{ij}^{K} - \psi_{ij}^{K-1} \right| \leq .00002 \qquad \text{.....[4-9]}$$

These values are consistent with tolerances used by others e.g., Mills (1) used .0004 and .000015 for ζ and ψ respectively, while Lee and Fung (12) used .001 and .00002. In the present study, the vorticity convergence was found to be of major concern, for if it satisfied equation (4-8) the stream function usually met its condition also.

The solution times for the runs were dependent upon the orifice diameter ratio and the Reynolds number plus the number of grid points under consideration. For Re = 0, solution times were found to be the

shortest, typically 5 minutes of UNIVAC 1108 computer time, whereas, an Re = 10, required about 25 minutes for convergence. The smallest orifice considered in this study was for a d/D ratio of .3. Computer running times for this size were the longest and for the largest Reynolds number investigated at this diameter ratio (Re = 5) nearly one hour of computer time was necessary to satisfy the convergence conditions of equations (4-8) and (4-9).

A rule of thumb developed from the computer program, for it was found that approximately 72,000 grid points could be swept in one minute of computation. Therefore, a field of 1800 nodal points (say 67 x 27) could be covered 40 times each minute. Typically 500 iteration were required to attain a converged solution, hence this example would require about 12-1/2 minutes for solution (it should be noted that this time estimate also includes the time required for the χ and $\int$ interpolations, differential pressure calculations and velocity computations).

A Test Problem - Poiseuille Flow

In order to verify the computer program and the solution method, runs were made to determine whether the program was capable of predicting the classical Poiseuille flow results starting with zeros at all of the node points of a given mesh. In effect, this is the same as solving the trivial case of flow through an orifice of d/D = 1.

Others have similarly used this computation test in evaluation the merits of their numerical scheme and some of the results of these past efforts are presented in the first portions of Tables (4-1) and (4-2).

Source	Re	Grid Size	Iter No	r/R=0	.25	.50	.75	1.0
Ex. Value	-	-	-	0.	1.0	2.0	3.0	4.0
Hung (18)	10	1/8	20	0.	-.002914	-.010186	-.020784	-.031450
			60	0.	-.002908	-.010164	-.020724	-.031386
			100	0.	-.002908	-.010164	-.020724	-.031386
	39.5	1/16	32	0.	-.037070	-.002570	-.000426	+.024624
			128	0.	-.000032	-.007372	-.004440	-.008814
Mills (1)	5	1/8	20	0.	+.012178	+.014782	-.025394	-.121806
			100	0.	-.001312	-.005882	-.015962	-.031700
		1/16	50	0.	+.153986	+.315804	+.286030	-.211602
			100	0.	+.002506	-.000094	-.013340	-.029610
	10	1/8	20	0.	+.002262	+.006172	+.006514	-.035040
			100	0.	+.001094	-.002488	-.014680	-.034554
		1/16	50	0.	-.001736	+.084702	+.271430	+.169452
			100	0.	+.000226	+.001690	+.002954	-.005698
Lee & Fung (12)	5	1/8	30	0.	-.01418	-.02974	-.04180	-.02106
			60	0.	+.00010	+.00014	+.00012	-.00018
PRESENT STUDY								
Single Precision	5	1/8	20	0.	+.0492134	+.1141405	+.1282063	-.0256042
			40	0.	-.0000822	-.0004683	-.0014410	-.0021257
			60	0.	-.0000063	-.0000076	+.0000725	+.0002203
			80↑	0.	-.0000016	+.0000172	+.0000830	+.0002165
Double Precision			20	0.	+.0492168	+.1141292	+.1281323	-.0258066
			40	0.	-.0000814	-.0004834	-.0015125	-.0022836
			60	0.	-.0000065	-.0000029	-.0000073	+.0000211
			80	0.	+.0000001	+.0000002	+.0000003	+.0000002
			100↑	0.	.0000000	.0000000	.0000000	.0000000
Double Precision		1/16	200	0.	-.0000973	-.0001431	+.0000877	+.0008440
			300	0.	+.0000005	+.0000009	+.0000005	-.0000013
			360↑	0.	.0000000	.0000000	.0000000	.0000000
Sing. Prec.		Grad.	100	0.	+.0178413	+.0966520	+.2954588	+.4506140
Double			200	0.	+.0008180	+.0046058	+.0119424	+.0154036
Precision			300	0.	+.0000301	+.0001697	+.0004350	+.0005544
			400	0.	+.0000011	+.0000061	+.0000157	+.0000201
			500	0.	.0000000	+.0000001	+.0000003	+.0000008
			600↑	0.	.0000000	.0000000	.0000000	.0000000

Note: Table values = $\int$ (exact) - $\int$ (computed)

Table (4-1)

Poiseuille Flow Vorticity Comparison

Source	Re	Grid Size	Iter No.	r/R=0	.25	.50	.75	1.0
Ex. Value	-	-	-	0	-.0605469	-.2187500	-.4042969	-.5000000
Hung (18)	10	1/8	20	0	+.000581	+.000862	+.000507	0
			60	0	+.000581	+.000858	+.000583	0
			100	0	+.000581	+.000858	+.000583	0
	39.5	1/16	32	0	+.000249	-.000364	-.000393	0
			128	0	+.000129	+.000198	+.000115	0
Mills (1)	5	1/8	20	0	+.001023	+.002234	+.001687	0
			100	0	+.000499	+.000744	+.000465	0
		1/16	50	0	-.001437	-.002122	+.000667	0
			100	0	+.000325	+.000828	+.000479	0
	10	1/8	20	0	+.000243	+.000146	+.000211	0
			100	0	+.000523	+.000802	+.000507	0
		1/16	50	0	-.004363	-.010102	-.005435	0
			100	0	-.000003	-.000066	-.000015	0
Lee & Fung (12)	5	1/8	30	0	+.00035	+.00085	+.00044	0
			60	0	-.00001	+.00001	+.00000	0
PRESENT STUDY								
Single Precision	5	1/8	20	0	-.0004666	-.0010530	-.0002907	0
			40	0	+.0000186	+.0000497	+.0000329	0
			60	0	-.0000009	-.0000127	-.0000030	0
			80↑	0	-.0000009	-.0000127	-.0000030	0
Double Precision			20	0	-.0004658	-.0010504	-.0002879	0
			40	0	+.0000193	+.0000521	+.0000255	0
			60	0	-.0000001	-.0000002	-.0000003	0
			80	0	.0000000	.0000000	.0000000	0
			100↑	0	.0000000	.0000000	.0000000	0
Double Precision		1/16	200	0	-.0000007	-.0000057	-.0000093	0
			300	0	.0000000	.0000000	.0000000	0
			360↑	0	.0000000	.0000000	.0000000	0
Sing. Prec.		Grad.	100	0	-.0059371	-.0178425	-.0095335	0
Double			200	0	-.0002279	-.0006678	-.0003452	0
Precision			300	0	-.0000083	-.0000242	-.0000125	0
			400	0	-.0000003	-.0000009	-.0000005	0
			500	0	.0000000	.0000000	.0000000	0
			600↑	0	.0000000	.0000000	.0000000	0

Note: Table Values = ψ(Exact) - ψ (Computed)

Table (4-2)

Poiseuille Flow Stream Function Comparison

Disagreement between exact and computed values of Poiseuille flow in these previous works are thought to be due to a combination of truncation and round off errors. For example, the ψ equation used by both Mills and Hung is in error with the exact result by the amount of $2h^2(1-r_j-h^2)$ as may be checked by direct substitution.

The results of the present Poiseuillean check reveals several important facts which can be confirmed by reference to the tables:

1. For the grid sizes considered, double precision arithmetic is vital in reducing the difference between the computed values and the exact values.

2. The finer the mesh the larger the total number of iterations necessary to attain the same degree of accuracy.

3. For a graded mesh:

   a. Double precision of necessity must be used.

   b. Considerably more iterations are required to attain the same degree of accuracy as a square mesh field containing the same number of grid points.

CHAPTER V

RESULTS AND DISCUSSION

In this chapter, results of the computer runs will be presented and discussed. In all, 27 numerical solutions were obtained for Reynolds numbers ranging from 0 to 12.5 and for orifice to pipe diameter ratios of .3, .4, .5, .6, and .7 (although for the .4 and .6 diameter ratios, only vanishing Reynolds number flows were considered). The thickness of the orifice plate was taken to be 1/8th of the pipe radius. Five of the solutions obtained apply to a sharp-edged orifice beveled at 45° and facing downstream i.e., forming a diverging passage in the direction of flow.

Square-Edged Orifice Results

The bulk of the results obtained in this thesis are contained in this section. In that so many solutions were obtained, it is unfortunately not possible to present all of the information extracted from these solutions. Therefore, in many of the figures about to be displayed, only representative situations will be exhibited.

Figures 5-1 through 5-3 show axial distributions of various constant values of stream function and vorticity. These streamline patterns and vorticity contours are presented for a low (zero), moderate, and high (relatively speaking) Reynolds number for three d/D ratios: .3, .5, and .7. The change from complete axial symmetry at zero Reynolds number to the asymmetric patterns as the Reynolds number increases is very pronounced. The reason for this alteration of flow pattern is attributed to the fact that the larger Reynolds numbered flows produce greater

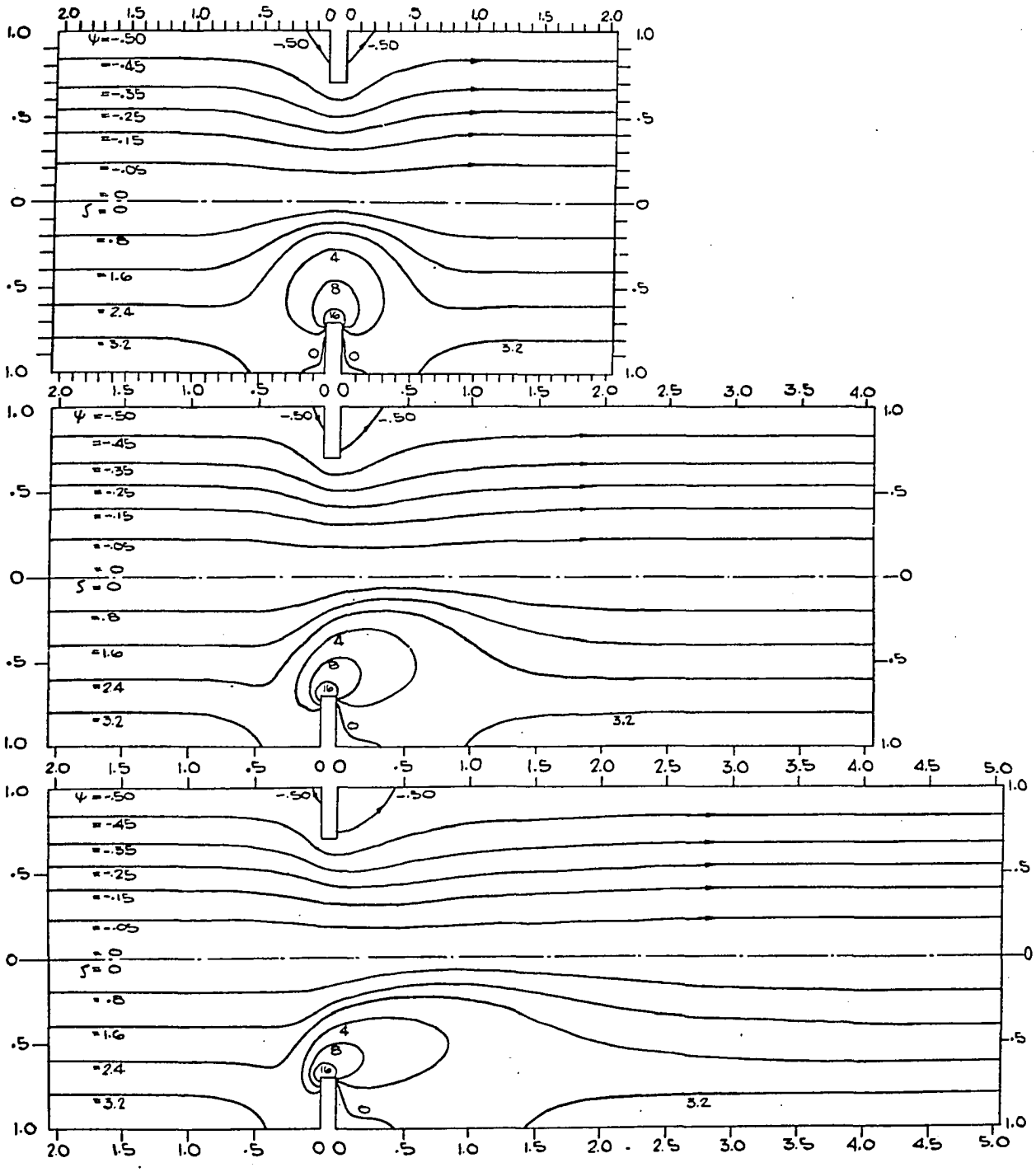

Figure 5-1

Streamlines and Vorticity Contours for
d/D = .7, Re = 0, 5, 10

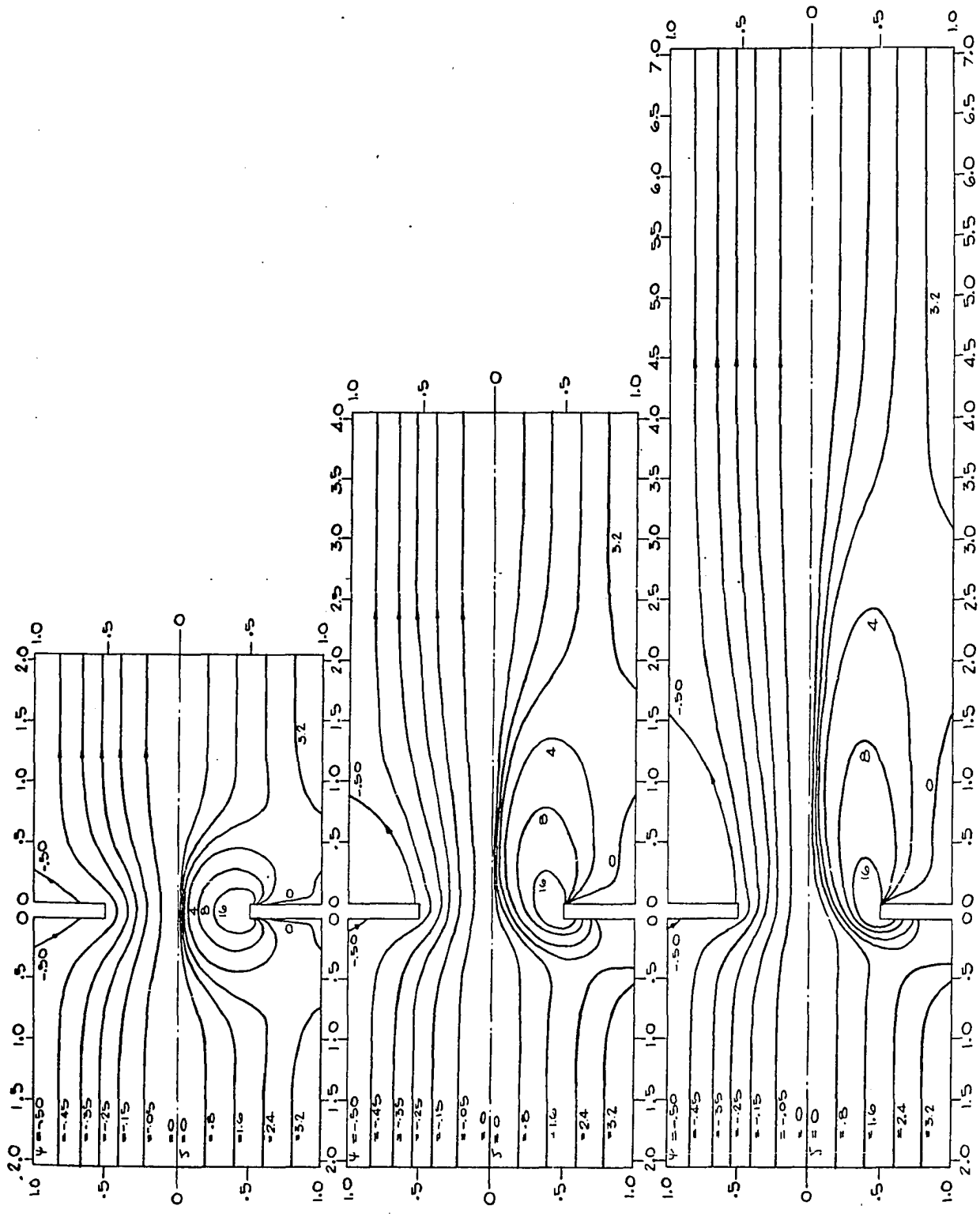

Figure 5-2

Streamlines and Vorticity Contours for
d/D = .5, Re = 0, 5, 10

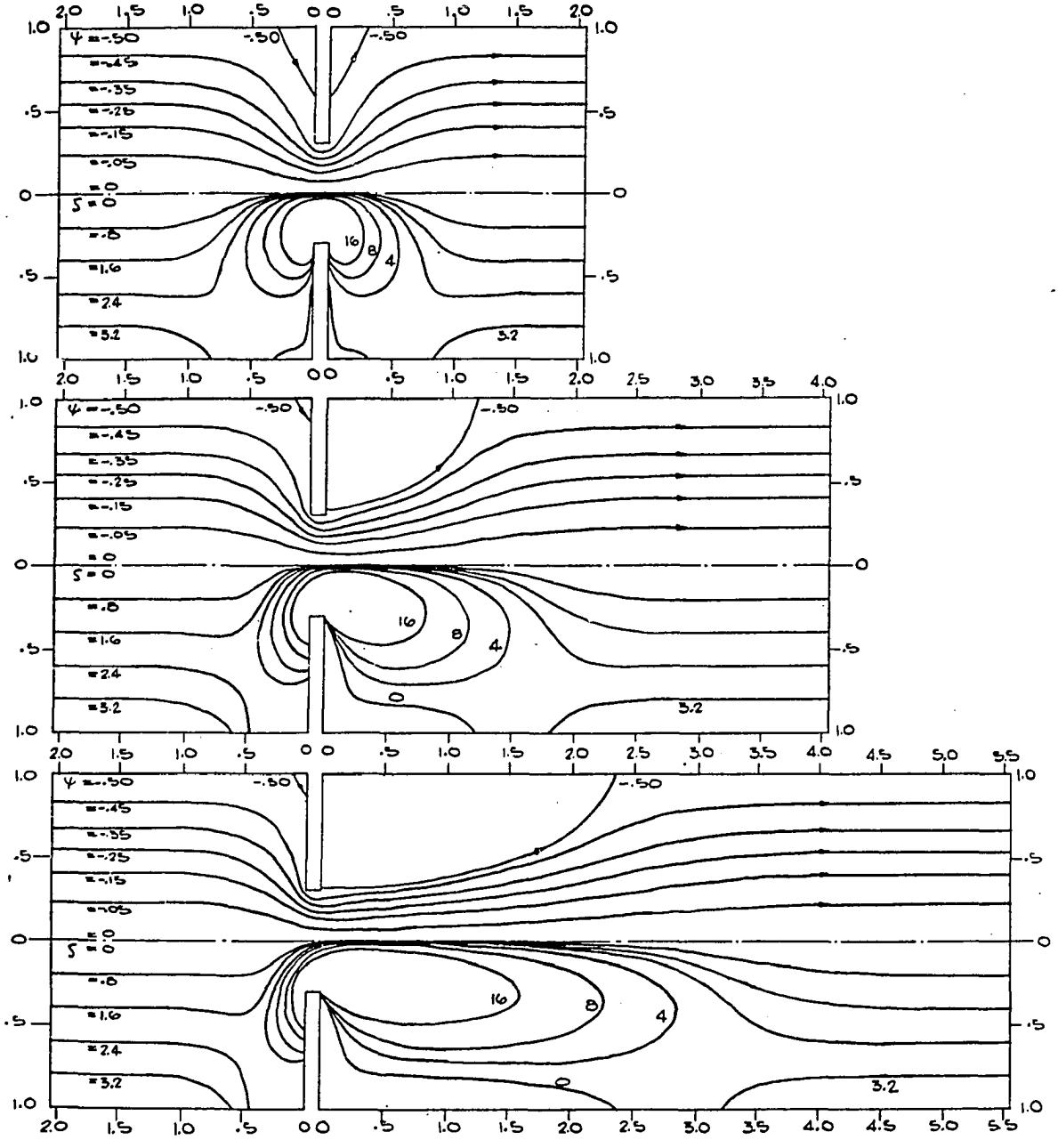

Figure 5-3

Streamlines and Vorticity Contours for
d/D = .3, Re = 0, 2.5, 5

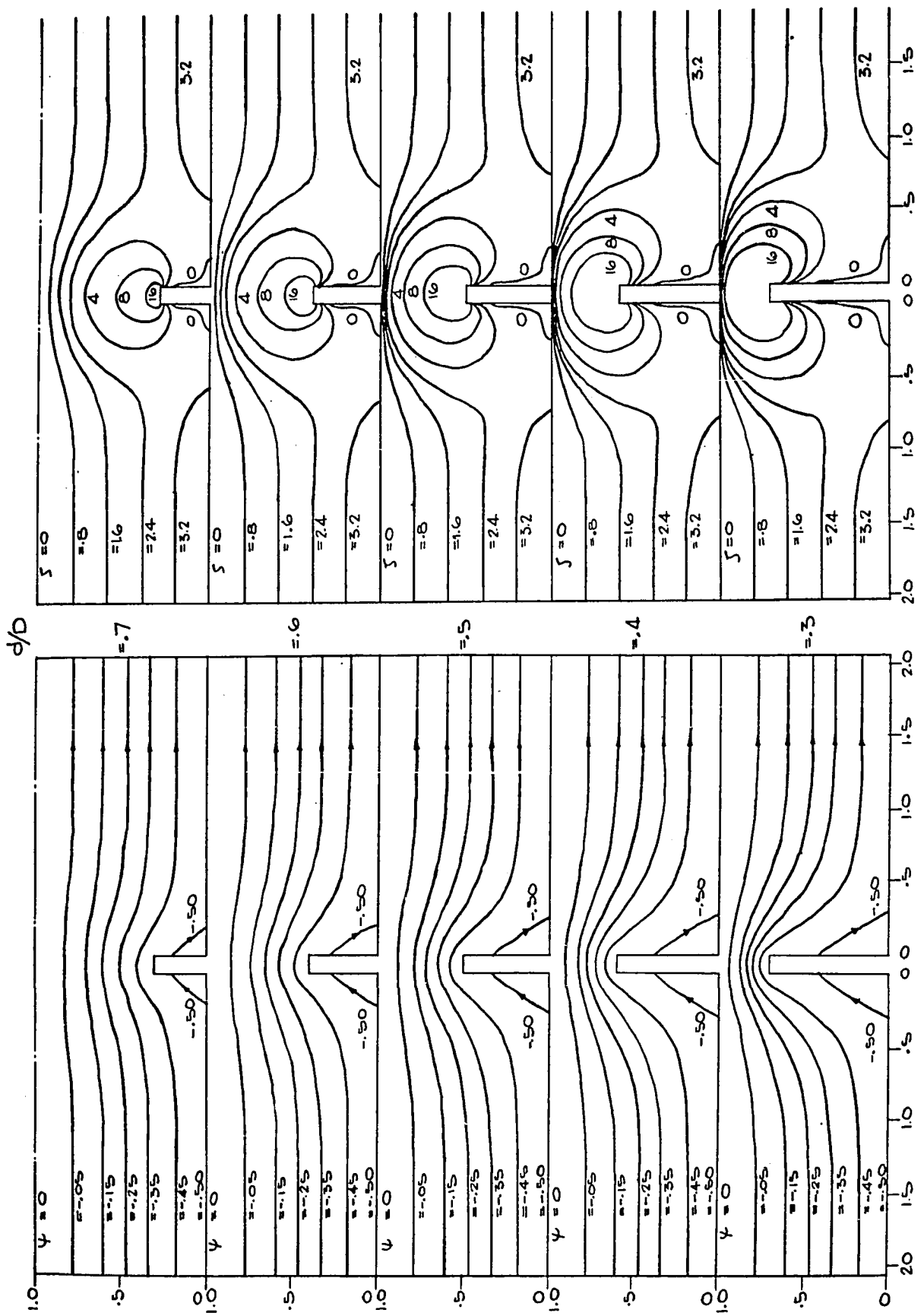

Figure 5-4

Streamlines and Vorticity Contours for Various d/D for Creeping Flow

amounts of vorticity at the solid surfaces in the forward half of the flow field (this will be shown in a later plot of the wall vorticity distribution). Moreover, the larger inertial forces existing in the higher Reynolds number flows cause the vorticity contours to be stretched in the direction of motion.

Figure 5-4 gives the creeping flow (Re = 0) streamline patterns and vorticity contours for five orifice diameter ratios. Due to the symmetry about the mid plane, flow can be considered from either left to right or right to left. In the vanishing Reynolds number case, the non-linear convective terms in the vorticity transport equation are dominated by the linear viscous terms and are therefore neglected. It is of some interest to examine a case where the inertial terms are small but not quite negligible when compared with the viscous terms in order to discover whether results scarcely different from the creeping flow solution could be obtained. Figure 5-5 shows the dividing streamline for the corner eddies for a d/D of .5 at a Reynolds numbers of 0 and .1. It can be seen that the results are about as might be expected, for the upstream eddy shape is slightly decreased in length and height while the downstream eddy is slightly elongated in both the axial and radial direction because of the increased convection.

From the above figures, it should be noticed that corner eddies exist on <u>both</u> faces of the orifice plate for all Reynolds numbers investigated. Furthermore, the separation point was found to be <u>below</u> the sharp corner in all cases. The separation point and the point of reattachment are located on the boundaries at the position where the vorticity vanished as is shown in Figure 5-6.

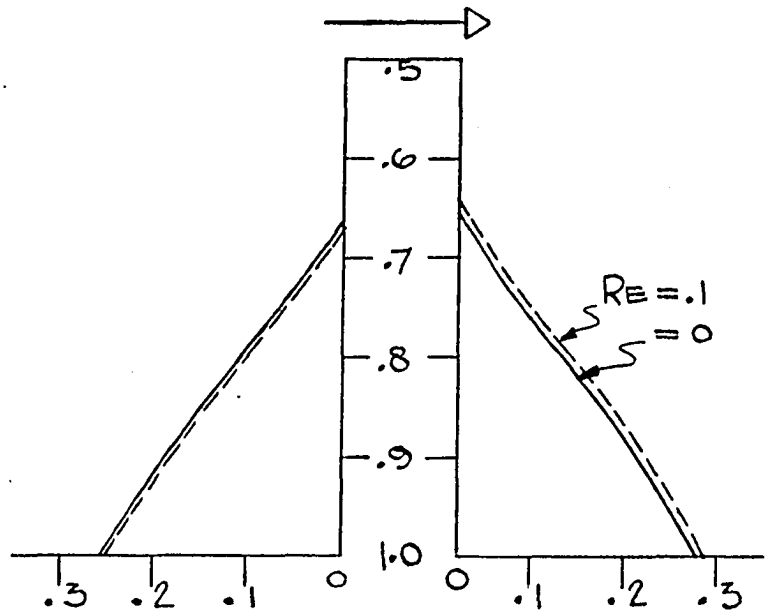

Figure (5-5)

Comparison of Dividing Streamlines For
A Square Edged Orifice At Two Reynolds Nos 0 and .1

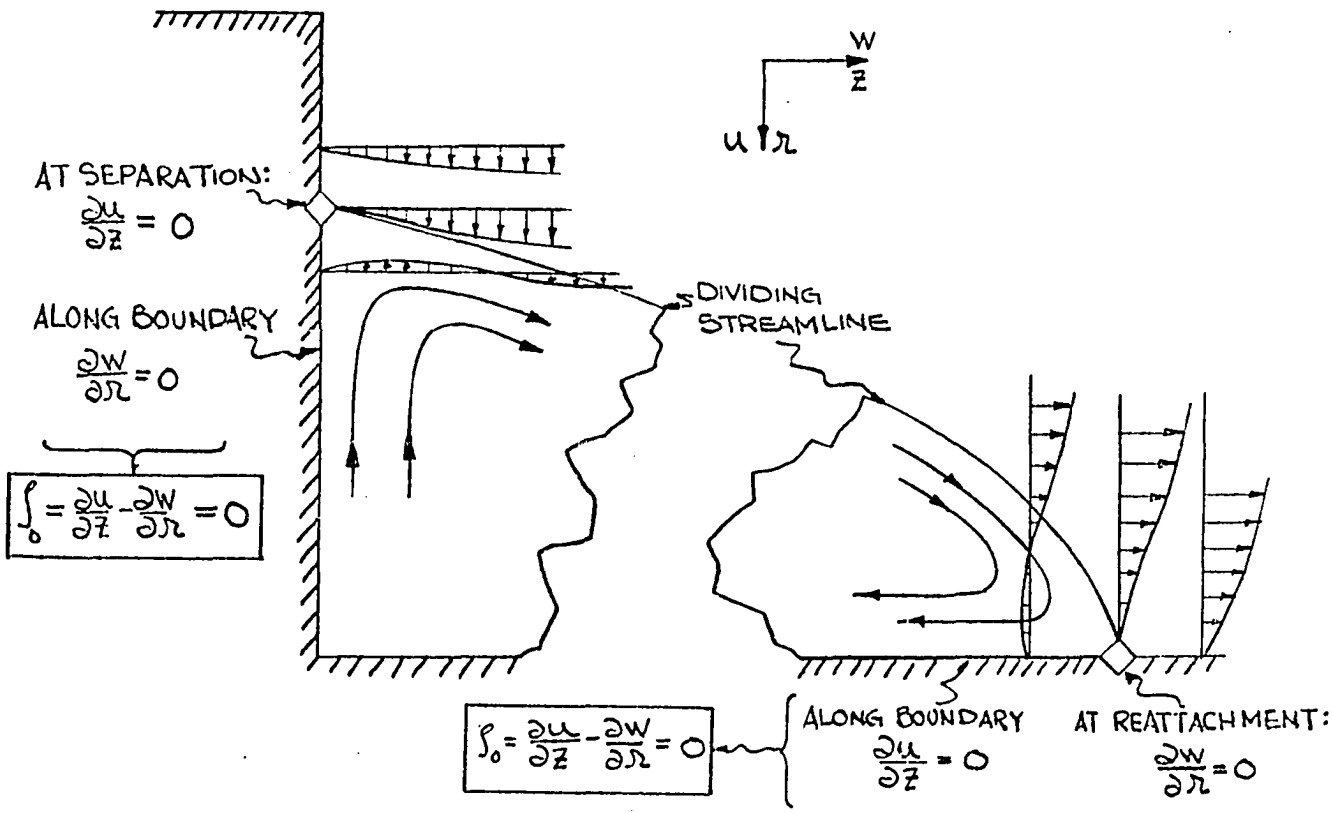

Figure (5-6)

Separation and Reattachment

For several reasons these results are especially interesting. First of all, the more familiar situations of flow around a sphere or a cylinder are generally thought to have a critical Reynolds number below which no separation takes place. For example, Underwood in (31), using a semi-analytical method in calculations of incompressible flow around a circular cylinder, found no wake region for an Re less than 5.75. The sphere study of Jenson (25) indicated that separation first appeared at a Reynolds number of 17. On the other hand, Rimon and Cheng (32) have challenged this result and raise questions as to whether a critical Reynolds number for separation really exists. Probably even more surprising than producing solutions which allow a wake for zero Reynolds number flow, is the fact that the flow separates on the face of the orifice plate rather than at the sharp intruding corner. It would not seem possible that the flow could negotiate the nearly 90° turn around the square corner. Yet, others have also indicated that separation can take place below an intruding corner. The analytical studies of Weinbaum (33) and of Schubert (34), the numerical studies of Mills, of Hung and Macano (35) and of Roache (36) and the experimental investigations of Hamma (37) and Donaldson (38), (to name a few) have indicated situations for which a dividing streamline originates below a corner or edge.

Another interesting feature of the flow is that a recirculatory region stands ahead of the orifice plate. Again, this is somewhat contrary to intuition based upon past experiences with cylinders and spheres. In those flows, the fluid is accelerated by a favorable pressure gradient over the upstream portion of the body and is decelerated against an adverse pressure gradient over its afterbody. Lacking suf-

ficient flow energy, the fluid is pushed away from the surface in the retarded flow area and a backflow region is established. In the case of the orifice plate, the flow not only sees an adverse pressure gradient on its downstream side, but the upstream facing side also produces a pressure rise near the pipe wall (as will be seen in subsequent axial pressure plots). Apparently, the pressure increases along the pipe wall are sufficient to cause the flow to detach from the surface ahead of the orifice plate. As the Reynolds number of the flow is increased, greater inertial forces act upon the fluid and enable the flow to advance closer to the orifice plate before being separated from the pipe wall. In addition, the increased convection of the flow demands that a greater amount of fluid must pass through the constricted portion of the pipe. The influence of the somewhat weak adverse pressure gradient is reduced and the forward wake region is forced, by the main stream, to diminish itself radially. Figure 5-7 which shows the variation of the upstream and downstream lengths of the separation region with Reynolds number for three orifice diameter ratios confirm this. It is interesting to note that after a Reynolds number of 5, the front eddy length is virtually identical in size for all the diameter ratios considered. The relation between the rear recirculation region length and Reynolds number is nearly linear. Linearity is more evident for higher d/D ratios and larger Re. For comparison purposes, Mills' rear wake length variation, which was obtained from his curves, is also shown. It can be seen that disagreement between that work and the present is less pronounced as the Reynolds number approaches zero.

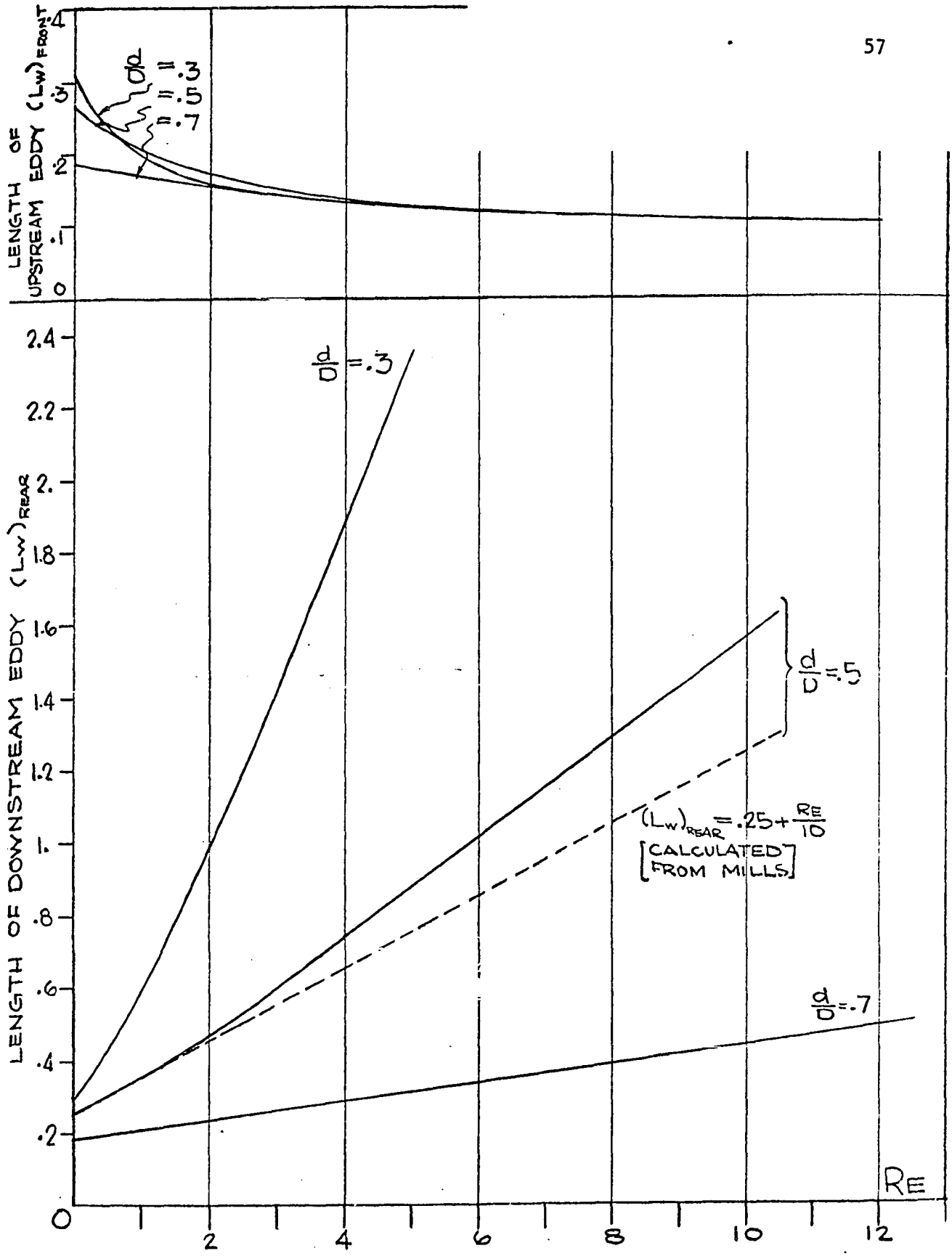

Figure 5-7

Upstream and Downstream Wake Length vs Re for Various d/D Ratios

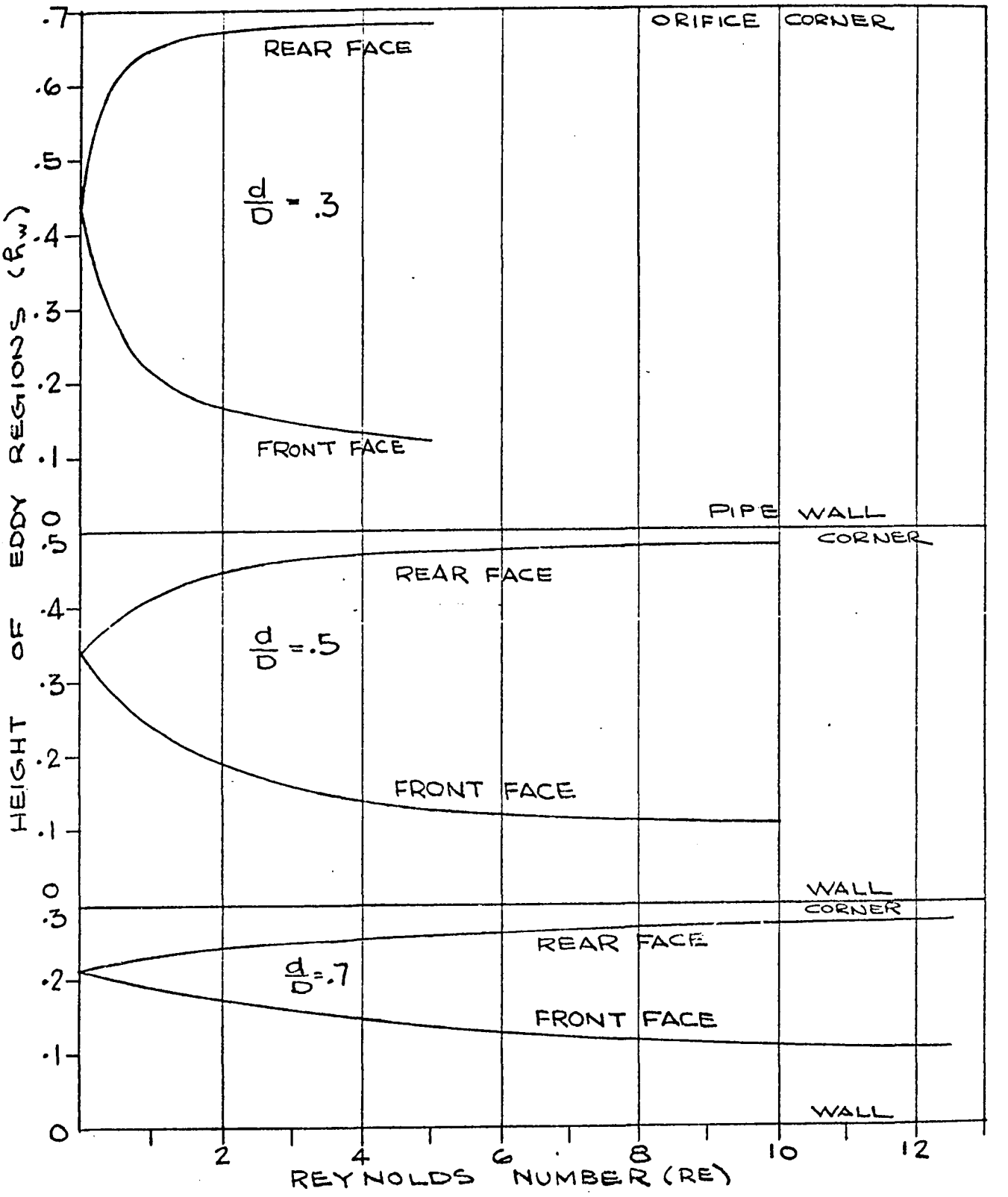

Figure (5-8)

Upstream and Downstream Wake Height vs Re for Various d/D Ratios

The distance from the pipe wall to the point of separation on the rear face of the orifice plate and the corresponding point of reattachment on the front face are shown in Figure 5-8 as a function of the Reynolds number for three d/D ratios. It is evident from this figure that the front side eddy height, like the frontal eddy length, all yield nearly the same value after a Reynolds number of about 5, independent of the orifice diameter ratio. In fact, the forward values h_w and L_w are found to be equal after this Reynolds number is reached. There does not seem to be any clear reason why this frontal eddy zone should contract to a region of equal height and length as the above results have indicated. It should also be noticed that the rear separation point approaches the sharp corner with increasing Re, and at the last computed Reynolds number, separation occurred within 3% of the total height of the orifice face from the corner for the d/D = .3, 4% for d/D = .5 and within 8% for d/D .7.

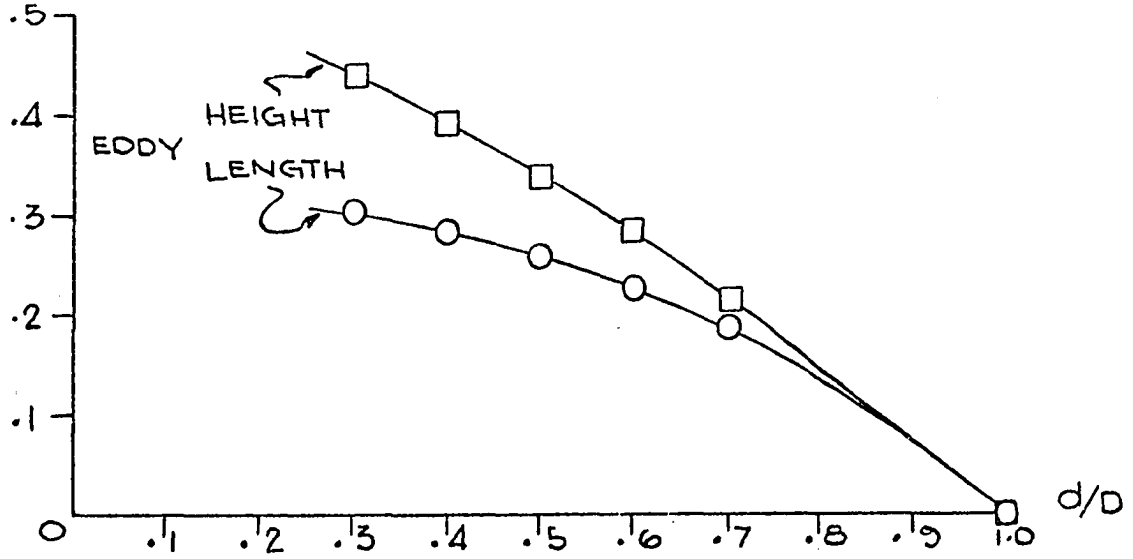

Figure (5-9)

Creeping Flow Eddy Height and Length
Vs Orifice to Pipe Diameter Ratio

Figure 5-9 gives the length and height variation of the recirculating region with orifice diameter ratio for the limiting creeping flow situation. For comparison purposes, Mills had an estimated wake length and height of .25 and .33 respectively, as contrasted to the .260 and .339 values predicted here.

It is of interest to show the details of the wake region. Since smaller orifice to pipe diameter ratios have the largest recirculation areas, the d/D = .3 results were chosen to demonstrate the closed streamlines of this portion of the flow field. Figure 5-10 contains the streamlines for the values of stream function indicated. Note that the curves have purposely not been smoothed so that an idea of the fine grain nature of the grid structure can be realized. A "•" is used to denote the so-called center of the wake which is defined as the point where the axial velocity profile and the radial velocity component both change sign. The determination of this point for the case of Re = .25 is presented in Figure 5-11. As the mainstream Reynolds number increases so too does the strength of the recirculatory wake. The wake streamline pattern of Figure 5-10 conveys this fact since the flow rate within the eddy zone, as characterized by the difference in ψ between two streamlines, is seen to increase as the Reynolds number of the flow is advanced. For a sufficiently high Reynolds number flow, it is possible to obtain a secondary wake region within the confines of the primary eddy zone. Unfortunately, a high enough Reynolds number to cause this formation of the second recirculation was not attempted.

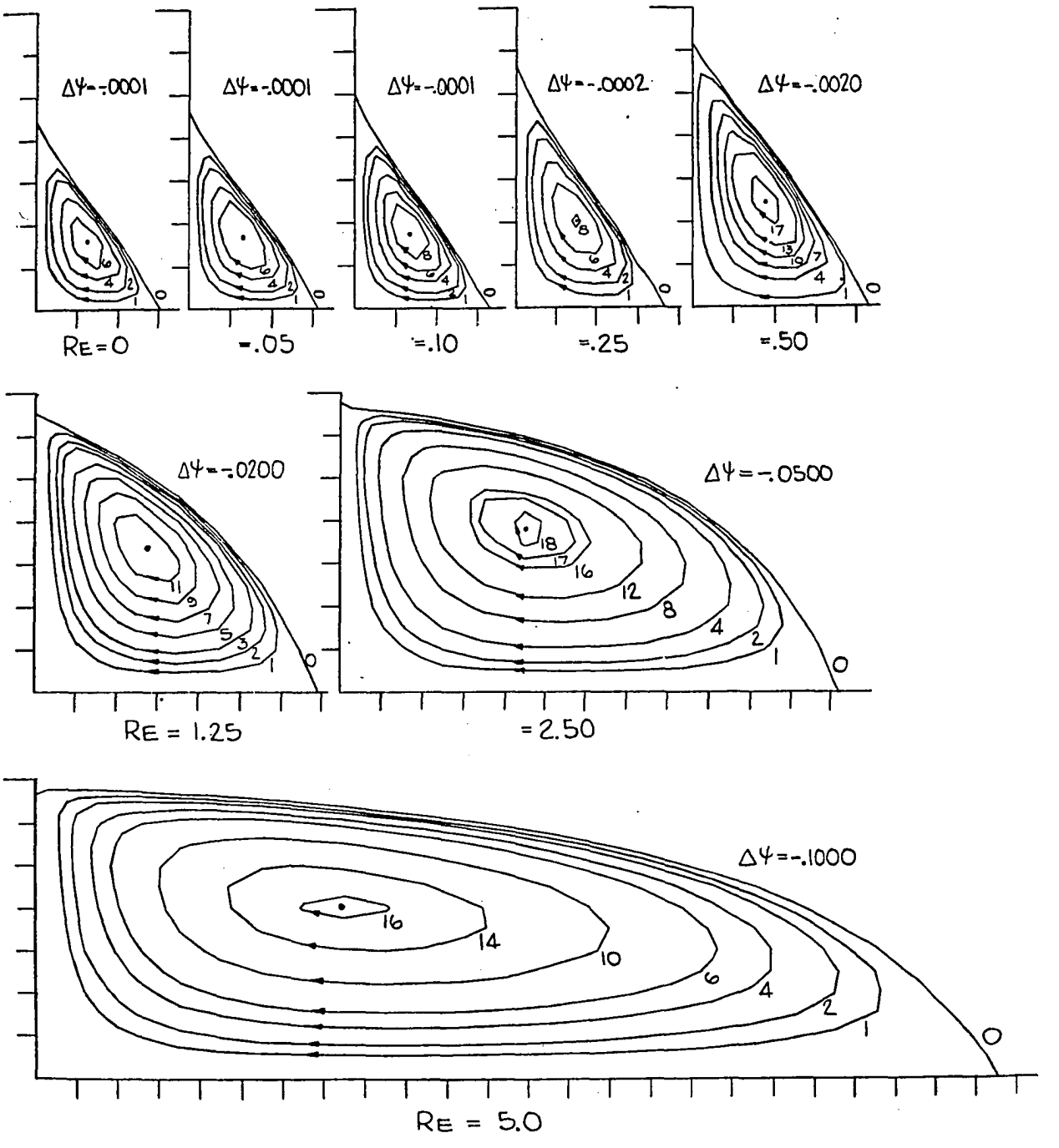

Figure 5-10

Closed Wake Streamlines for d/D = .3 at Various Re

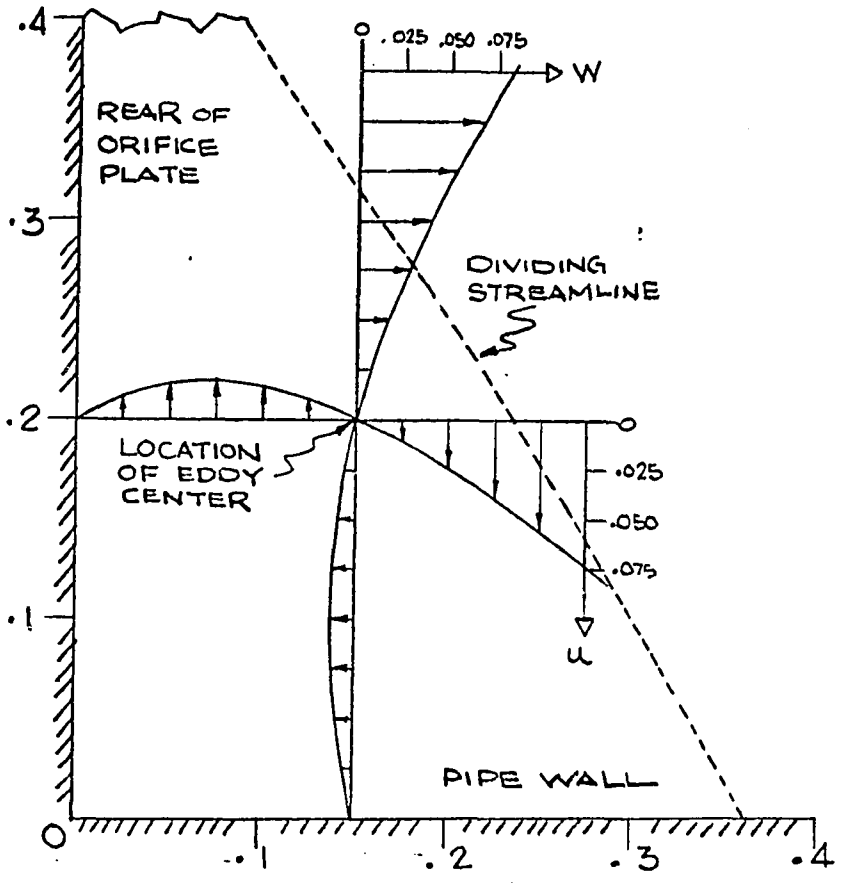

Figure (5-11)

Location of Eddy Center for d/D = .3, at Re = .25

Figure (5-12) shows the location of the core of the wake region and how its position changes with Reynolds number for a d/D = .3. The curves bear a resemblance to those of h_w and L_w of Figures (5-7) and (5-8). The axial location of the wake center appears to vary linearly with Re except at the low end of the curve. The radial distance appears to be approaching some asympotic value which undoubtedly varies with the diameter ratio. Accurate locations are not easily found because a double interpolation is required and also because the grid structure is not as fine as would be desired at that particular point in the flow field.

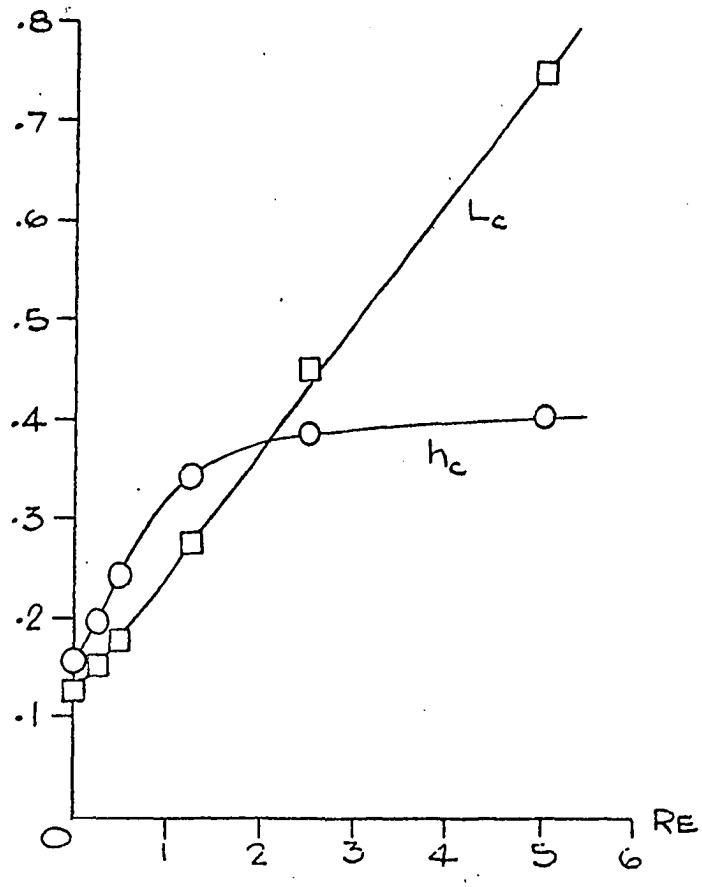

Figure (5-12)

Radial and Axial Locations of Eddy Center Vs Re for d/D = .3

The axial pressure distribution along the wall and the centerline are presented in Figure (5-13). These distributions were obtained by performing the numerical integrations required by equations (3-30) and (3-31). Note that a direct evaluation of the ratio ψ/r in equation (3-30) at the centerline would result in the indeterminate 0/0. To resolve this, Lester (20) is followed wherein $(\psi/r)_{\ell}$ was replaced by its limiting form: $(\partial\psi/\partial r)_{\ell}$ . . . . The symmetry about the mid-plane of the orifice plate is apparent in the creeping flow cases as seen in Figure (5-14). One half of the pressure loss occurs on the upstream

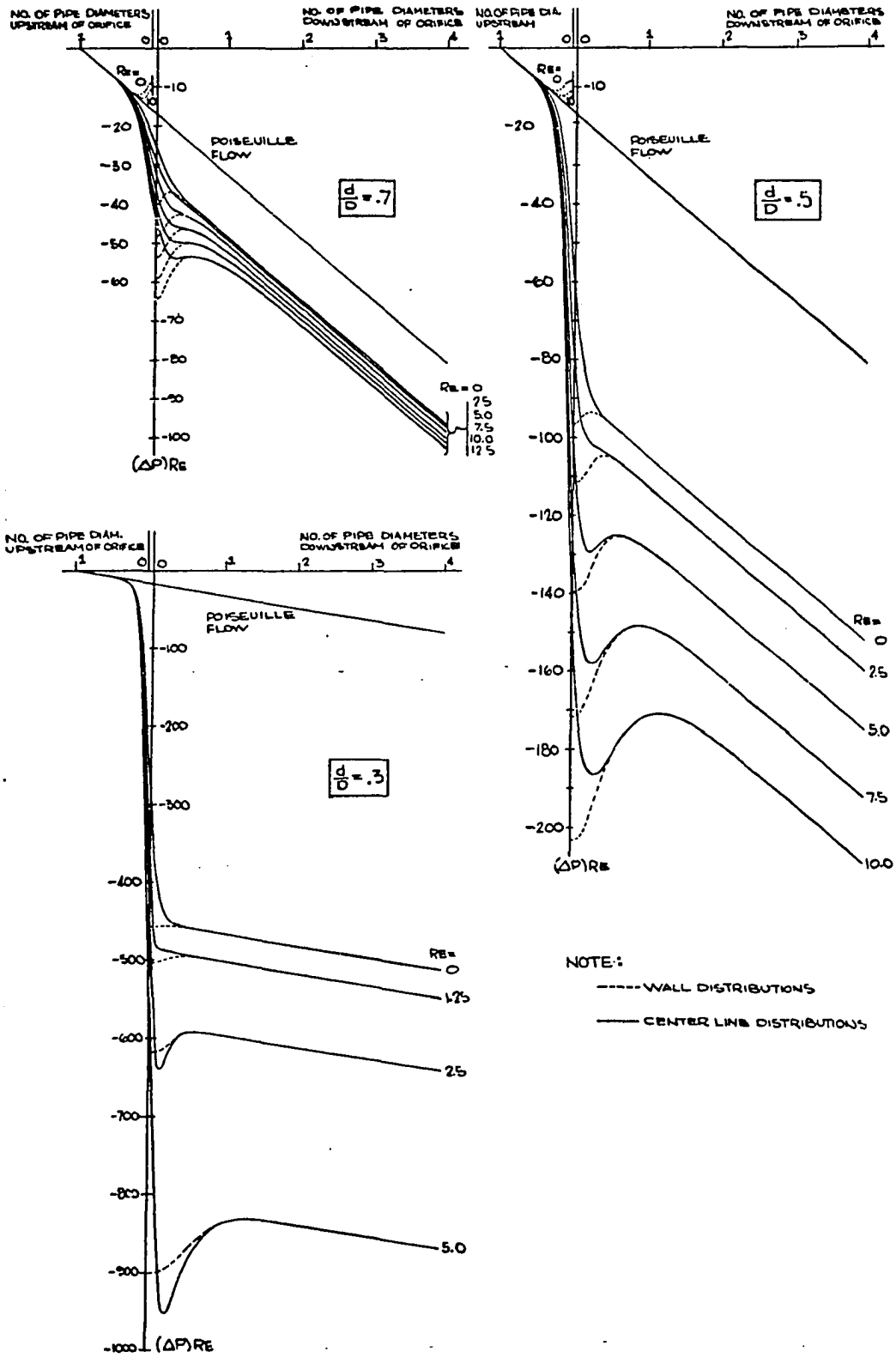

Figure 5-13

Axial Pressure Distributions, Square-Edged Plate, at Various Reynolds Numbers for d/D = .7, .5, .3

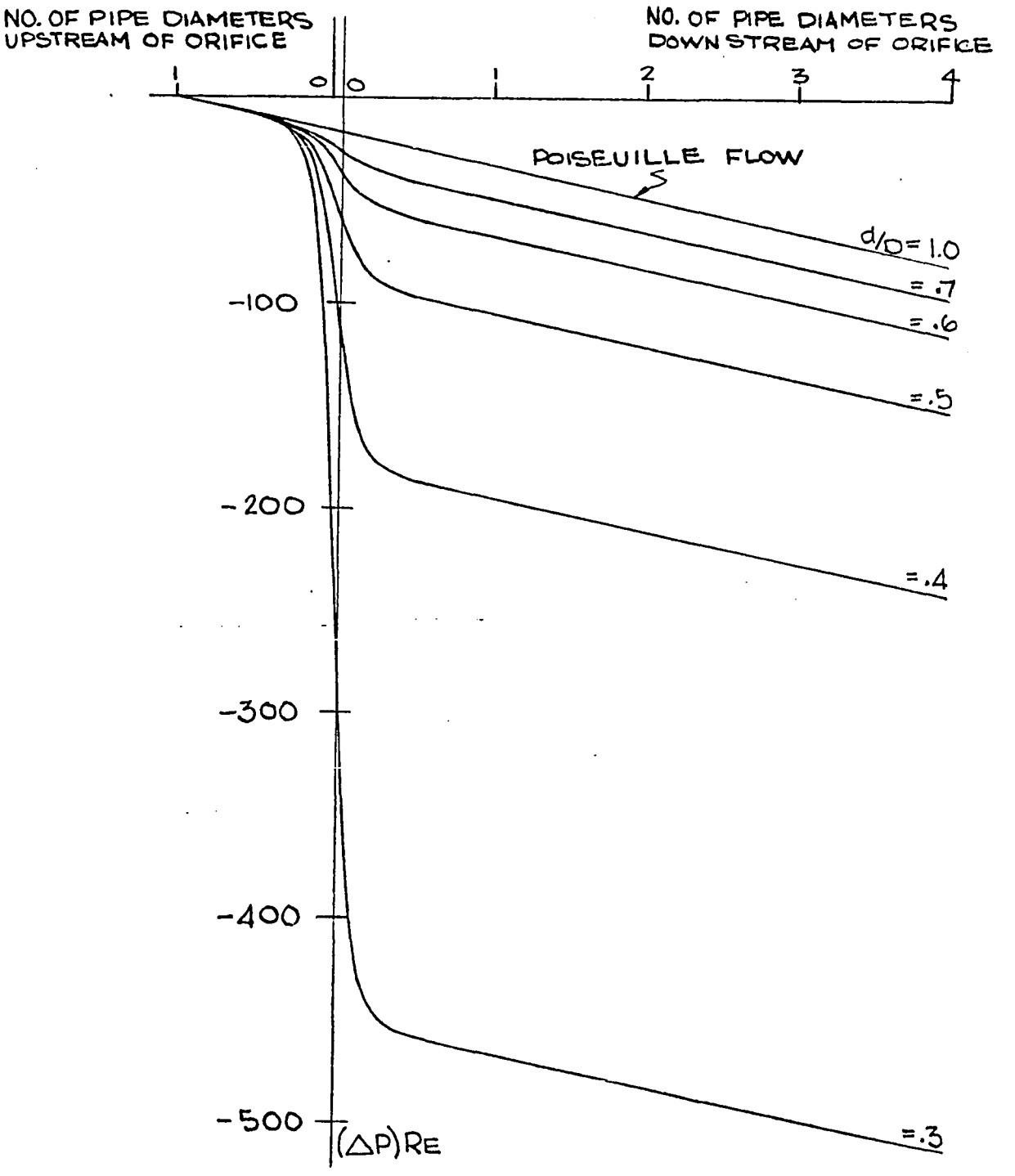

Figure (5-14)

Center Line Pressure Distributions for Square Edge Orifices with Various Diameter Ratios for Re = 0

side of the line which divides the plate in two and the other half is lost on the downstream side. As the Reynolds number is increased, a greater percentage of the drop occurs in the forward portion of the plate. The curve of pressure drop for Poiseuille flow is shown for reference. Notice that after passing through the orifice section, the pressure differences between wall and centerline disappear and the resulting distribution correctly parallels the Poiseuille curve. Another interesting feature of the figure is that for all Reynolds numbers investigated there is little difference between the wall and centerline pressure distributions on the front side of the orifice. In fact, it may be seen that the difference becomes smaller as the Reynolds number is made larger. On the other hand, there is considerable difference in the distributions on the downstream side of the orifice. Except for two of the cases (Re = 2.5 and 5.0 at d/D = .3), both the maximum and the minimum pressure drop occur on the pipe wall. At present, it is not clear whether or not the other orifice diameter ratios will also allow the centerline distributions to exceed that of the pipe wall for higher values of Reynolds number.

Figure (5-15) gives plots of the pipe wall vorticity and its variation with Reynolds number for the three orifice diameter ratios considered throughout this section. Since the wall vorticity equals the negative of the wall shear stress times the Reynolds number, equation (3-33), these curves may be regarded as plots of the pipe wall shear stress and for that matter, the local value of the friction coefficient. As can be seen, the major changes of the shearing stress on the pipe wall take place downstream of the orifice within the recirculation wake

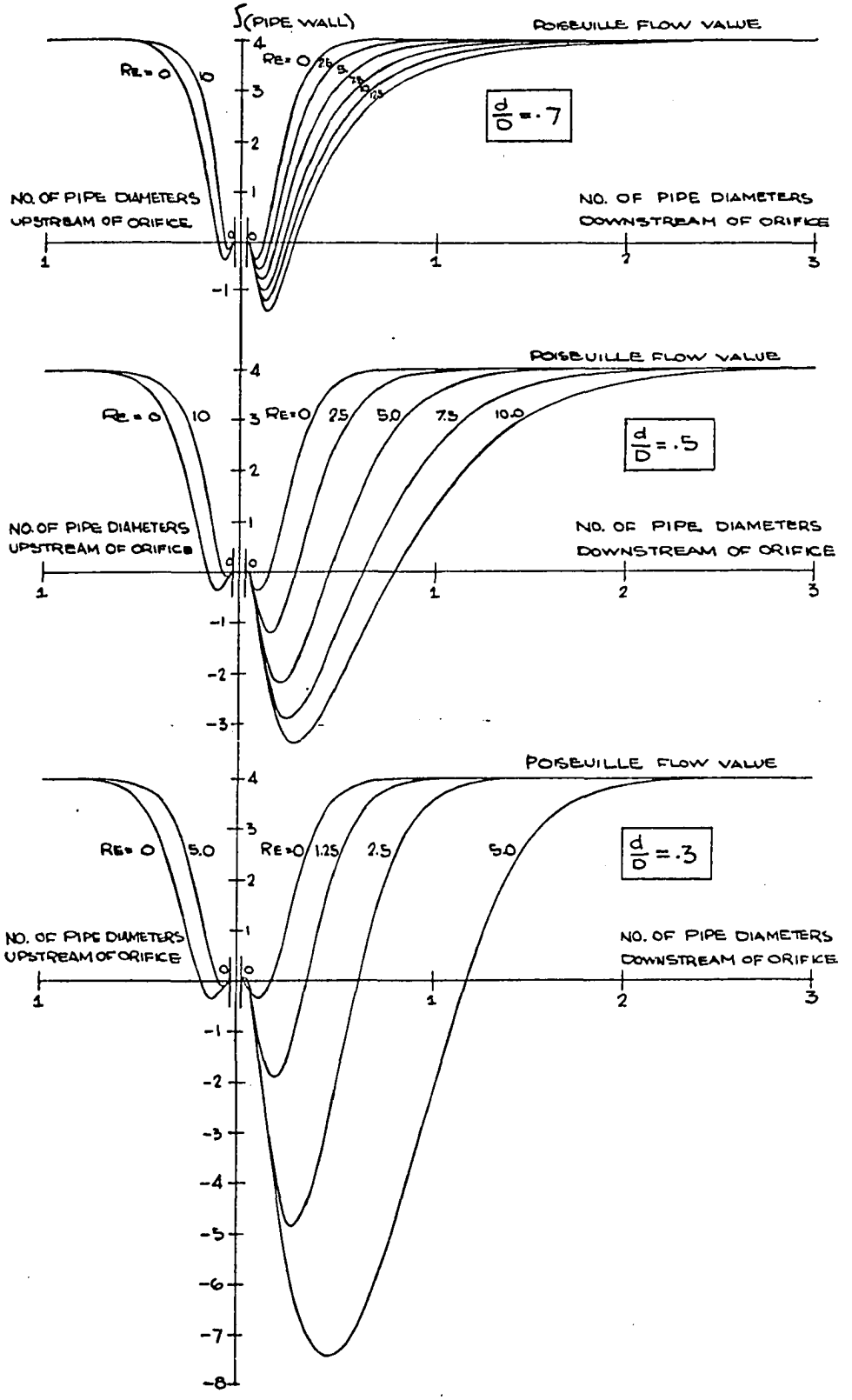

Figure 5-15

Distribution of Vorticity on Pipe Wall for Various Reynolds Numbers, d/D = .7, .5, .3

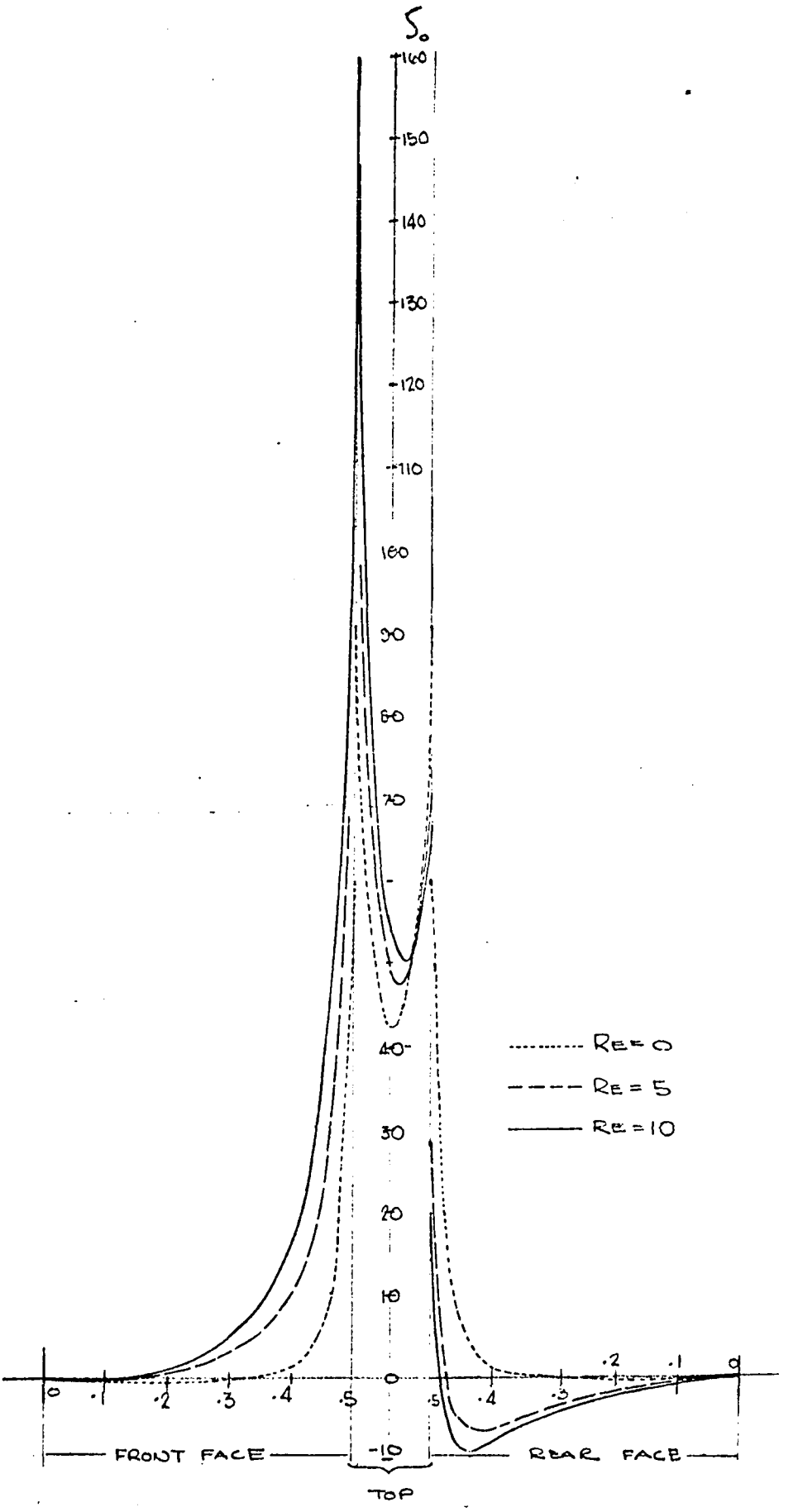

Figure 5-16

Distribution of Vorticity on Surface of Orifice Plate, Square-Edged, d/D = .5

region. The largest values of shear occur on the orifice plate. This is shown in Figure (5-16) which presents the vorticity on the faces of the orifice plate for an orifice to pipe diameter ratio of .5 at various Reynolds numbers. The values of the vorticity at the sharp edges, Figure (5-17), are presented in Table 5-1. It is apparent that as the Reynolds number is increased the downstream corner vorticity, ζ_4, is decreased until eventually $\zeta_4 \leq 0$, wherein separation will occur. Note also that the upstream corner vorticities, ζ_1 and ζ_2, are approaching each other with increasing Reynolds number and appear to be tending towards some asympotic value.

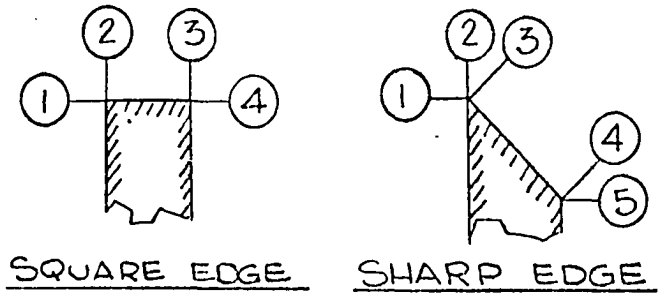

Figure (5-17)

Numbering of Corner Vorticities

CORNER VORTICITY						
d/D	Re	ζ_1	ζ_2	ζ_3	ζ_4	ζ_5
.7	0	23.338	36.692	36.698	23.346	-
.7	2.5	29.242	42.088	33.145	18.525	-
.7	5.0	34.495	47.213	31.741	15.742	-
.7	7.5	39.086	51.660	31.185	14.000	-
.7	10.0	43.184	55.537	30.942	12.757	-
.7	12.5	46.922	58.967	30.766	11.739	-
.6	0	36.700	55.960	55.955	36.691	-
.5	0	59.927	90.482	90.482	59.927	-
.5	0.1	60.978	91.322	89.675	58.891	-
.5	2.5	86.509	112.578	75.666	38.121	-
.5	5.0	108.906	131.320	70.800	28.437	-
.5	7.5	128.199	146.608	68.666	23.321	-
.5	10.0	145.411	159.459	67.173	19.777	-
.4	0	106.003	161.391	161.391	106.004	-
.3	0	216.603	339.398	339.398	216.604	-
.3	.05	220.168	342.089	336.736	213.055	-
.3	.10	223.746	344.801	334.094	209.493	-
.3	.25	234.454	353.021	326.354	198.877	-
.3	.50	252.091	366.835	314.262	181.683	-
.3	1.25	302.108	406.821	286.229	138.166	-
.3	2.50	375.350	464.130	263.871	98.928	-
.3	5.00	496.149	550.435	248.666	68.425	-
			SHARP-EDGED			
.5	0	68.906	147.719	78.904	16.997	14.794
.5	2.5	95.188	162.513	75.447	6.166	3.871
.5	5.0	118.839	179.605	76.383	-0.043	-2.491
.5	7.5	139.442	194.251	77.574	-3.593	-6.013
.5	10.0	157.791	206.470	78.344	-6.045	-8.357

Table (5-1)

Values of Corner Vorticity

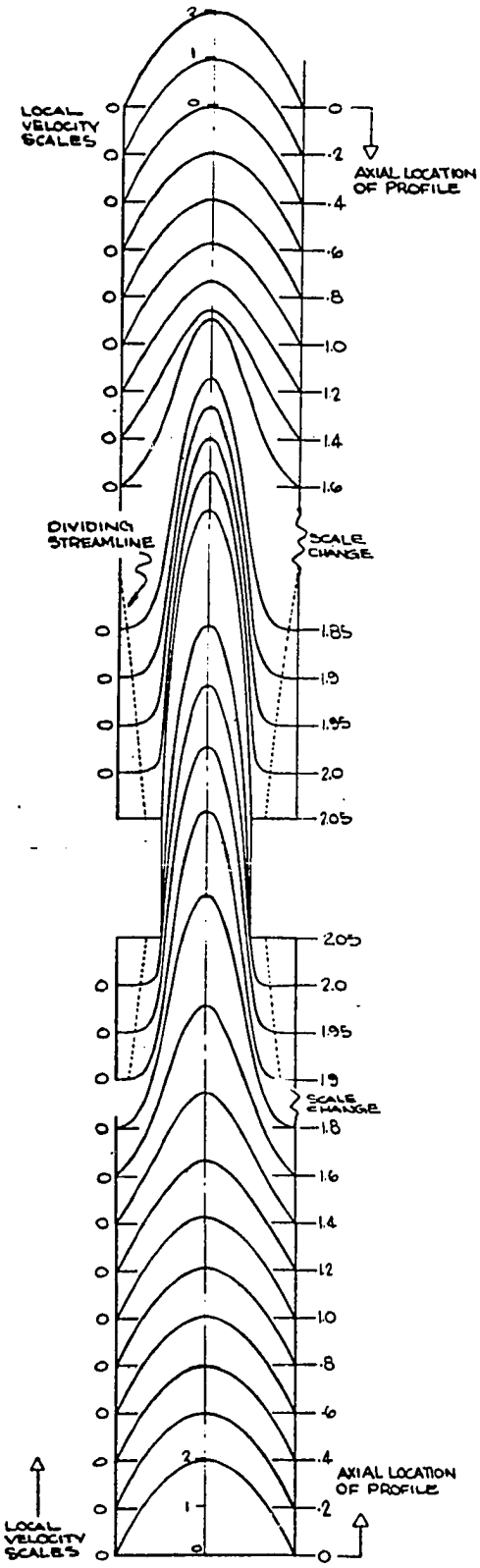

Figure 5-18

Development of the Axial Velocity Component in Creeping Flow for a Square-Edged Orifice, d/D = .5

The velocity distributions are probably the most difficult quantities to represent graphically because they range over a rather widespread of values. The radial distributions are especially cumbersome to handle. Figure (5-18), which shows the axial velocity component development for a diameter ratio of .5 at Re = 0, bears out this claim. In as much, the description of the velocity distributions will be held to a minimum herein. Figure (5-19) shows how the axial velocity component along the centerline varies with Reynolds number. As may be seen, the peak nondimensionalized velocity decreases and its position moves downstream as the Reynolds number is increased. The lowering of the maximum velocity verifies the fact that the velocity profile at the orifice mid-plane becomes blunter with increasing Reynolds number. One further point worth noting, it was found that the maximum velocity usually, but not always, lay on the centerline. As the Reynolds number was elevated, the point of maximum velocity in the vicinity of the orifice plate shifted to a radial location about one grid point below the centerline. Lee and Fung have also shown this in their study and at present it is not known whether this is of a numerical or fluid dynamic origin.

Sharp-Edged Orifice Results

In this section results of flow through an orifice plate with a top surface beveled to cause a flow area increase in the direction of the flow are discussed. This configuration was chosen for two reasons. First, it demonstrates the utility of the graded mesh scheme in handling a problem with a boundary which requires a locally fine mesh without the

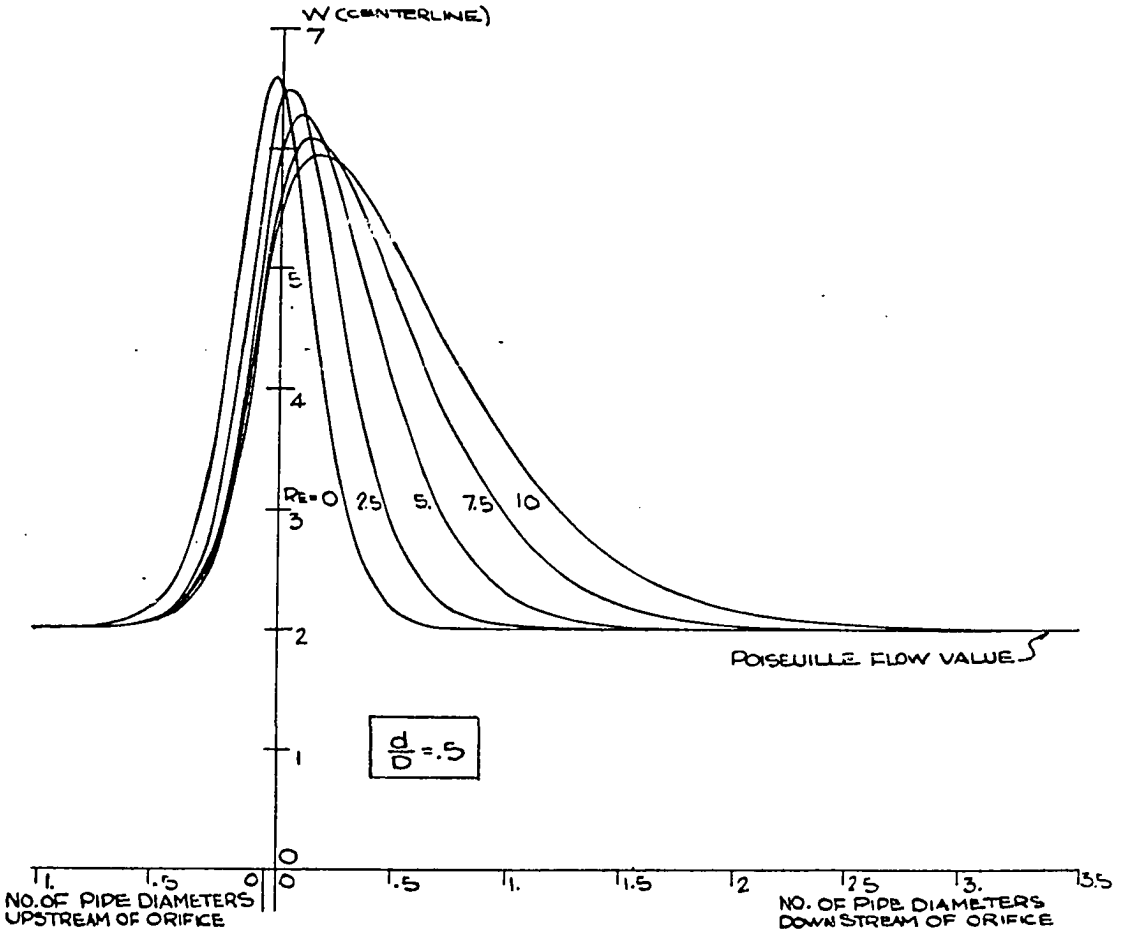

Figure 5-19

Centerline Axial Velocity Component vs Reynolds Number, Square-Edged Plate, d/D = .5

necessity of resorting to a specification of a small grid size over the entire field. Secondly, the shape gives a closer representation of the orifice plate used in a widely referenced experimental work against which the numerical results obtained herein will be compared.

Only one configuration was studied. The diameter at the narrowest section was one half of that of the pipe. The slanted face was angled at 45° clockwise from the horizontal. The thickness was again taken as one sixteenth of the pipe diameter. Thus the largest diameter of the orifice section was 5/8 of D. A further reason for selecting a 45 degree bevel was so that the radial and axial grid lines would cross at the orifice surface, i.e., so that node points would be located on the slanting surface of the orifice plate. This occurred because the mesh was uniform in the vicinity of the orifice surface. For other angles, it may be possible to adjust the grid structure near the orifice so that node points would still appear on the solid surface. This could be done by creating a rectangular net near the orifice. If such a procedure is not followed, special techniques to handle the irregular lengths between nodes would have to be worked out.

Results similar to those shown in the previous section for the square-edged orifice are shown in the following figures.

Figure (5-20) shows the streamline pattern and the vorticity contours for three Reynolds numbers. Because of the asymmetry of the orifice plate, the vanishing Reynolds number solution is not symmetric about the orifice plate midplane. Also note that in the creeping flow plot that the wake on the downstream side of the orifice is smaller than that on the upstream side. As the Reynolds number is increased however, the

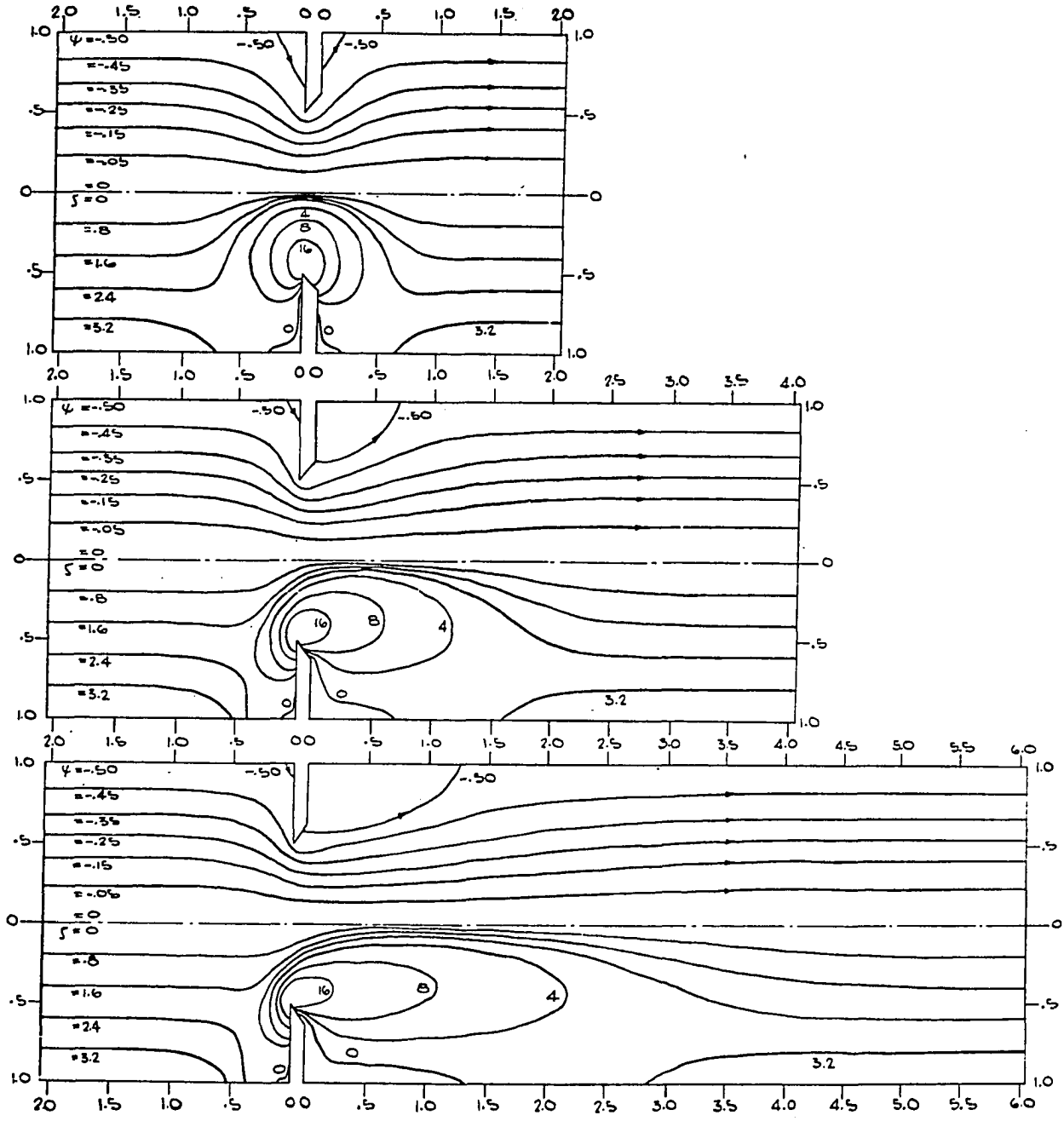

Figure 5-20

Streamlines and Vorticity Contours for d/D = .5,
Re = 0, 5, 10 for a Sharp-Edged Orifice

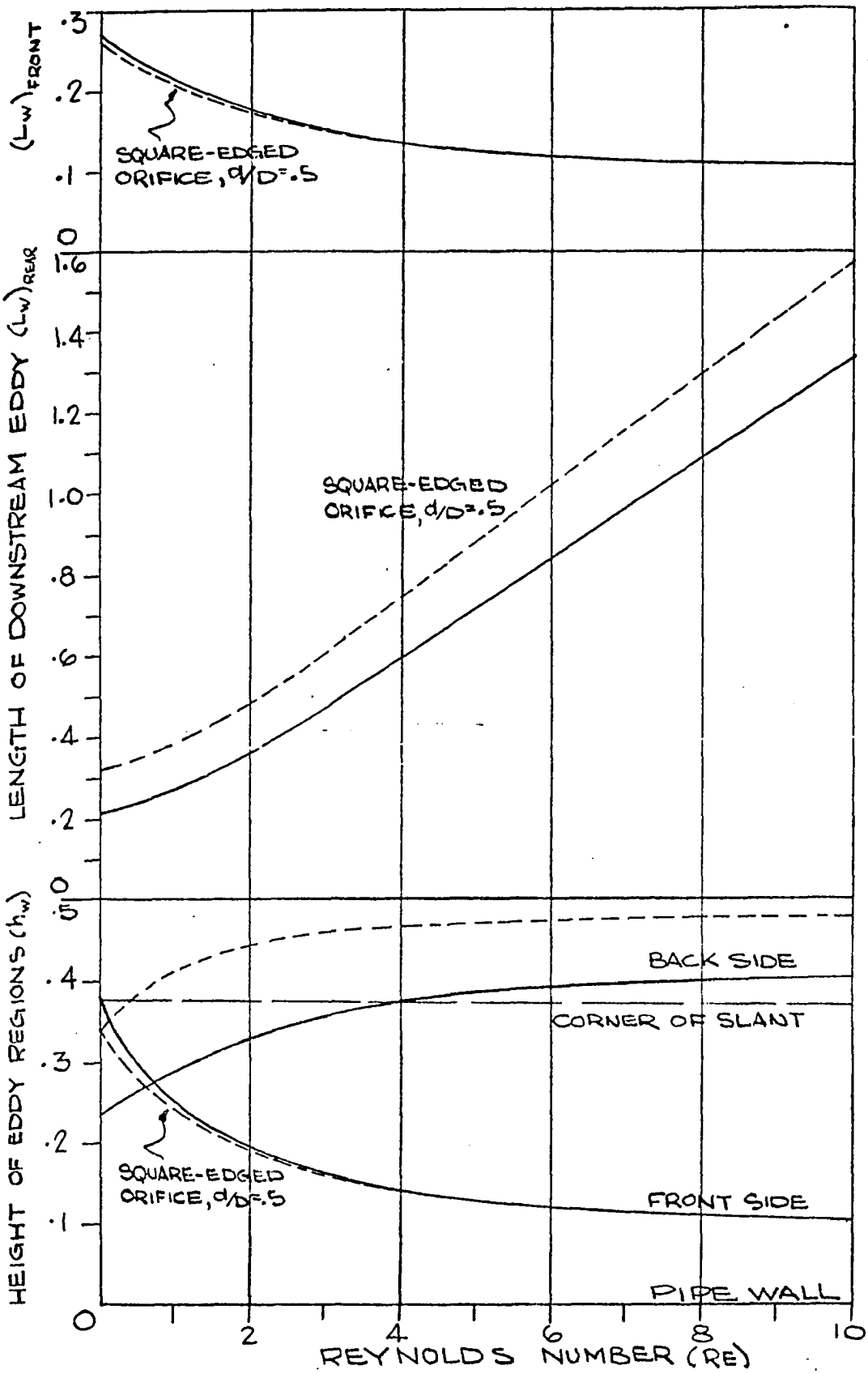

Figure 5-21

Radial and Axial Dimensions of Wake Region vs Reynolds Number, Sharp-Edged Orifice Plate

size of the frontal eddy zone is diminished and that of the rear recirculatory region is enlarged. If the Reynolds number is made large enough, it is found that the rear dividing streamline will originate on the beveled surface. Figure (5-21) presents the radial and axial dimensions of the wake region as a function of the Reynolds number. The square-edged orifice results are also shown for comparison. From the figure, the creeping flow eddy region in front of the sharp-edged plate is found to be slightly larger than that found in front of the square-edged orifice, but as the Reynolds number increases, this difference disappears and the two eventually have the same size frontal eddy. Hence, for all but very small Reynolds numbers the size of the forward recirculation region is independent of edge geometry as well as orifice diameter ratio. On the other hand, the sharp-edged plate has a smaller wake region both radially and axially, than does its square edge counterpart. Note that after a Reynolds number of about 4, the rear wake begins to separate from the sloped orifice face.

Figure (5-22) shows the axial pressure drop on the wall and along the centerline as a function of Reynolds number. By comparing this figure with that of (5-13), it is found that the pressure drops for the sharp-edged plate are not as large as in the square-edged orifice plate situation. This is due to the diffuser like action that the diverging section offers to the flow.

Figure (5-24) shows how the pipe wall vorticity (or equivalently, the wall shear stress) varies with the Reynolds number. Figure (5-23) presents the distribution of the axial velocity component along the centerline as a function of the Reynolds number. In both of these plots,

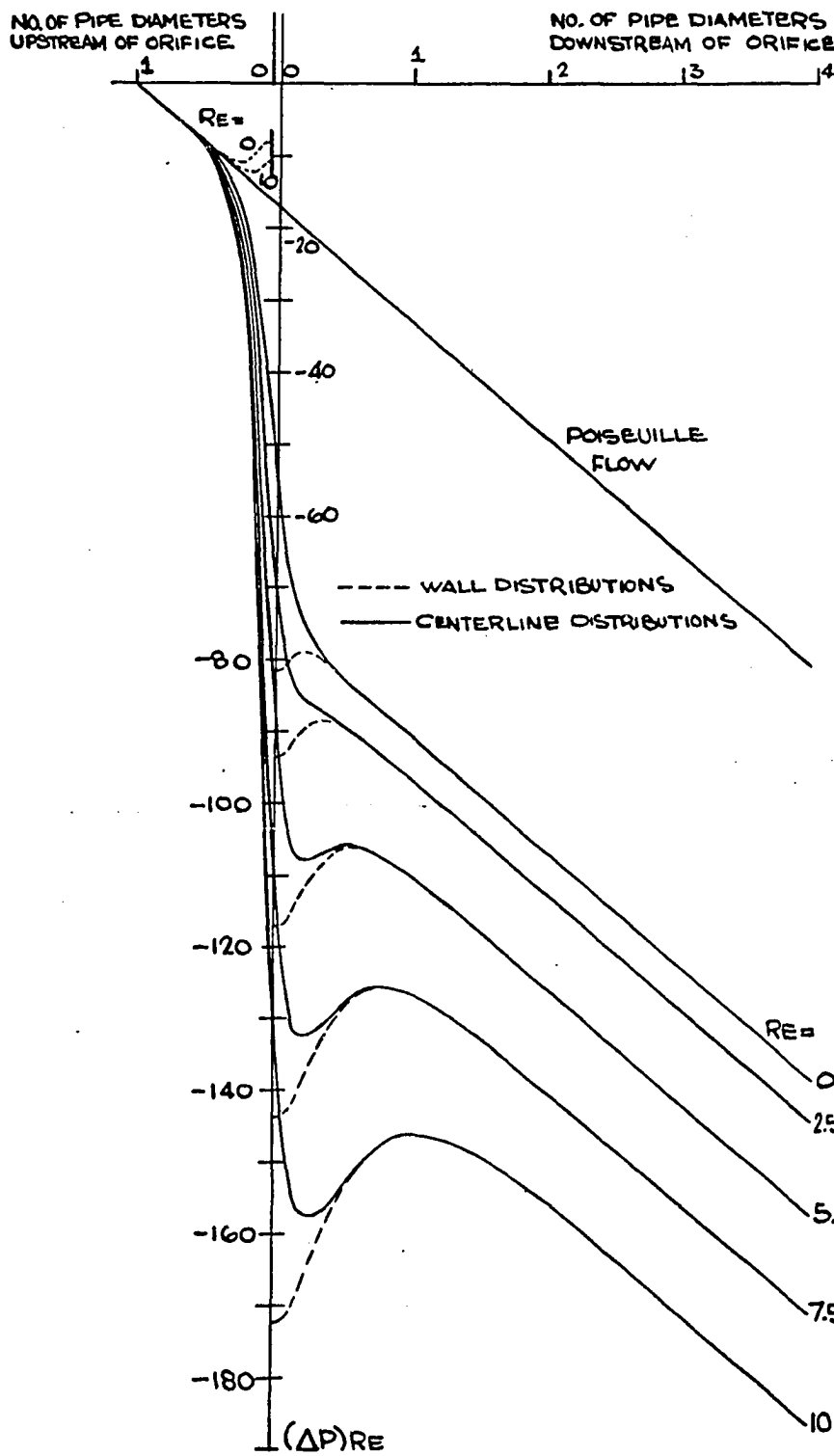

Figure 5-22

Axial Pressure Distribution, Sharp-Edged Orifice, d/D = .5

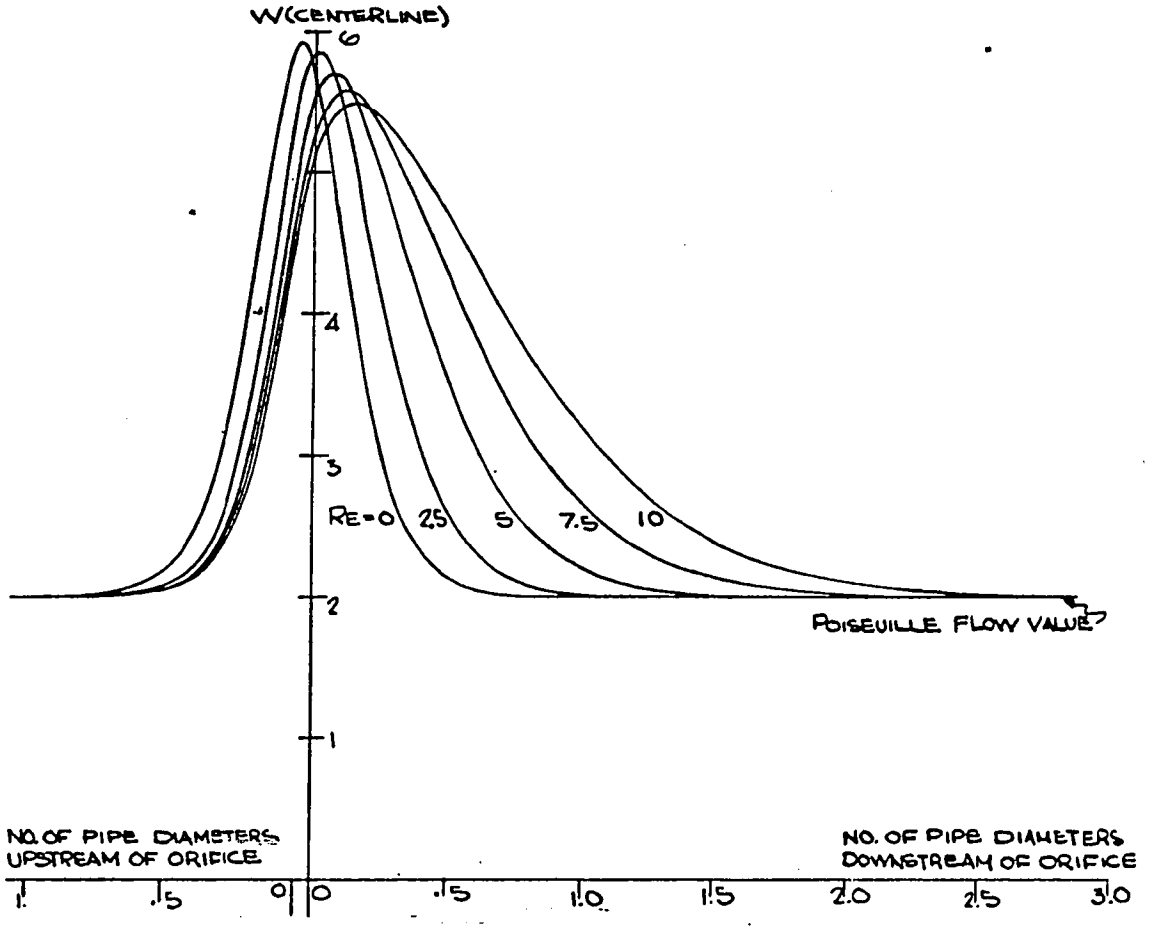

Figure 5-23

Centerline Axial Velocity Component vs Reynolds Number, Sharp-Edged Plate, d/D = .5

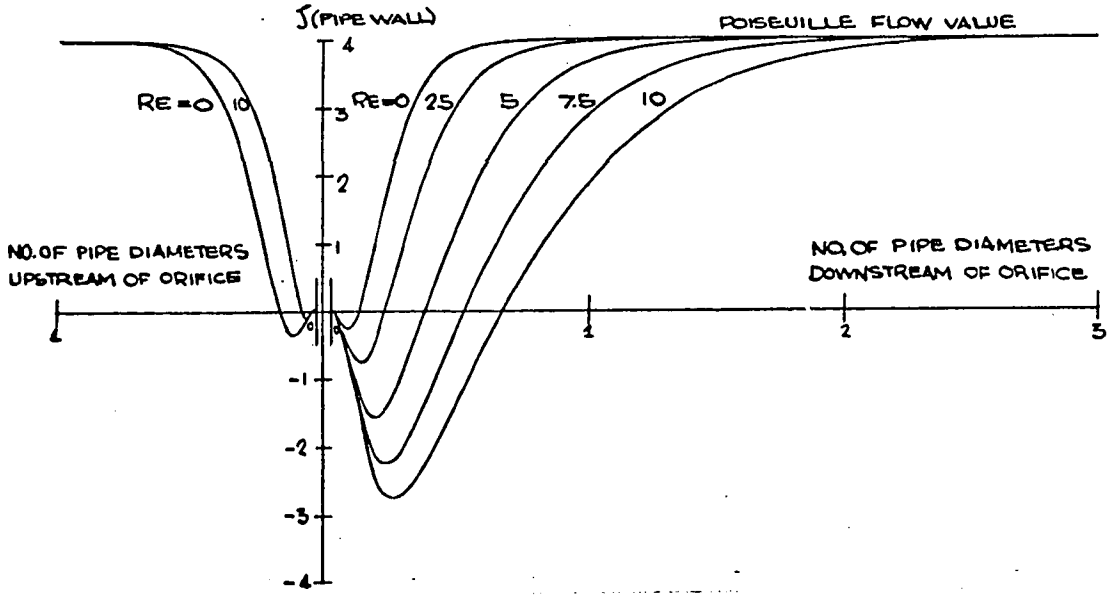

Figure 5-24

Distribution of Vorticity on Pipe Wall, Sharp-Edged Orifice Plate, d/D = .5

the magnitudes are less than the corresponding values found in the square-edged orifice case.

Comparison With Existing Experimental Results

In order to verify the results of any numerical study, comparisons to either analytical solutions or to experimental data must be made. Generally, there are no analytical solutions available and one must rely upon empirical results to confirm any predictions. Furthermore, unless experiments are performed first hand, it is unlikely that the numerical and physical situations will be exactly the same and in as much, some doubt often persists.

Earlier in this thesis, it was mentioned that there is not a great deal of experimental information available for low Reynolds number orifice flow. Of the existing material, the discharge coefficient is the most detailed, and it is this quantity to which the numerical results will be compared.

The flow rate through the orifice can be expressed as (39):

$$\dot{m}' = \rho (K A_t) \sqrt{2 \frac{\Delta P'}{\rho}} \qquad \text{.....[5-1]}$$

$$= \rho A_p \bar{W}_p$$

The flow coefficient K can be written as:

$$K = \frac{C_D}{\sqrt{1-\beta^4}} \qquad \text{.....[5-2]}$$

where: $\beta \equiv d/D$

Substituting equation (5-2) into (5-1) and nondimensionalizing gives:

$$C_D = \sqrt{\frac{1-\beta^4}{2\beta^4}}\ \frac{1}{\sqrt{\Delta P}} \qquad \text{.....[5-3]}$$

The pressure drop is taken across the orifice plate corners at the pipe wall by numerically integrating equations (3-30) and (3-31) along the path shown in Figure (5-25). Notice that the radial pressure drops

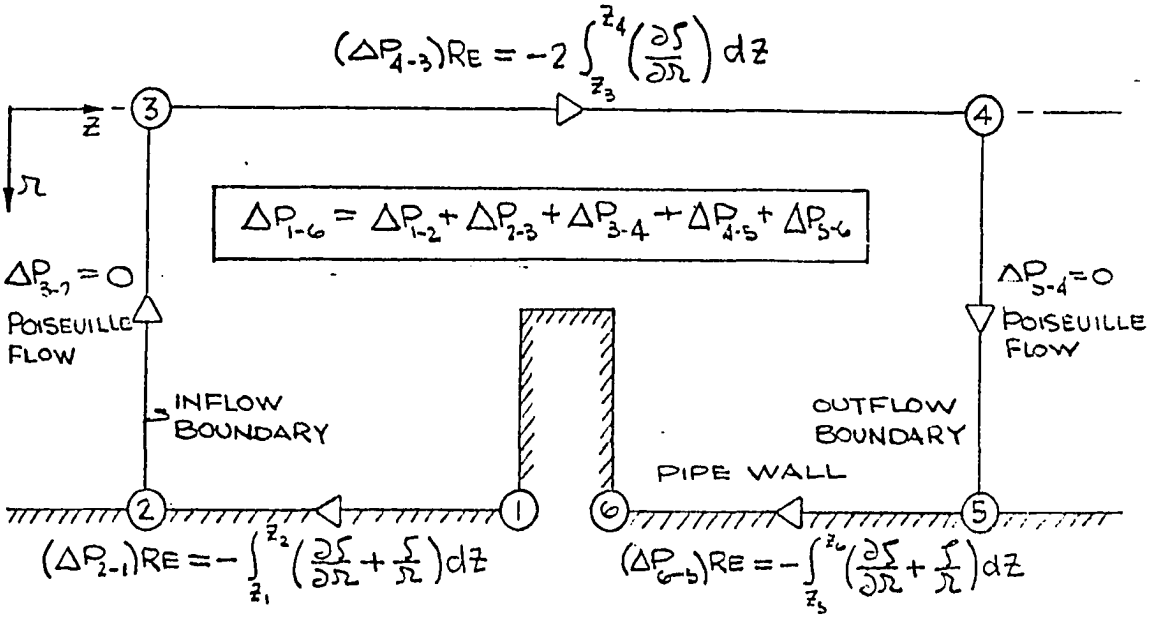

Figure (5-25)

Path of Orifice Pressure Drop Integration

$P_3 - P_2$ and $P_5 - P_4$ are both zero because they are evaluated at the inflow and outflow boundaries where a uniform pressure is assumed to exist across the tube. This method of integration was chosen because it simultaneously produced the centerline and wall axial pressure distributions which have already been presented in the two preceding sections. The pressure drop could also have been calculated by integrating along

other routes since the pressure changes between any two points in the field are independent of the path joining them. For example, the integration could have been performed around the outline of the orifice plate, however the vorticity gradients, which must be evaluated, are the largest in the vicinity of the orifice surface. In addition, the sharp corners of the plate present a serious computation problem, hence, this path would probably not yield a very accurate result.

The major experimental work was performed by Johansen (2) over 40 years ago. The experimental values of discharge coefficients were obtained from Johansen's curves. These results, along with the values obtained by Mills in (1) and the results of the present investigation are given in Table 5-2. All of these coefficients are shown plotted in Figure (5-26).

As can be seen, the values predicted here agree favorably with the experimental results of Johansen (the two generally are within 5% of each other). The square-edged results typically under estimate C_D while the sharp-edged plate results are higher than the experimental values. Agreement is better with increasing orifice to pipe diameter ratio.

In addition to the discharge coefficient experiments, Johansen conducted some flow visualization studies. His description of the flow is in disagreement with that given above. For $Re_d \leq 10$, he found the flow to be symmetrical about the orifice mid plane and "for this almost perfectly steady condition fluid from near the walls of the pipe is deflected at right angles and adheres closely to the diaphragm on both sides of the orifice". In fact, Johansen first found a separation region at an Re_d of 30 with a length of about 1/2 pipe diameter. At an

PREDICTED C_D VALUES:

Re_d	d/D =.3	Re_d	d/D = .5 (Mills)	Square	Sharp	Re_d	d/D =.7
0	0	0	0	0	0	0	0
0.33	.082	5	.342	-	-	7.14	.348
0.67	.116	10	.462	.429	.476	14.29	.461
1.67	.184	20	.581	.528	.578	21.43	.527
3.33	.258	30	-	.593	.651	28.57	.576
8.33	.394	40	-	.622	.683	35.71	.609
16.67	.526	50	.690	-	-		
33.33	.588						

EXPERIMENTAL C_D VALUES:

(Johansen)

Re_d	d/D = .209	.401	.595	.794
0	0	0	0	0
1	.18	.15	.13	.12
4	.32	.30	.27	.25
9	.45	.43	.42	.37
16	.53	.53	.51	.46
25	.58	.58	.60	.55
36	.63	.62	.65	.61
49	.65	.65	.70	.67
64	.66	.67	.72	.69
81	.67	.68	.73	.73
100	.68	.70	.74	.76

Table (5-2)

Orifice Discharge Coefficients

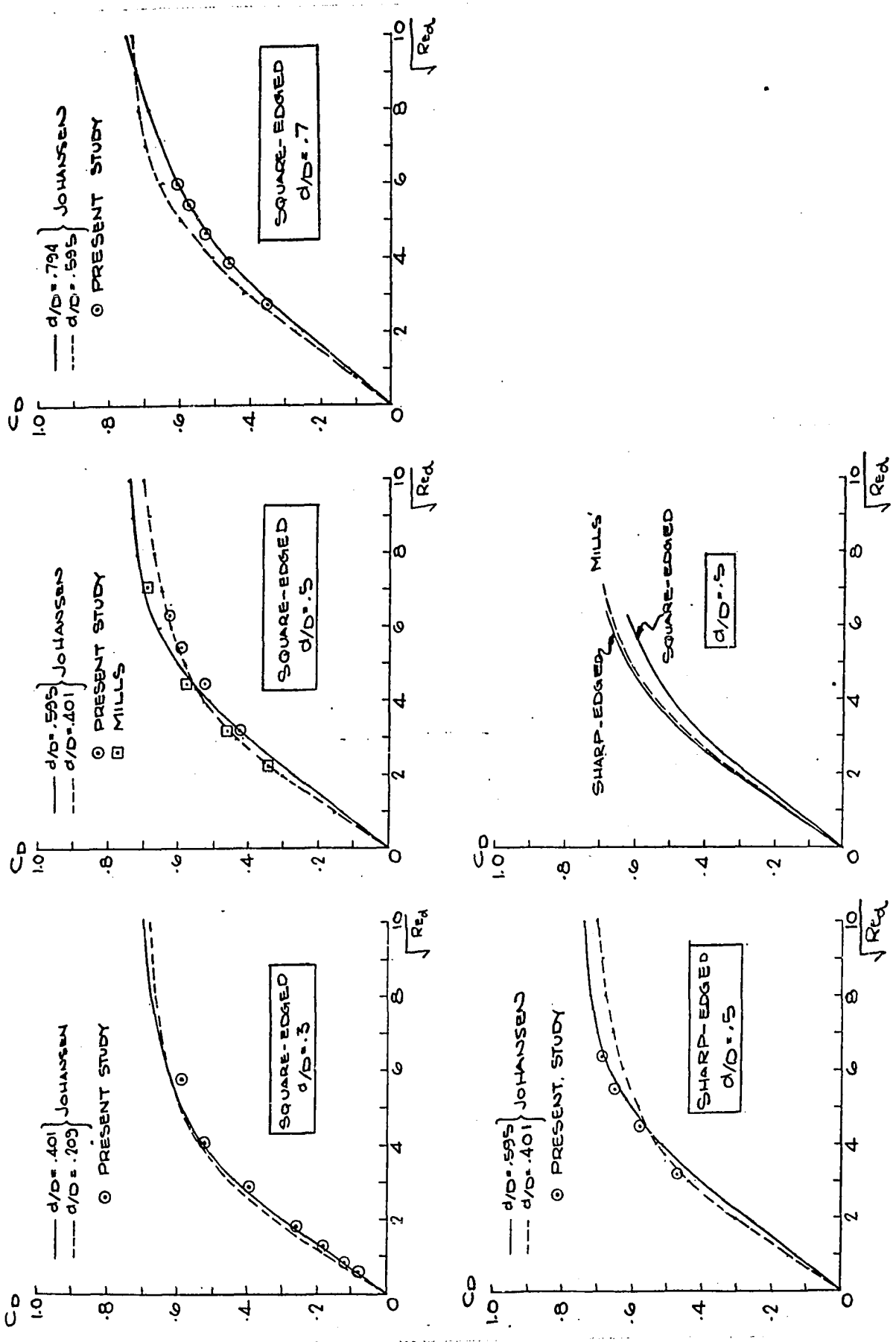

Figure 5-26

Discharge Coefficients

Re_d of 100, the length was found to be between one and two pipe diameters. No forward based eddy was observed. The difficulty with these visualization studies is that they were carried out using water as a test fluid. It is easy to see however that this fluid, with its rather low coefficient of viscosity, allows only a very small average pipe velocity for realistic pipe diameters and in as much the flow can be altered by even minute disturbances and can also be influenced by unavoidable convection currents which have comparable velocities.

Comparisons With an Existing Numerical Study

Throughout this thesis, reference has been made to Mills since his study was a forerunner of the present study. Not all of the results obtained above agree completely with Mills' numerical data and therefore it is useful to discuss some of these differences in order to identify some possible explanations for the discrepancies.

In an earlier section, dealing with the boundary conditions, it was mentioned that, except at very small Re, longer downstream field lengths were used in the current study compared to those of Mills. Later plots, which compared the predicted wake lengths, indicated that, except at low values of Re, shorter eddy zones were estimated by Mills than those predicted in the current investigation. If a fore-shortened flow field had been used by Mills at the higher Reynolds numbers, it is likely that interior flow results would be similarly contracted. This could therefore account (at least partially) for the differences in wake length prediction. Of course there is no guarantee, short of repeating the calculations, that an abbreviated flow field could fully

account for the disagreement, for it is known that the recirculation region will also be somewhat smaller if the vorticity production at the solid surfaces is conservatively estimated.

The pressure predictions of Mills as expressed through the orifice discharge coefficient, were found to be higher than the numerical values contained herein. Yet, it should be noted that Mills' results are rather close to the experimental data of Johansen, although slightly higher. Mills expressed some surprise over the agreement in light of the fact that his orifice plate was of a different thickness, a different edge geometry and had different pressure tappings. With regard to the orifice thickness, Figure (5-27) is presented. It shows the values of the thicknesses used in Johansen (1/12d), in Mills (1/16R) and in the present study (1/8R). It should also be mentioned that Mills' orifice plate had a square edge whereas the orifice plate used in Johansen's investigation was beveled at 45°. Because of the good agreement between predicted values and experimental results, Mills concluded that orifice geometry was a secondary factor compared with the Reynolds number in the determination of C_D. This conclusion was clearly not substantiated in the current study as it may be recalled that a sharp-edged discharge coefficient was higher than a square-edged value for a given Re and therefore the edge geometry did have an influence upon this coefficient. Since the sharp-edged orifice can accommodate the flow better than the square-edged orifice plate, it is understandable that the pressure drop should be less and in as much should produce a somewhat higher value of C_D than the square-edged orifice. The fact that Mills' values were higher than the experimental values does not appear to be correct.

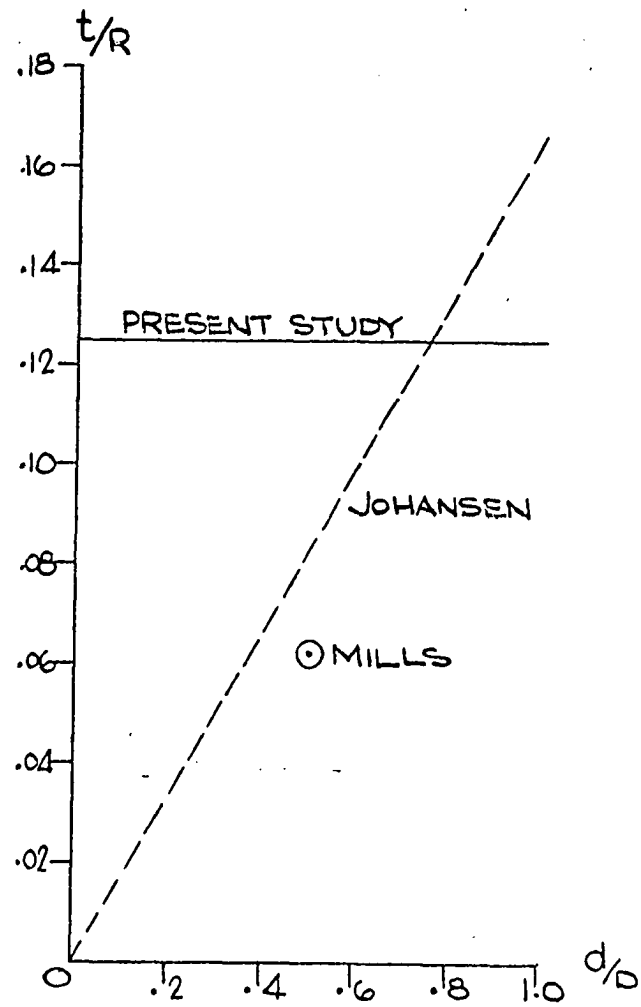

Figure (5-27)

Orifice Thicknesses Used in Various Investigations

With respect to the numerical technique, the procedure is essentially the same for both of the studies, however the use of five point operators, use of a finer flow net near the troublesome intruding corners and use of double place accuracy would indicate a greater precision was possible in the current investigation. This was proven in the elementary Poiseuille computational test.

CHAPTER VI

CONCLUSION

In this study, a considerable amount of knowledge concerning the steady laminar flow of an incompressible fluid through a circular pipe orifice plate has been obtained from the numerical solutions of the axisymmetric form of the Navier-Stokes equations. The solutions have provided information about the flow patterns, the pressure drop, the velocity and vorticity distributions, the discharge coefficient and the wall shear stress for various orifice sizes and for two plate edges: one square and the other sharp.

In the investigation involving the square-edged plate, the streamline patterns and the vorticity contours were found to change from the perfectly symmetric profile of creeping flow to an asymmetric shape as the Reynolds number of the stream was increased. Two recirculation regions were identified within the flow field: one on the forward side of the orifice plate and one on the rear. As the Reynolds number of the flow was increased, the size of the frontal eddy region was found to diminish. Moreover, it was discovered that the reduction produced a limiting forward eddy size which was independent of the orifice to pipe diameter ratio. On the other hand, the rear recirculation region was found to grow, especially in the axial direction, with increasing Reynolds number. Separation occurred below the intruding corner on the downstream face of the orifice plate for all Reynolds numbers considered. Analysis of the creeping flow results revealed that the distance from the pipe wall to the point of separation on the rear orifice face

varied inversely with orifice to pipe diameter ratio. The length of the separation region (measured from the back face of the orifice plate to the point of reattachment on the pipe wall) was found to vary linearly with Reynolds number for sufficiently high values of the latter parameter, e.g., with a d/D of .5, the point of linearity occurred at Re of about 3. The eddy center of the rear recirculation region was found to move downstream with increasing Reynolds number. However, the center location appeared to approach a radial asymptotic value. The pressure drop along the centerline was found to be greater on the upstream face of the orifice than on the downstream side, but the difference between the two was seen to vanish as the Reynolds number was decreased. The adverse pressure gradient upstream of the orifice plate was found to diminish as the Reynolds number increased. In the vicinity of the orifice plate, velocity profiles became blunter as the Reynolds number was advanced. The maximum value of velocity was not always found on the centerline. The point of maximum vorticity occurred at the forward corner of the square-edged plate. Larger Reynolds number flow produced greater amounts of vorticity in the forward portion of the flow field. The increased vorticity was swept downstream producing vorticity contours that were elongated in the direction of the flow. Predicted values of orifice discharge coefficient agree favorably with experimental values of Johansen. The numerical values are approximately 5% lower than the experimental data. Agreement is better for larger values of orifice to pipe diameter ratio.

Results similar to those of the square-edge plate were found for an orifice with an edge beveled at 45° in the downstream direction.

Again, two eddy regions were detected. Unlike the creeping flow recirculation regions of the square-edged plate, which produced two eddy zones of equal size, the sharp-edged plate created a smaller separation region on the downstream side of the plate than on the upstream side. However, as the Reynolds number was increased, the front eddy size was reduced while the rear eddy grew. At a sufficiently high Reynolds number, the rear eddy size is larger than that of the front. The rear separation point was found to occur on the vertical portion of the downstream facing side of the plate, but as the Reynolds number was elevated, the point of separation moved up this vertical face and eventually separation occurred on the slanted portion of the plate. For all Reynolds numbers investigated, the size of the rear recirculation region for the sharp-edged plate was smaller than that of the square-edged orifice. The results revealed that there is a limiting size of the frontal eddy region and this size was found to be the same as that obtained for the square edged plate. Therefore, it was concluded that the size is independent of the orifice geometry. The centerline pressure drop was found to be less than that of the corresponding square-edged plate. Moreover, the wall vorticity and axial velocity component values are both found to be smaller than those of the corresponding square-edged orifice. Predicted values of the orifice discharge coefficient were found to be slightly larger than the experimental values of Johansen. The slight discrepancy was attributed to the differences (mainly the plate thickness) in the orifice geometry.

Clearly, the results obtained are only as reliable as the numer-

ical methods used to obtain them will permit. In as much, a considerable amount of care has been exercised in employing numerical techniques. Truncation error, due to the finite difference approximations, was kept small by using five point differences instead of the more conventional three point form. Round off error, was kept small by requiring that all arithmetic was carried out in double precision. For the UNIVAC 1108 computer, this meant that 18 decimal places of accuracy were specified. To give the orifice plate boundaries better definition and to produce greater flow field resolution in the high gradient area occurring at the intruding sharp corners of the orifice plate, the grid network was structured. The structuring of the net was performed in such a way as to partition sections of the flow field into areas of either uniform or rectangular grids. Some of these areas contained a fine mesh while others had a more coarse subdivision. Difference operators capable of passing from one partitioned area to another were used. Realistic solution times of approximately 15 minutes were obtained. In order to extend the maximum value of Reynolds number capable of producing a stable solution, under-relaxation was used. The smaller the relaxation factor, the larger the computer time required to produce converged results. Trial and error methods were used to obtain the under-relaxation values.

APPENDIX A

5-POINT FINITE DIFFERENCE OPERATORS

From known values of a function $f(x,y)$ at 5 points (not necessarily evenly spaced) along a line y = constant, the derivatives $\partial f/\partial x$ and $\partial^2 f/\partial x^2$ are to be numerically evaluated. The evaluation takes place at a nodal site which can lie one point ahead of the middle data point producing backward differences, at the middle point producing central differences, or at one grid point to the rear of the middle point producing forward differences.

FIRST DERIVATIVES

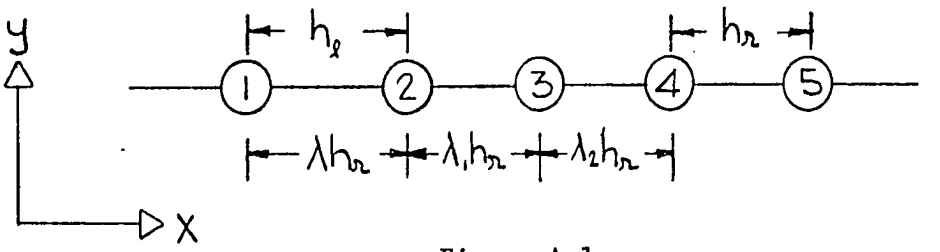

Figure A-1

Grid Nomenclature

Backward differences: Writing a Taylor series expansion about the point 4 of Figure A-1 and truncating the series at the $(\partial^5 f/\partial x^5)$ term, yields the following:

$$f_5 = f_4 + \sum_{i=1}^{4} \frac{(h_r)^i}{i!}\left(\frac{\partial^i f}{\partial x^i}\right)_4 \qquad \text{.....[A-1]}$$

$$f_3 = f_4 + \sum_{i=1}^{4} (-1)^i \frac{(\lambda_2 h_r)^i}{i!}\left(\frac{\partial^i f}{\partial x^i}\right)_4 \qquad \text{.....[A-2]}$$

$$f_2 = f_4 + \sum_{i=1}^{4} (-1)^i \frac{[(\lambda_1+\lambda_2) h_r]^i}{i!}\left(\frac{\partial^i f}{\partial x^i}\right)_4 \qquad \text{.....[A-3]}$$

$$f_1 = f_4 + \sum_{i=1}^{4} (-1)^i \frac{[(\lambda+\lambda_1+\lambda_2) h_r]^i}{i!}\left(\frac{\partial^i f}{\partial x^i}\right)_4 \qquad \text{.....[A-4]}$$

Solving for $(\partial f/\partial x)_4$ gives:

$$\left(\frac{\partial f}{\partial x}\right)_4 = \frac{-A_1(f_5-f_4)+A_2(f_3-f_4)-A_3(f_2-f_4)+A_4(f_1-f_4)}{D\, h_r} \qquad \text{.....[A-5]}$$

where:

$$A_1 = \lambda\lambda_1\lambda_2(\lambda+\lambda_1)(\lambda_1+\lambda_2)(\lambda+\lambda_1+\lambda_2)$$

$$A_2 = \lambda(1+\lambda+\lambda_1+\lambda_2)(1+\lambda_1+\lambda_2)(\lambda_1+\lambda_2)(\lambda+\lambda_1+\lambda_2)/\lambda_2$$

$$A_3 = \lambda_2(1+\lambda+\lambda_1+\lambda_2)(1+\lambda_2)(\lambda+\lambda_1+\lambda_2)(\lambda+\lambda_1)/(\lambda_1+\lambda_2)$$

$$A_4 = \lambda_1\lambda_2(1+\lambda_1+\lambda_2)(1+\lambda_2)(\lambda_1+\lambda_2)/(\lambda+\lambda_1+\lambda_2)$$

$$D = -A_1 - A_2\lambda_2 + A_3(\lambda_1+\lambda_2) - A_4(\lambda+\lambda_1+\lambda_2)$$

Four distributions are possible: 3 h_ℓ (intervals) + 1 h_r, 2 h_ℓ + 2 h_r h_ℓ + 3 h_r, and 4 h_r. Consideration of these four distributions result in the following difference equations:

<u>3 h_ℓ + h_r ($\lambda_1 = \lambda_2 = \lambda$)</u>

$$\left(\frac{\partial f}{\partial x}\right)_4 = \frac{-12\lambda^4(f_5-f_4)+6(1+2\lambda)(1+3\lambda)(f_3-f_4)-3(1+\lambda)(1+3\lambda)(f_2-f_4)+\frac{2}{3}(1+\lambda)(1+2\lambda)(f_1-f_4)}{\left[-12\lambda^4-6(1+2\lambda)(1+3\lambda)\lambda+6(1+\lambda)(1+3\lambda)\lambda-2(1+\lambda)(1+2\lambda)\lambda\right] h_r} \qquad \text{.....[A-6]}$$

$2\,h_\ell + 2\,h_r \quad (\lambda_1 = \lambda,\ \lambda_2 = 1)$

$$\left(\frac{\partial f}{\partial x}\right)_4 = \frac{\lambda^2(1+\lambda)(1+2\lambda)(f_5-f_4) - (1+\lambda)^2(1+2\lambda)(2+\lambda)(f_3-f_4) + 4(1+2\lambda)(f_2-f_4) - \frac{(1+\lambda)(2+\lambda)}{(1+2\lambda)}(f_1-f_4)}{\left[\lambda^2(1+\lambda)(1+2\lambda) + (1+\lambda)^2(1+2\lambda)(2+\lambda) - 4(1+2\lambda)(1+\lambda) + (1+\lambda)(2+\lambda)\right] h_r} \qquad \text{.....[A-7]}$$

$h_\ell + 3\,h_r, \quad (\lambda_1 = \lambda_2 = 1)$

$$\left(\frac{\partial f}{\partial x}\right)_4 = \frac{2(2+\lambda)(1+\lambda)\lambda(f_5-f_4) - 6\lambda(2+\lambda)(3+\lambda)(f_3-f_4) + (1+\lambda)(2+\lambda)(3+\lambda)(f_2-f_4) - \frac{12}{(2+\lambda)}(f_1-f_4)}{\left[2(2+\lambda)(1+\lambda)\lambda + 6\lambda(2+\lambda)(3+\lambda) - 2(1+\lambda)(2+\lambda)(3+\lambda) + 12\right] h_r} \qquad \text{.....[A-8]}$$

$4\,h_r \quad (\lambda = \lambda_1 = \lambda_2 = 1)$

$$\left(\frac{\partial f}{\partial x}\right)_4 = \frac{3(f_5-f_4) - 18(f_3-f_4) + 6(f_2-f_4) - (f_1-f_4)}{12\,h_r} \qquad \text{.....[A-9]}$$

Central differences: Expanding about point 3 of Figure A-1 and truncating at $(\partial^5 f/\partial x^5)_3$ produces:

$$f_5 = f_3 + \sum_{i=1}^{4} \frac{[(1+\lambda_2)h_r]^i}{i!}\left(\frac{\partial^i f}{\partial x^i}\right)_3 \qquad \text{.....[A-10]}$$

$$f_4 = f_3 + \sum_{i=1}^{4} \frac{(\lambda_2 h_r)^i}{i!}\left(\frac{\partial^i f}{\partial x^i}\right)_3 \qquad \text{.....[A-11]}$$

$$f_2 = f_3 + \sum_{i=1}^{4} (-1)^i \frac{(\lambda_1 h_r)^i}{i!}\left(\frac{\partial^i f}{\partial x^i}\right)_3 \qquad \text{.....[A-12]}$$

$$f_1 = f_3 + \sum_{i=1}^{4} (-1)^i \frac{[(\lambda+\lambda_1)h_r]^i}{i!}\left(\frac{\partial^i f}{\partial x^i}\right)_3 \qquad \text{.....[A-13]}$$

Solving for $(\partial f/\partial x)_3$ results in:

$$\left(\frac{\partial f}{\partial x}\right)_3 = \frac{-A_1(f_5-f_3)+A_2(f_4-f_3)-A_3(f_2-f_3)+A_4(f_1-f_3)}{D\,h_r} \qquad \text{.....[A-14]}$$

where:

$$A_1 = \lambda\lambda_1\lambda_2(\lambda_1+\lambda_2)(\lambda+\lambda_1)(\lambda+\lambda_1+\lambda_2)/(1+\lambda_2)$$
$$A_2 = \lambda\lambda_1(1+\lambda_2)(\lambda+\lambda_1)(1+\lambda_1+\lambda_2)(1+\lambda+\lambda_1+\lambda_2)/\lambda_2$$
$$A_3 = \lambda_2(1+\lambda+\lambda_1+\lambda_2)(\lambda+\lambda_1+\lambda_2)(\lambda+\lambda_1)(1+\lambda_2)/\lambda_1$$
$$A_4 = \lambda_1\lambda_2(1+\lambda_2)(1+\lambda_1+\lambda_2)(\lambda_1+\lambda_2)/(\lambda+\lambda_1)$$
$$D = -A_1(1+\lambda_2) + A_2\lambda_2 + A_3\lambda_1 - A_4(\lambda+\lambda_1)$$

3 h_ℓ + h_r ($\lambda_1 = \lambda_2 = \lambda$)

$$\left(\frac{\partial f}{\partial x}\right)_3 = \frac{-12\lambda^4 f_5 + 2(1+\lambda)^2(1+2\lambda)(1+3\lambda)f_4 + [3(1+\lambda)^2(1+2\lambda-4\lambda^2)+12\lambda^4]f_3 - 6(1+\lambda)^2(1+3\lambda)f_2 + (1+\lambda)^2(1+2\lambda)f_1}{6\lambda(1+\lambda)(1+2\lambda)(1+3\lambda)h_r} \qquad \text{.....[A-15]}$$

2 h_ℓ + 2 h_r ($\lambda_1 = \lambda$, $\lambda_2 = 1$)

$$\left(\frac{\partial f}{\partial x}\right)_3 = \frac{-\lambda^3(1+2\lambda)f_5 + 8\lambda^3(2+\lambda)f_4 + [15\lambda+6-\lambda^3(15+6\lambda)]f_3 - 8(1+2\lambda)f_2 + (2+\lambda)f_1}{[\lambda^3(14+4\lambda)+\lambda(4+14\lambda)]h_r} \qquad \text{.....[A-16]}$$

h_ℓ + 3 h_r ($\lambda_1 = \lambda_2 = 1$)

$$\left(\frac{\partial f}{\partial x}\right)_3 = \frac{-\lambda(1+\lambda)^2(2+\lambda)f_5 + 6\lambda(1+\lambda)^2(3+\lambda)f_4 - [3(1+\lambda)^2(\lambda^2+2\lambda-4)+12]f_3 - 2(1+\lambda)^2(3+\lambda)(2+\lambda)f_2 + 12f_1}{6\lambda(1+\lambda)(2+\lambda)(3+\lambda)h_r} \qquad \text{.....[A-17]}$$

4 h_r ($\lambda = \lambda_1 = \lambda_2 = 1$)

$$\left(\frac{\partial f}{\partial x}\right)_3 = \frac{-f_5 + 8f_4 - 8f_2 + f_1}{12\,h_r} \qquad \text{.....[A-18]}$$

Forward differences: Expanding about point (2) of Figure A-1 and neglecting terms of the order $(h_r)^5$:

$$f_5 = f_2 + \sum_{i=1}^{4} \frac{[(1+\lambda_1+\lambda_2)h_r]^i}{i!}\left(\frac{\partial^i f}{\partial x^i}\right)_2 \qquad \text{.....[A-19]}$$

$$f_4 = f_2 + \sum_{i=1}^{4} \frac{[(\lambda_1+\lambda_2)h_r]^i}{i!}\left(\frac{\partial^i f}{\partial x^i}\right)_2 \qquad \text{.....[A-20]}$$

$$f_3 = f_2 + \sum_{i=1}^{4} \frac{(\lambda_1 h_r)^i}{i!}\left(\frac{\partial^i f}{\partial x^i}\right)_2 \qquad \text{.....[A-21]}$$

$$f_1 = f_2 + \sum_{i=1}^{4} (-1)^i \frac{(\lambda h_r)^i}{i!}\left(\frac{\partial^i f}{\partial x^i}\right)_2 \qquad \text{.....[A-22]}$$

Solving for $(\partial f/\partial x)_2$

$$\left(\frac{\partial f}{\partial x}\right)_2 = \frac{A_1(f_5-f_2)-A_2(f_4-f_2)+A_3(f_3-f_2)-A_4(f_1-f_2)}{D\,h_r} \qquad \text{.....[A-23]}$$

where:

$$A_1 = \lambda\lambda_1\lambda_2(\lambda_1+\lambda_2)(\lambda+\lambda_1)(\lambda+\lambda_1+\lambda_2)/(1+\lambda_1+\lambda_2)$$
$$A_2 = \lambda\lambda_1(1+\lambda_1+\lambda_2)(1+\lambda+\lambda_1+\lambda_2)(1+\lambda_2)(\lambda+\lambda_1)/(\lambda_1+\lambda_2)$$
$$A_3 = \lambda(1+\lambda_1+\lambda_2)(1+\lambda_1+\lambda_2+\lambda)(\lambda_1+\lambda_2)(\lambda+\lambda_1+\lambda_2)/\lambda_1$$
$$A_4 = \lambda_1\lambda_2(\lambda_1+\lambda_2)(1+\lambda_2)(1+\lambda_1+\lambda_2)/\lambda$$
$$D = A_1(1+\lambda_1+\lambda_2) - A_2(\lambda_1+\lambda_2) + A_3\lambda_1 + A_4\lambda$$

3 h_ℓ + h_r $(\lambda_1 = \lambda_2 = \lambda)$

$$\left(\frac{\partial f}{\partial x}\right)_2 = \frac{\frac{12\lambda^4}{(1+2\lambda)}(f_5-f_2) - (1+\lambda)(1+2\lambda)(1+3\lambda)(f_4-f_2) + 6(1+2\lambda)(1+3\lambda)(f_3-f_2) - 2(1+\lambda)(1+2\lambda)(f_1-f_2)}{[12\lambda^4 - 2\lambda(1+\lambda)(1+2\lambda)(1+3\lambda) + 6\lambda(1+2\lambda)(1+3\lambda) + 2\lambda(1+2\lambda)(1+\lambda)]}$$

.....[A-24]

$2\,h_\ell + 2\,h_r \quad (\lambda_1 = \lambda,\ \lambda_2 = 1)$

$$\left(\frac{\partial f}{\partial x}\right)_2 = \frac{\left[\frac{\lambda^3(1+\lambda)(1+2\lambda)}{2+\lambda}\right](f_5-f_2)-4\lambda^3(2+\lambda)(f_4-f_2)+(1+\lambda)^2(1+2\lambda)(2+\lambda)(f_3-f_2)-(1+\lambda)(2+\lambda)(f_1-f_2)}{\left[\lambda^3(1+\lambda)(1+2\lambda)-4\lambda^3(2+\lambda)(1+\lambda)+\lambda(2+\lambda)(1+\lambda)^2(1+2\lambda)+\lambda(1+\lambda)(2+\lambda)\right]h_r}$$

.....[A-25]

$h_\ell + 3\,h_r \quad (\lambda_1 = \lambda_2 = 1)$

$$\left(\frac{\partial f}{\partial x}\right)_2 = \frac{\frac{2\lambda(1+\lambda)(2+\lambda)}{3}(f_5-f_2)-3\lambda(1+\lambda)(3+\lambda)(f_4-f_2)+6\lambda(2+\lambda)(3+\lambda)(f_3-f_2)-\frac{12}{\lambda}(f_1-f_2)}{\left[\lambda^3(1+\lambda)(1+2\lambda)-4\lambda^3(2+\lambda)(1+\lambda)+\lambda(2+\lambda)(1+\lambda)^2(1+2\lambda)+\lambda(1+\lambda)(2+\lambda)\right]h_r}$$

.....[A-26]

$4\,h_r \quad (\lambda_1 = \lambda_2 = \lambda = 1)$

$$\left(\frac{\partial f}{\partial x}\right)_2 = \frac{(f_5-f_2)-6(f_4-f_2)+18(f_3-f_2)-3(f_1-f_2)}{12\,h_r}$$

.....[A-27]

SECOND DERIVATIVES

The second derivative calculation produces results which are more complicated than those of the first derivative and in as much it is better to solve for particular distributions directly.

Backward differences: Solving equations (A-1) through (A-4) for $(\partial^2 f/\partial x^2)_4$ yields:

$3\,h_\ell + h_r$

$$\left(\frac{\partial^2 f}{\partial x^2}\right)_4 = \frac{-22\lambda^5(f_5-f_4)+(5\lambda+19\lambda^2-36\lambda^4)(f_3-f_4)-(4\lambda+13\lambda^2-9\lambda^4)(f_2-f_4)+\frac{3\lambda+7\lambda^2-4\lambda^4}{3}(f_1-f_4)}{h_r^2\left[-6\lambda^6-3\lambda^3(1+2\lambda)(1+3\lambda)+3\lambda^3(1+3\lambda)(1+\lambda)-\lambda^3(1+\lambda)(1+2\lambda)\right]}$$

.....[A-28]

$2\,h_\ell + 2\,h_r$

$$\left(\frac{\partial^2 f}{\partial x^2}\right)_4 = \frac{-4\lambda^3(3+6\lambda+2\lambda^2)(f_5-f_4)+4\lambda(1-2\lambda^2)(2+\lambda)(1+\lambda)(f_3-f_4)-16\lambda(f_2-f_4)+4\frac{\lambda(2+\lambda)}{1+2\lambda}(f_1-f_4)}{\left[-2\lambda(1+\lambda)(2+\lambda)-2(1+2\lambda)(1+\lambda)\lambda^3-2(2+\lambda)\lambda(1+\lambda)^2(1+2\lambda)+8(1+2\lambda)(1+\lambda)\lambda\right]h_r^2} \quad \text{.....[A-29]}$$

$h_\ell + 3\,h_r$

$$\left(\frac{\partial^2 f}{\partial x^2}\right)_4 = \frac{-(8\lambda+11\lambda^2+3\lambda^2)(f_5-f_4)-(9\lambda^2+3\lambda^3)(f_3-f_4)-(\lambda^2+4\lambda+3)(f_2-f_4)+\frac{6}{2+\lambda}(f_1-f_4)}{\left[-(2+\lambda)(1+\lambda)\lambda-3(2+\lambda)(3+\lambda)\lambda+(1+\lambda)(2+\lambda)(3+\lambda)-6\right]} \quad \text{.....[A-30]}$$

$4\,h_r$

$$\left(\frac{\partial^2 f}{\partial x^2}\right)_4 = \frac{11(f_5-f_4)+6(f_3-f_4)+4(f_2-f_4)-(f_1-f_4)}{12\,h_r^2} \quad \text{.....[A-31]}$$

Central differences: Solving equations (A-10) to (A-13) for the second derivative results in:

$3\,h_\ell + h_r$

$$\left(\frac{\partial^2 f}{\partial x^2}\right)_3 = \frac{-6\lambda^4 f_5+(1+\lambda)(3+\lambda)(1+2\lambda)(1+3\lambda)f_4-3(1+3\lambda)(1+2\lambda)(2+3\lambda)f_3+3(1+\lambda)(1+3\lambda)^2 f_2-\lambda(1+\lambda)(1+2\lambda)f_1}{3\lambda^2(1+\lambda)(1+2\lambda)(1+3\lambda)h_r^2} \quad \text{.....[A-32]}$$

$2\,h_\ell + 2\,h_r$

$$\left(\frac{\partial^2 f}{\partial x^2}\right)_3 = \frac{(4\lambda^6-7\lambda^4-3\lambda^3)f_5+(-8\lambda^6+56\lambda^4+48\lambda^3)f_4+(4\lambda^6-49\lambda^4-90\lambda^3-49\lambda^2+4)f_3+(48\lambda^3+56\lambda^2-8)f_2-(3\lambda^3+7\lambda^2-4)f_1}{2\lambda^2(1+\lambda)^2(1+2\lambda)(2+\lambda)h_r^2} \quad \text{.....[A-33]}$$

$h_\ell + 3\,h_r$

$$\left(\frac{\partial^2 f}{\partial x^2}\right)_3 = \frac{-2\lambda(1+\lambda)(2+\lambda)f_5+6\lambda(1+\lambda)(3+\lambda)^2 f_4-(12\lambda^4+78\lambda^3+162\lambda^2+108\lambda)f_3+2(1+\lambda)(2+\lambda)(3+\lambda)(1+3\lambda)f_2-12f_1}{(6\lambda^4+36\lambda^3+66\lambda^2+36\lambda)h_r^2} \quad \text{.....[A-34]}$$

4 hr

$$\left(\frac{\partial^2 f}{\partial x^2}\right)_3 = \frac{-f_5+16f_4-30f_3+16f_2-f_1}{12\,h_R^2} \qquad \text{.....[A-35]}$$

Forward differences: Solving equations (A-19) thru (A-22) for $(\partial^2 f/\partial x^2)_2$ gives:

3 h_ℓ + h_r

$$\left(\frac{\partial^2 f}{\partial x^2}\right)_2 = \frac{-\frac{6\lambda^3}{1+2\lambda}(f_5-f_2)+(3\lambda^2+4\lambda+1)(f_4-f_2)+\frac{9\lambda+3}{\lambda}(f_3-f_2)+\frac{8\lambda^2+11\lambda+3}{\lambda}(f_1-f_2)}{(9\lambda^3+12\lambda^2+3\lambda)\,h_R^2}$$

.....[A-36]

2 h_ℓ + 2 h_r

$$\left(\frac{\partial^2 f}{\partial x^2}\right)_2 = \frac{-\frac{\lambda^3(1+2\lambda)}{2+\lambda}(f_5-f_2)+4\lambda^3(f_4-f_2)+\frac{2+6\lambda+3\lambda^2-3\lambda^3-2\lambda^4}{\lambda}(f_3-f_2)+\frac{3\lambda^2+6\lambda+2}{\lambda}(f_1-f_2)}{(4\lambda^3+6\lambda^2+2\lambda)\,h_R^2}$$

.....[A-37]

h_ℓ + 3 h_r

$$\left(\frac{\partial^2 f}{\partial x^2}\right)_2 = \frac{-\lambda(3\lambda^3+7\lambda^2-4)(f_5-f_2)+3\lambda(4\lambda^3+13\lambda^2-9)(f_4-f_2)-3\lambda(5\lambda^3+19\lambda^2-36)(f_3-f_2)+66(f_1-f_2)}{3\lambda(\lambda^3+6\lambda^2+11\lambda+6)\,h_R^2}$$

.....[A-38]

4 h_r

$$\left(\frac{\partial^2 f}{\partial x^2}\right)_2 = \frac{-f_5+4f_4+6f_3-20f_2+11f_1}{12\,h_R^2} \qquad \text{.....[A-39]}$$

Three grid ratios were used in this study: λ = 2, 1 and 1/2. The derivatives in each case are as follows:

$\lambda = 2$ ($h_\ell = 2\ h_r$)

$3\ h_\ell + h_r$

$$\left(\frac{\partial f}{\partial x}\right)_{\begin{bmatrix}4\\3\\2\end{bmatrix}} = \frac{\begin{bmatrix}192/7\\-64/7\\64/7\end{bmatrix} f_5 + \begin{bmatrix}-5\\30\\-25\end{bmatrix} f_4 + \begin{bmatrix}-30\\-5\\50\end{bmatrix} f_3 + \begin{bmatrix}9\\-18\\-27\end{bmatrix} f_2 + \begin{bmatrix}-10/7\\15/7\\-50/7\end{bmatrix} f_1}{60\ h_r} \quad \text{.....[A-40]}$$

$$\left(\frac{\partial^2 f}{\partial x^2}\right)_{\begin{bmatrix}4\\3\\2\end{bmatrix}} = \frac{\begin{bmatrix}352/7\\-32/7\\-32/7\end{bmatrix} f_5 + \begin{bmatrix}-80\\25\\10\end{bmatrix} f_4 + \begin{bmatrix}35\\-40\\5\end{bmatrix} f_3 + \begin{bmatrix}-6\\21\\-24\end{bmatrix} f_2 + \begin{bmatrix}5/7\\-10/7\\95/7\end{bmatrix} f_1}{60\ h_r^2} \quad \text{.....[A-41]}$$

$2\ h_\ell + 2\ h_r$

$$\left(\frac{\partial f}{\partial x}\right)_{\begin{bmatrix}4\\3\\2\end{bmatrix}} = \frac{\begin{bmatrix}75/4\\-10\\15\end{bmatrix} f_5 + \begin{bmatrix}32\\64\\-64\end{bmatrix} f_4 + \begin{bmatrix}-225/4\\-45\\90\end{bmatrix} f_3 + \begin{bmatrix}25/4\\-10\\-35\end{bmatrix} f_2 + \begin{bmatrix}-3/4\\1\\-6\end{bmatrix} f_1}{60\ h_r} \quad \text{.....[A-42]}$$

$$\left(\frac{\partial^2 f}{\partial x^2}\right)_{\begin{bmatrix}4\\3\\2\end{bmatrix}} = \frac{\begin{bmatrix}115/2\\5\\-10\end{bmatrix} f_5 + \begin{bmatrix}-112\\32\\32\end{bmatrix} f_4 + \begin{bmatrix}105/2\\-60\\-15\end{bmatrix} f_3 + \begin{bmatrix}5/2\\25\\-20\end{bmatrix} f_2 + \begin{bmatrix}-1/2\\-2\\13\end{bmatrix} f_1}{60\ h_r^2} \quad \text{.....[A-43]}$$

$h_\ell + 3\,h_r$

$$\left(\frac{\partial f}{\partial x}\right)_{\begin{bmatrix}4\\3\\2\end{bmatrix}} = \frac{\begin{bmatrix}16\\-6\\8\end{bmatrix} f_5 + \begin{bmatrix}45\\45\\-45\end{bmatrix} f_4 + \begin{bmatrix}-80\\-10\\120\end{bmatrix} f_3 + \begin{bmatrix}20\\-30\\-80\end{bmatrix} f_2 + \begin{bmatrix}-1\\1\\-3\end{bmatrix} f_1}{60\,h_x} \quad \text{.....[A-44]}$$

$$\left(\frac{\partial^2 f}{\partial x^2}\right)_{\begin{bmatrix}4\\3\\2\end{bmatrix}} = \frac{\begin{bmatrix}56\\-4\\-16\end{bmatrix} f_5 + \begin{bmatrix}-105\\75\\75\end{bmatrix} f_4 + \begin{bmatrix}40\\-140\\-80\end{bmatrix} f_3 + \begin{bmatrix}10\\70\\10\end{bmatrix} f_2 + \begin{bmatrix}-1\\-1\\11\end{bmatrix} f_1}{60\,h_x^2} \quad \text{.....[A-45]}$$

$\lambda = 1$ ($h_r = h_\ell$) evenly distributed case

All distributions: $4\,h_r$

$$\left(\frac{\partial f}{\partial x}\right)_{\begin{bmatrix}4\\3\\2\end{bmatrix}} = \frac{\begin{bmatrix}15\\-5\\5\end{bmatrix} f_5 + \begin{bmatrix}50\\40\\-30\end{bmatrix} f_4 + \begin{bmatrix}-90\\0\\90\end{bmatrix} f_3 + \begin{bmatrix}30\\40\\-50\end{bmatrix} f_2 + \begin{bmatrix}-5\\5\\-15\end{bmatrix} f_1}{60\,h_x} \quad \text{.....[A-46]}$$

$$\left(\frac{\partial^2 f}{\partial x^2}\right)_{\begin{bmatrix}4\\3\\2\end{bmatrix}} = \frac{\begin{bmatrix}55\\-5\\-5\end{bmatrix} f_5 + \begin{bmatrix}-100\\80\\20\end{bmatrix} f_4 + \begin{bmatrix}30\\-150\\30\end{bmatrix} f_3 + \begin{bmatrix}20\\80\\-100\end{bmatrix} f_2 + \begin{bmatrix}-5\\-5\\55\end{bmatrix} f_1}{60\,h_x^2} \quad \text{.....[A-47]}$$

$\lambda = 1/2$ ($h_\ell = 1/2\ h_r$)

$3\ h_\ell + h_r$

$$\left(\frac{\partial f}{\partial x}\right)_{\begin{bmatrix}4\\3\\2\end{bmatrix}} = \frac{\begin{bmatrix}6\\-2\\2\end{bmatrix} f_5 + \begin{bmatrix}160\\60\\-40\end{bmatrix} f_4 + \begin{bmatrix}-240\\20\\160\end{bmatrix} f_3 + \begin{bmatrix}90\\-90\\-90\end{bmatrix} f_2 + \begin{bmatrix}-16\\12\\-32\end{bmatrix} f_1}{60\ h_r} \quad \text{.....[A-48]}$$

$$\left(\frac{\partial^2 f}{\partial x^2}\right)_{\begin{bmatrix}4\\3\\2\end{bmatrix}} = \frac{\begin{bmatrix}44\\-4\\-4\end{bmatrix} f_5 + \begin{bmatrix}40\\280\\40\end{bmatrix} f_4 + \begin{bmatrix}-320\\-560\\160\end{bmatrix} f_3 + \begin{bmatrix}300\\300\\-420\end{bmatrix} f_2 + \begin{bmatrix}-64\\-16\\224\end{bmatrix} f_1}{60\ h_r^2} \quad \text{.....[A-49]}$$

$2\ h_\ell + 2\ h_r$

$$\left(\frac{\partial f}{\partial x}\right)_{\begin{bmatrix}4\\3\\2\end{bmatrix}} = \frac{\begin{bmatrix}12\\-2\\3/2\end{bmatrix} f_5 + \begin{bmatrix}70\\20\\-25/2\end{bmatrix} f_4 + \begin{bmatrix}-180\\90\\225/2\end{bmatrix} f_3 + \begin{bmatrix}128\\-128\\-64\end{bmatrix} f_2 + \begin{bmatrix}-30\\20\\-75\end{bmatrix} f_1}{60\ h_r} \quad \text{.....[A-50]}$$

$$\left(\frac{\partial^2 f}{\partial x^2}\right)_{\begin{bmatrix}4\\3\\2\end{bmatrix}} = \frac{\begin{bmatrix}52\\-2\\-2\end{bmatrix} f_5 + \begin{bmatrix}-80\\25\\10\end{bmatrix} f_4 + \begin{bmatrix}-60\\-60\\210\end{bmatrix} f_3 + \begin{bmatrix}128\\32\\-448\end{bmatrix} f_2 + \begin{bmatrix}-40\\5\\230\end{bmatrix} f_1}{60\ h_r} \quad \text{.....[A-51]}$$

$h_\ell + 3\,h_r$

$$\left(\frac{\partial f}{\partial x}\right)_{\begin{bmatrix}4\\3\\2\end{bmatrix}} = \frac{\begin{bmatrix}100/7\\-30/7\\20/7\end{bmatrix} f_5 + \begin{bmatrix}54\\36\\-18\end{bmatrix} f_4 + \begin{bmatrix}-100\\10\\60\end{bmatrix} f_3 + \begin{bmatrix}50\\-60\\10\end{bmatrix} f_2 + \begin{bmatrix}-128/7\\128/7\\-384/7\end{bmatrix} f_1}{60\,h_r} \qquad \text{.....[A-52]}$$

$$\left(\frac{\partial^2 f}{\partial x^2}\right)_{\begin{bmatrix}4\\3\\2\end{bmatrix}} = \frac{\begin{bmatrix}380/7\\-40/7\\20/7\end{bmatrix} f_5 + \begin{bmatrix}-96\\84\\-24\end{bmatrix} f_4 + \begin{bmatrix}20\\-160\\140\end{bmatrix} f_3 + \begin{bmatrix}40\\100\\-320\end{bmatrix} f_2 + \begin{bmatrix}-128/7\\-128/7\\1408/7\end{bmatrix} f_1}{60\,h_r^2} \qquad \text{.....[A-53]}$$

As a test as well as a check on the validity of the above, the first and second derivatives of the function:

$$f = \tfrac{1}{2}(x^4 - 2x^2) \qquad \text{.....[A-54]}$$

which is the same form as the stream function in Poiseuille flow in a circular tube, are computed. Also evaluated for comparison are the three point central differences which are readily obtained by a simultaneous solution of Taylor series expansion about Point 2 of Figure A-2:

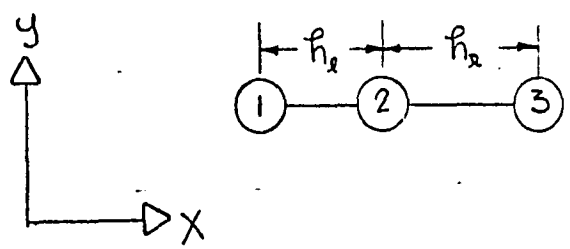

Figure A-2

Grid Nomenclature

$$f_3 = f_2 + \sum_{i=1}^{2} \frac{h_r^i}{i!} \left(\frac{\partial^i f}{\partial x^i}\right)_2$$

$$f_1 = f_2 + \sum_{i=1}^{2} (-1)^i \frac{h_l^i}{i!} \left(\frac{\partial^i f}{\partial x^i}\right)_2$$

Note that the series have been truncated at the (h_r^3) term solving for the first and second derivatives:

$$\left(\frac{\partial f}{\partial x}\right)_2 = \frac{\lambda^2(f_3 - f_2) - (f_1 - f_2)}{(1+\lambda)\lambda h_r} \qquad \text{.....[A-55]}$$

$$\left(\frac{\partial^2 f}{\partial x^2}\right)_2 = \frac{2\lambda(f_3 - f_2) - 2(f_1 - f_2)}{(1+\lambda)\lambda h_r^2}$$

The truncation errors are respectively of the order $(\lambda\ h_r^2)$ and $(1 - \lambda)\ h_r$. The second derivative calculation is quite inaccurate for all λ except where $h_l = h_r$ i.e., $\lambda = 1$ where the accuracy improves to the order of h_r^2.

It should be mentioned that the truncation error of the 5 point forms was h_r^4 for the first derivative and h_r^3 for the second.

The derivatives were evaluated at the point X = 1/2 with a grid spacing of: $h_r = 1/10$. All arithmetic was done in double precision so that the effects of round off error would be diminished. The results of the calculations are as follows:

° The five point forms of equations (A-40) through (A-53) allowed the derivative at the desired point to be correctly calculated

(-.75 and -.5 for the first and second derivative respectively).

° The three point form of equation (A-55) gave first derivative values of: -.7310000, -.7400000 and -.7290000, for grid ratios of: λ = 2, 1, 1/2 respectively and gave second derivative values of: -.6700000, -.4900000, -.2700000 for the indicated grid ratios.

APPENDIX B

A SURVEY OF LITERATURE CONCERNED WITH FINITE DIFFERENCE SOLUTIONS OF THE NAVIER-STOKES EQUATIONS

Efforts to solve the Navier-Stokes equations by using finite difference methods have been so extensive that it is worthwhile to assemble a list of these works. Consultation of this list will then provide a clearer picture of the ground already covered by others. Unfortunately, such a reference tabulation cannot hope to be exhaustive because work in this area has taken so many directions. Nevertheless, 195 references have been incorporated into this index. The entries have been listed chronologically so that they may be easily located and so that they may also be expanded to include any overlooked works.

1928 Thom, A., "An Investigation of Fluid Flow in Two Dimensions," A.R.C. R.&M., No. 1194 (Nov 1928)

1932 Thom, A., "Arithmetical Solution of Certain Problems in Steady Viscous Flow," A.R.C. R.& M., No. 1475 (May 1932)

1933 Thom, A., "The Flow Past Circular Cylinders at Low Speeds," Proc. Roy. Soc. A. VOL 141 pp 651-669 (April 1933)

1934 Thom, A., "Arithmetical Solution of Equations of the Type $\nabla^4\psi$ = Constant," A.R.C. R.& M., No. 1604 (1934)

1950 Kawaguti, M., Rep. Inst. Sci., Tokyo, VOL 4, p 154 (Flow Around a Sphere at a Reynolds Number of 20 - in Japanese)

1952 Thom, A., "The Flow at the Mouth of a Stanton Pitot," A.R.C. R.& M., No. 2984, (Oct 1952)

1953 Thom, A., "The Arithmetic of Field Equations," Aero. Quart. IV Part 3. (Aug 1953)

1953 Kawaguti, M., "Numerical Solution of the Navier-Stokes Equations for the Flow Around a Circular Cylinder at Reynolds Number 40," Journ. of Phy. Soc. of Jap VOL 8, No. 6, pp 747-757 (Nov 1953)

1953 Lister, M. Ph.D. Thesis, London, (Flow Around a Sphere for Reynolds Numbers of 0, 1, 10, 20)

1954 Woods, L. C., "A Note on the Numerical Solution of Fourth-order Differential Equations," Aero. Quart. V. Pt. 3, (Sept 1954)

1955 Allen, D. N. and Southwell, R. V., "Relaxation Methods Applied to Determine the Motion in Two Dimensions of a Viscous Fluid Past a Circular Cylinder," Quart. Journ. of Mech. and Applied Math, VOL 8, Pt. 2, pp 129-145 (1955)

1956 Thom, A. and Apelt, C. J., "Note on the Convergence of Numerical Solutions of the Navier-Stokes Equations," A.R.C. R& M., No. 3061, (June 1956)

1956 Payne, R. B., A.R.C. R.& M., No. 3047 (1956) (Nonsteady Flow)

1957 Janssen, E., "Flow Past a Flat Plate at Low Reynolds Numbers," Journ. of Fluid Mech., VOL 3, pp 329-343 (1957)

1958 Payne, R. B., "Calculation of Unsteady Viscous Flow Past a Circular Cylinder," Journ. of Fluid Mech., VOL 4, pp 81-86 (May 1958)

1958 Thom, A., "Boundary Troubles in Arithmetical Solutions of the Navier-Stokes Equations," A.R.C. 20, 289 (July 1958)

1958 Apelt, J. D., "The Steady Flow of a Viscous Fluid Past a Circular Cylinder at Reynolds Numbers 40 and 44," A.R.C. R& M. No. 3175 (Oct 1958)

1959 Jenson, V. G., "Viscous Flow Round a Sphere at Low Reynolds Numbers (<<40)," Proc. Roy. Soc. (London), VOL A 249, pp 346-366

1959 Kawaguti, M., "Note on Allen and Southwell's paper 'Relaxation Methods Applied to Determine the Motion, in Two Dimensions, of a Viscous Fluid Past a Cylinder'," Quart. J. Mech. 12 pp 261-63 (1959)

1960 Lester, W. G. S., "Some Convergence Problems in the Numerical Solution of the Navier-Stokes Equations," A.R.C. R.& M. No. 3239 (July 1960)

1960 Lester, W. G. S., "The Flow Past a Pitot Tube at Low Reynolds Numbers:

Part I - The Numerical Solution of the Navier-Stokes Equations for Steady Viscous Axi-symmetric Flow

Part II - The Effects of Viscosity and Orifice Size on a Pitot Tube at Low Reynolds Numbers,"

A.R.C. R.&M. No. 3240 (July 1960)

1960 Hellums, J. D., Finite Difference Computations of Natural Convection Heat Transfer Ph.D. Thesis, University of Michigan

1961 Thom, A. and Apelt, J. D., Field Computations in Engineering and Physics, D. Van Nostrand Co.

1961 Filler, L. and Ludloff, H. F., "Stability Analysis and Integration of the Viscous Equations of Motion," Math of Comp., VOL 15, pp 261-274 (July 1961)

1961 Kawaguti, M., "Numerical Solution of the Navier-Stokes Equations for the Flow in a Two-Dimensional Cavity," Journ. of the Phy. Soc. of Jap., VOL 16, No. 12 (Nov 1961)

1961 Thompson, P. D., Numerical Weather Analysis and Prediction, New York, MacMillan

1962 Gillis, J., Numerical Integration of the Navier-Stokes Equations," Tech Rep No. 2 Dept of Appl. Math, The Weizmann Inst. of Sci., Rehovot, Israel (Jan 1962)

1962 Hellums, J. D. and Churchill, S. W., "Transient Natural Convection," A.I.Ch.E. Journ., 8 pp 690-695

1963 Fromm, J. E., "A Method for Computing Non Steady, Incompressible, Viscous Fluid Flows," Los Alamos Sci. Rept No. LA 2910 (May 1963)

1963 Fromm, J. E. and Harlow, F. H., "Numerical Solution of the Problem of Vortex Street Development," The Phys. of Fluids, VOL 6, No. 7, pp 975-982, (July 1963)

1963 Hellums, J. D. and Churchill, S. W., "Computation of Natural Convection by Finite Difference Methods," Int. Devel. in Heat Transfer - Proceedings, pp 985-994

1963 Wang, Y. L., Ph.D Thesis, Part 2, Calif. Inst. Tech.

1963 Wilkes, J. O., Ph.D. Thesis, University of Michigan, The Finite Difference Computation of Natural Convection in an Enclosed Rectangular Cavity.

1964 Harlow, F. H. and Fromm, J. E., "Dynamics and Heat Transfer in the Von Karman Wake of a Rectangular Cylinder," Phys of Fluids, VOL 7 pg 1147

1964 Wang, Y. L. and Longwell, P. A., "Laminar Flow in the Inlet Section of Parallel Plates," A.I.Ch.E. Journ., Vol 10, No. 3 pp 323-329 (May 1964)

1964 Greenspan, D., et al., "Numerical Studies of the Navier-Stokes Equations," Math. Res. Cent., Tech Summary Rept No. 482, U. S. Army, University of Wisconsin, (Clearinghouse order No. AD-605639), (May 1964)

1964 Simuni, L. M., "The Numerical Solution of Several Problems in the Flow of a Viscous Fluid," Eng. Journ. of Academy of USSR, VOL 4, pp 446-450, (in Russian)

1964 Gillis, J. and Brandt, A., "Numerical Integration of the Equations of Motion of a Viscous Fluid," Weizmann Inst. of Sci., SR No. 1, (Clearinghouse order No. AD-614915) (Oct 1964)

1964 Fromm, J. E., "The Time Dependent Flow of an Incompressible Viscous Fluid," Methods of Comput. Phy., VOL 3, pp 345-382, Academic Press

1965 Harlow, F. H., "Numerical Fluid Dynamics," American Math. Monthly, VOL 72, No. 2 pp 84-91, (Feb 1965)

1965 Harlow, F. H. and Fromm, J. E., "Computer Experiments in Fluid Dynamics," Scientific American, VOL 212, No. 3 p 104 (Mar 1965)

1965 Kawaguti, M., "Numerical Solutions of the Navier-Stokes Equations for Flow in a Channel with a Step," Math. Res. Center, Tech. Summary Rept No. 574, University of Wisconsin, (Clearinghouse order No. AD-620108) (May 1965)

1965 Brailovskaya, I. Y., "A Difference Scheme for Numerical Solution of the Two-Dimensional, Non Steady, Navier-Stokes Equations for a Compressible Gas," Soviet Physics-Doklady, VOL 10, No. 2, pp 107-110, (Aug 1965)

1965 Macagno, E. O., "Some New Aspects in Similarity in Hydraulics," La Houille Blanche, No. 8, pp 751-758

1965 Fromm, J. E., "Numerical Solutions of the Nonlinear Equations of a Heated Fluid Layer," Phys. Fluids VOL 8, p 1757

1965 Mills, R. D., "Numerical Solutions of the Viscous Flow Equations for a Class of Closed Flows," Journ. Roy. Aero. Soc., VOL 69 pp 714-718, (Oct 1965)

1965 Crocco, L., "A Suggestion for the Numerical Solution of the Steady Navier-Stokes Equations," AIAA Journ., VOL 3, No. 10 pp 1824-1832, (Oct 1965), (also reprinted in Computational Fluid Dynamics, Chu, C. K., ed. pp 105-113, (July 1968))

1965 Paris, J. and Whitaker, S., "Confined Wakes: A Numerical Solution of the Navier-Stokes Equations," A.I.Ch.E. Journ., VOL 11, No. 6 pp 1033-1041, (Nov 1965)

1965 Pearson, C. E., "A Computational Method for Viscous Flow Problems," Journ. Fluid Mech., VOL 21, Part 4, pp 611-622

1965 Pearson, C. E., "Numerical Solutions for the Time Dependent Viscous Flow Between Two Rotating Coaxial Disks," Journ. Fluid Mech., VOL 21, Part 4, pp 622-633

1965 Harlow, F. H. and Welch, E. J., "Numerical Calculation of Time Dependent Viscous, Incompressible Flow of Fluid with a Free Surface," Phys Fluids, VOL 8, No. 12, pp 2182-2189, (Dec 1965)

1965 Aziz, K., Ph.D. Thesis, Rice University

1966 Burggraf, O. R., "Analytical and Numerical Studies of the Structure of Steady Separated Flow," Journ Fluid Mech., VOL24, Part 1, pp 113-151.

1966 Bye, J. T., "Obtaining Solutions of the Navier-Stokes Equations by Relaxation Processes," Computer Journ., VOL 8, No. 1, pp 53-56

1966 Wilkes, J. O. and Churchill, S. W., "The Finite Difference Computation of Natural Convection in a Rectangular Enclosure," A.I.Ch.E. Journ., VOL 12, No. 1, pp 161-166, (Jan 1966)

1966 Arakawa, A., "Computational Design for Long-term Numerical Integration of the Equations of Fluid Motion: Two Dimensional Incompressible Flow Part I," Journ. Comp. Phys. VOL 1, p 119

1966 Barakat, H. Z. and Clark, J. A., "Analytical and Experimental Study of the Transient Laminar Natural Convection Flows in Partially Filled Containers," Proc. Third Int. Heat Transf. Conf. VOL II, p 152

1966 Micheal, P., "Steady Motion of a Disk in a Viscous Fluid," Phys. of Fluids, VOL 9, No. 3, pp 466-471, (Mar 1966)

1966 Kurzrock, J. W., Exact Numerical Solutions of the Time-Dependent Compressible Navier-Stokes Equations, Ph.D. Thesis, Cornell U., (Feb 1966)

1966 Welch, J. L., Harlow, F. H. Shannon, J. P., and Daly, B. J., "The MAC Method -- A Computing Technique for Solving Viscous, Incompressible, Transient Fluid Flow Problems Involving Free Surfaces," Los Alamos Sci. Lab., LA-3424, (Mar 1966)

1966 Tejeira, E. J., Numerical and Experimental Investigations of a Two-Dimensional Laminar Flow, Ph.D. Thesis, U. of Tennessee (July 1966)

1966 Thoman, D. C. and Szewczyk, A. A., "Numerical Solutions of the Time Dependent Two Dimensional Flow of a Viscous, Incompressible Fluid Over Stationary and Rotating Cylinders," Heat Trans. and Fluid Lab. Dept. M.E., U. of Notre Dame, T.R. 66-14 (July 1966)

1966 Bye, J. T., "Numerical Solutions of the Steady-State Vorticity Equation in Rectangular Basins," Journ. Fluid Mech., VOL 26, part 3, pp 577-598.

1966 Hung, T. K., Laminar Flow in Conduit Expansions, Ph.D. Thesis, U. of Iowa, (Aug 1966)

1966 Kawaguti, M. and Jain, P., "Numerical Study of a Viscous Fluid Flow Past a Circular Cylinder," Journ. Phy. Soc. Jap. VOL 21, No. 10, pp 2055-2062, (Oct 1966)

1966 Keller, H. B. and Takami, H., "Numerical Studies of Steady Viscous Flow about Cylinders," from Numerical Solutions of Nonlinear Differential Equations, John Wiley & Sons, pp 115-140 (May 1966)

1966 Vrentas, J. S., Duda, J. L. and Bargeron, K. G., "Effect of Axial Diffusion of Vorticity on Flow Development in Circular Conduits: Part I Numerical Solutions," A.I.Ch.E. Journ., VOL 12, No. 5, pp 837-844, (Sept 1966)

1966 Runchal, A. K. and Wolfshtein, M., "A Finite Difference Procedure for the Integration of the Navier-Stokes Equations," Dept M.E. Imperial College, London, Ref. N ST/TN/1 (1966)

1966 Roslyakov, G. S. and Chudov, L. A., Editors of, Numerical Methods in Gas Dynamics, (A collection of papers of the Computational Center of the Moscow State University). Trans. from Russian-Israel Program for Sci. Trans., NASA, TT F-36C
Relevant articles:
Krylov, A. L., "Finite-Dimensional Models for Equations of Mathematical Physics," pp 114-120
Krylov, A. L. and Proizvolova, E. K., "Numerical Study of Flow Between Rotating Cylinders," pp 121-126
Krylov, A. L. and Misnik, A. F., "Stability of Viscous Flow Between Two Rotating Cylinders," pp 127-131
Chudov, L. A. and Kuskova, T.V., "Application of Difference Schemes to Computation of Nonstationary Flow of Viscous Incompressible Fluid," pp 132-144

1966 Hung, T. K. and Macagno, E. O., "Laminar Eddies in a Two-Dimensional Conduit Expansion," La Houille Blanche, No. 4, pp 391-400

1966 Kurtzrock, J. W. and Mates, R. E., "Exact Numerical Solutions of the Time-Dependent Compressible Navier-Stokes Equations," AIAA paper No. 66-30, 3rd Aerospace Science Meeting

1966 Kruzhivitski, A. and Ladyzhenskaya, O., "A Grid Method for the Navier-Stokes Equations," Soviet Physics - Doklady VOL 11, pp 212-213, (1966)

1966 Pearson, J. D., Numerical Solution of the Navier-Stokes Equations for the Entrance Region of Suddenly Accelerated Parallel Plates, Ph.D. Thesis, Iowa State University

1967 Macagno, E. O. and Hung, T. K., "Computational and Experimental Study of a Captive Annular Eddy," Journ. Fluid Mech., VOL 28 Part 1, pp 43-64.

1967 Macagno, E. O. and Hung, T. K., "Pressure, Bernoulli Sum, and Momentum and Energy Relations in a Laminar Zone of Separation," Physics of Fluids, VOL 10, No. 1, pp 78-82 (Jan 1967)

1967 Aziz, K. and Hellums, J. D., "Numerical Solution of the Three Dimensional Equations of Motion for Laminar Natural Convection," Physics of Fluids, VOL 10, No. 2, pp 314-324, (Feb 1967)

1967 Hamielec, A. E., Hoffman, T. W., Ross, L. L., "Numerical Solution of the Navier-Stokes Equations for Flow Past Spheres: Part I Viscous Flow Around Spheres with and without Radial Mass Efflux," A.I.Ch.E. Journ., VOL 13, No. 2, pp 212-219, (Mar 1967)

1967 Hamielec, A. E., Johnson, A. I., and Haughton, W. T., "Numerical Solution of the Navier-Stokes Equation for Flow Past Spheres: Part II Viscous Flow Around Circulating Spheres of Low Viscosity," A.I.Ch.E. Journ. VOL 13, No. 2, pp 220-224 (Mar 1967)

1967 Chorin, A. E., "A Numerical Method for Solving Incompressible Viscous Flow Problems," Journ. Comp. Phys., VOL 2, No. 1, pp 12-26, (Aug 1967)

1967 Meyer, K., "Time Dependent Numerical Study of Taylor Vortex Flow," Phys Fluids, VOL 10, No. 9, pp 1874-1879, (Sept 1967)

1967 Numerical Methods for Viscous Flows, AGARD Conf. Proceedings No. 60 (Abstracts of papers presented at seminar held by Fluid Dynamics Panel of AGARD at the Nat. Phy. Lab., Teddington, U.K.) (Sept 1967), (Clearinghouse order No. AD-708697)
Relevant Abstracts:
Sears, W. R., "Solutions of the Navier-Stokes Equations," pg 2
Szewczyk, A., Thoman, D. C., and Kopfer, J., "Numerical Solutions of the Navier-Stokes Equations for Time Dependent Flow Past a Circular Cylinder," pg 11
Micheal, P., "Difference Approximation Solutions of the Acceleration of a Sphere in a Viscous Fluid," pg 12
Rimon, Y. and Cheng, S. I., "Numerical Solution of the Time-Dependent Incompressible Viscous Flows Over a Disk or a Sphere," pg 13

Legendre, R., "Ecoulement plan d'un fluide visqueux autour d'un obstacle s'etendant a l'infini aval," pg 16
Spalding, D. B., "A New Procedure for the Numerical Solution of the Elliptic Equations of Simultaneous Heat, Mass and Momentum Transfer," pg 20
Thommen, H. U., "Integration of the Unsteady Navier-Stokes Equations by Finite Difference," pp 28-29
Hirt, C. W., "Computer Studies of Time-dependent Flows," pp 34-35
Allen, J. S. and Cheng, S. I., "Numerical Solutions of the Compressible Navier-Stokes Equations for Laminar Near-wake in Supersonic Flow," pp 36-38
Scala, S. M. and Gordon, P., "Solution of the Time-dependent Navier-Stokes Equations for Supersonic Flows," pp 39-41

1967 Roache, P. J., Numerical Solutions of Compressible and Incompressible Laminar Separated Flows, Ph.D. Thesis, U. of Notre Dame, (Nov 1967)

1967 Dixon, T. N. and Hellums, J. D., "A Study of Stability and Incipient Turbulence in Poiseuille and Plane-Poiseuille Flow by Numerical Finite Difference Simulation," A.I.Ch.E. Journ., VOL 13, No. 5, pp 866-872, (Sept 1967)

1967 Richards, C. G. and Graebel, W. P., "A Numerical Study of the Flow Due to a Rotating Disk with a Center Sink," ASME Trans., Journ. of Basic Eng., p 807, (Dec 1967)

1967 Friedman, M. and Gillis, J., "Viscous Flow in a Pipe With Absorbing Walls," ASME Trans., Journ. of Appl. Mech., pp 819-822 (Dec 1967)

1967 Pan, F. and Acrivos, A., "Steady Flows in Rectangular Cavities," Journ. Fluid Mech., VOL 28, Part 4, pp 643-655

1967 Freudiger, F. A., Gallaher, W. H., and Thommen, H. U., "Numerical Calculation of the Low Reynolds Number Flow Over a Blunt Wedge with Rearward Facing Step," Office of Aerospace Research, ARL 67-0151

1967 Rhodes, J. M., Ph.D. Thesis, U. of Tennessee

1967 Chorin, A. J., "The Numerical Solution of the Navier-Stokes Equations for an Incompressible Fluid," Bull. Am. Math. Soc., 73, pp 928-931

1968 Petrishchev, V., "A Cylinder in a Viscous Incompressible Fluid Flow," Izvestia AN SSSR MZhG, No. 1

1968 Acrivos, A., Leal, L. G., Snowden, D. D., and Pan, F., "Further Experiments on Steady Separated Flows Past Bluff Objects," Journ. Fluid Mech., VOL 34, Part 1, pp 25-48

1968 Mills, R. D., "Numerical Solutions of Viscous Flow Through a Pipe Orifice at Low Reynolds Numbers," Journ. Mech. Eng. Sci., VOL 10, No. 2, pp 133-140, (Feb 1968)

1968 Scala, S. M. and Gordon, P., "Solution of the Time Dependent Navier-Stokes Equations for Flow Around a Circular Cylinder," AIAA Journ., VOL 6, No. 5, pp 815-822, (May 1968)

1968 Strawbridge, D. R. and Hooper, G. T. J., "Numerical Solutions of the Navier-Stokes Equations for Axisymmetric Flows," Journ. of Mech. Eng. Sci., VOL 10, No. 5, pp 389-401, (May 1968)

1968 Boyd, K. E. and Rice, W., "Laminar Inward Flow of an Incompressible Fluid Between Rotating Disks, with Full Peripheral Admission," ASME Trans. Journ. of Applied Mech., pp 229-237, (June 1968)

1968 Leclair, B. P. and Hamielec, A. E., Ind. Eng. Chem. Fund., VOL 7, p 542

1968 Allen, J. S., Numerical Solutions of the Compressible Navier-Stokes Equations for the Laminar Near Wake in Supersonic Flow, Ph.D. Thesis, Princeton University (June 1968)

1968 Chorin, A. J., "On the Convergence of Discrete Approximations to the Navier-Stokes Equations," NYO-1480-106, AEC Computing and Applied Math. Center, N.Y., (July 1968)

1968 Seventh Symposium of Naval Hydrodynamics, Office of Naval Research, Rome, Italy (Aug 1968)
Relevant papers:
Macagno, E. and Hung, T. K., "Growth of Eddies in a Flow Expansion," pp 1609-1613
Piacsek, S. A., "Some Problems in the Numerical Solution of Three Dimensional, Incompressible Fluid Flows," pp 1615-1618
Gauthier, M., "Numerical Solutions of the Two-Dimensional Navier-Stokes Equations," pp 1618-1619

1968 Taylor, P. J., "The Stability of Boundary Conditions in the Numerical Solution of the Time Dependent Navier-Stokes Equations," A.R.C. 30406, (Aug 1968), (Clearinghouse order No. AD-679436)

1968 Thompson, J. F., Jr., "Numerical Solution of the Incompressible Two-Dimensional, Time Dependent Navier-Stokes Equations for a Body Oscillating in Pitch in a Moving Fluid," Dept of Aerophysics and Aerospace Eng., Miss. St. U., Rept No. 86, (Oct 1968), (Clearinghouse order No. AD-678611)

1968 Torrance, K. E., "Comparison of Finite-Difference Computations of Natural Convection," Journ. of Res. of NB.S., VOL 72B, No. 4 (Oct 1968)

1968 Jenson, V. G., Horton, J. R. and Wearing, J. R., Trans. Inst. Chem. Engr., VOL 46 p. 177

1968 Masliyah, J. H. and Epstein, N., Ind. Eng. Chem. Fund., VOL 8, p. 602

1968 Friedmann, M., Gillis, J., and Liron, N., "Laminar Flow in a Pipe at Low and Moderate Reynolds Numbers," Applied Sci. Res., 19 pp 426-438, (Nov 1968)

1968 Heat and Mass Transfer in Recirculating Flows, Dept of M.E. Imperial College, Post Experience Course (Dec 1968)
Relevant Lectures:
Taylor, R. G., "The Basic Differential Equations," Lecture 1
Spalding, D. B., "Finite-Difference Equations," Lecture 2
Runchal, A. K., "Computation of Laminar Flow," Lecture 3
Gosman, A. D., "Structure of Computer Program," Lecture 6

1968 Chorin, A. J., "Numerical Solution of the Navier-Stokes Equations," Math of Computation, 22, pp 745-762

1968 Rimon, Y., "Numerical Solutions of the Time Dependent Incompressible Viscous Flow, Ph.D. Thesis, Princeton U. (Also see Aerospace Res. Lab Rept 69-0063, Clearinghouse order AD-691842)

1968 Textor, R. E., "A Numerical Investigation of a Confined Vortex Problem," Rept No. K-1732, Nuclear Div. Union Carbide Corp.

1968 Hwang, J., On Numerical Solutions of the General Navier-Stokes Equations for Two-Layered Stratified Flows, Ph.D. Thesis, Oregon State U.

1968 Beus, S., Compressible Viscous Flow in Varying Area Ducts, Ph.D. Thesis, Carnegie-Mellon U.

1968 Phillips, B., A Numerical Investigation of Laminar Newtonian Flow in a Sudden Expansion and Tee, Ph.D. Thesis, U. of Tennessee

1969 Son, J. S. and Hanratty, T. J., "Numerical Solution for Flow Around a Cylinder at Reynolds Numbers of 40, 200 and 500," Journ. of Fluid Mech., VOL 35, Part 2, pp 369-386

1969 Greenspan, D., "Numerical Studies of Steady, Viscous Incompressible Flow in a Channel with a Step," Journ. of Eng. Math., VOL 3, No. 1, pp 21-28 (Jan 1969)

1969 Hamielec, A. E. and Raal, J. D., "Numerical Studies of Viscous Flow Around Circular Cylinders," Phys. Fluids, VOL 12, No. 1 pp 11-17, (Jan 1969)

1969 Rimon, Y., "Numerical Solution of the Incompressible Time Dependent Viscous Flow Past a Thin Oblate Spheroid," NSRDL, Washington, D.C. Rept 2955, (Jan 1969)

1969 Rimon, Y. and Lugt, H. J., "On Laminar Flow Past Oblate Spheroids of Various Thicknesses," NSRDL, Washington, D.C., Appl. Math. Lab. Note AML 16-69, (Mar 1969)

1969 Runchal, A. K. and Wolfshtein, M., "Numerical Integration Procedure for the Steady State Navier-Stokes Equations," Journ. of Mech. Eng. Sci., VOL 11, No. 5, pp 445-453

1969 Rimon, Y. and Cheng, S. I., "Numerical Solution of a Uniform Flow Over a Sphere at Intermediate Reynolds Numbers," Phys. Fluids, VOL 12, No. 5, pp. 949-959, (May 1969)

1969 O'Leary, R. A. and Mueller, T. J., "Correlation of Physical and Numerical Experiments for Incompressible Laminar Separated Flows," Proj. THEMIS, Tech Rept UND-69-4, (July 1969)

1969 Dennis, S. C. R. and Chang, G. Z. . "Numerical Integration of the Navier-Stokes Equations in Two Dimensions," MRC Tech Sum. Rept 859, Univ. of Wisc. (July 1969), (Clearinghouse order No. AD-699001)

1969 Schonauer, W., "Solution of the Three-dimensional Time Dependent Navier-Stokes Equations by the Difference Method," (in German), (July 1969), (Clearinghouse order No. N70-38683)

1969 Atkinson, B., Brocklebank, M., Card, C., and Smith, J., "Low Reynolds Number Developing Flows," A.I.Ch.E. Journ., VOL 15, No. 4, pp 548-553, (July 1969)

1969 Beardsley, R. C., "Alternative Finite Difference Approximations for the Viscous Generation of Vorticity at a Stationary Fluid Boundary," M.I.T. Rept GFD/69-2, (Oct 1969), (Clearinghouse order No. AD-697669)

1969 Lugt, H. and Rimon, Y., "Finite-Difference Approximations of the Vorticity of Laminar Flows at Solid Surfaces," NSRDL, Washington, D.C., Appl. Math. Lab. Tech. Note, AML-67-69, (Sept 1969)

1969 Thompson, J. F., "Optimized Acceleration of Convergence of an Implicit Numerical Solution of the Time-Dependent Navier-Stokes Equations," AIAA Journ. Tech Notes, VOL 7, No. 11, pp 2186-2188, (Nov 1969)

1969 Thommen, H. U., "Calculation of High Reynolds Number Flow Fields by Numerical Methods," Off. of Aerospace Res., ARL 69-0194, (Nov 1969), (Clearinghouse AD-702144)

1969 Mehta, U. B. and Lavan, Z., "Flow in a Two-dimensional Channel with a Rectangular Cavity," ASME Trans. Journ. of Appl. Mech., pp 897-901, (Dec 1969)

1969 Rimon, Y. and Lugt, H. J., "Laminar Flows Past Oblate Spheroids of Various Thicknesses," Phys. Fluids, VOL 12, No. 12, pp 2465-2472 (Dec 1969)

1969 High Speed Computing in Fluid Dynamics, published as Physics of Fluids Supplement II, (Dec 1969)
Relevant articles:
Runchal, A. K., Spalding, D. B., Wolfshtein, M., "Numerical Solution for the Transport of Vorticity, Heat and Matter in Two-dimensional Flow," pp 21-28
Cheng, S.I., "Accuracy of Difference Formulation of Navier-Stokes Equations," pp 34-40
Takami, H. and Keller, H. B., "Steady Two Dimensional Viscous Flow of an Incompressible Fluid Past a Circular Cylinder," pp 51-56
Jain, P. C. and Rao, K. S., "Numerical Solution of Unsteady Viscous Incompressible Fluid Flow Past a Circular Cylinder," pp 57-64
Rimon, Y., "Numerical Solution of the Incompressible Time-dependent Viscous Flow Past a Thin Oblate Spheroid," pp 65-75
Thoman, D. C. and Szewczyk, A. A., "Time-dependent Viscous Flow Over a Circular Cylinder," pp 76-86
Takaisi, Y., "Numerical Studies of a Viscous Liquid Past a Circular Cylinder," pp 86-87
Dennis, S.C.R. and Chang, G. Z., "Numerical Integration of the Navier-Stokes Equations for Steady Two-dimensional Flow," pp 88-93
Kuwahara, K. and Imai, I., "Steady, Viscous Flow Within a Circular Boundary," pp 94-101
Kawaguti, M., "Numerical Study of the Flow of a Viscous Fluid in a curved channel" pp 101-104
Fromm, J. E., "Numerical Solutions of Two-dimensional Stall in Fluid Diffusers," pp 113-119

1969 Keller, H. B., (comments on), "Numerical Studies of Viscous Flow Around Circular Cylinder," Phys. Fluids, 13, pp 533-534

1969 Hamielec, A. E. and Raal, J. D., (Reply to comments by H. B. Keller), Phys. Fluids, 13, pp 534-535

1969 Williams, G. P., "Numerical Integration of the Three-dimensional Navier-Stokes Equations for Incompressible Flow," Journ. Fluid Mech., VOL 37, Part 4, pp 727-750

1969 Blaisdell, J., A Finite Difference Solution of the Viscous Flow Through Axisymmetric Channels, Ph.D. Thesis, North Carolina St.U.

1969 Hurd, A., Analysis of Flow Separation in a Confined Two-dimensional Channel, Ph.D. Thesis, U. of Nebraska

1969 Aung, W., Heat Transfer in the Separated Region Beyond a Rearward Facing Step, Ph.D. Thesis, U. of Minnesota

1970 Gromov, B. and Petrishchev. V., "The Temperature and Dynamic Conditions of a Cylinder in a Distributed Flow of a Viscous Fluid," Fourth Int. Heat Transf. Conf. VOL III Forced Convection, Paris 1970

1970 Krall, K. M. and Eckert, E. R. G., "Heat Transfer to a Transverse Circular Cylinder at Low Reynolds Numbers Including Rarefaction Effects," Fourth Int. Heat. Transf. Conf. VOL III Forced Concsction, Paris 1970

1970 Jarski, E. J. Dynamics of Viscous Fluid Oscillations in Hydraulic Lines, Ph.D. Thesis, U. of Maryland, (Jan 1970), also NSRDL Annapolis, Maryland Rept 3201

1970 Trulio, J. G. and Walitt, L., "Numerical Calculations of Viscous Compressible Fluid Flow Around a Stationary Cylinder,", NASA CR-1465, (Jan 1970)

1970 Allen, J. S. and Cheng, S. I., "Numerical Solutions of the Compressible Navier-Stokes Equations for the Laminar Near Wake," Phys of Fluids, VOL 13, No. 1, pp 37-52, (Jan 1970)

1970 Harlow, F. H., Fluid Dynamics-An Introductory Text, Los Alamos Rept LA 4100, (Feb 1970)

1970 Friedman, M., "Flow in a Circular Pipe with Recessed Walls," ASME Trans. Journ. of Applied Mech., pp 5-8, (Mar 1970)

1970 Lee, J. S. and Fung, Y. C., "Flow in Locally Constricted Tubes at Low Reynolds Numbers," ASME Trans. Journ. of Applied Mech., pp 9-16, (Mar 1970)

1970 Donovan, L. F., "A Numerical Solution of Unsteady Flow in a Two-dimensional Square Cavity", AIAA Journ., VOL 8, No. 3, pp 524-529, (Mar 1970)

1970 Roache, P. J. and Mueller, T. J., "Numerical Solution of Laminar Separated Flows," AIAA Journ. VOL 8, No. 3, pp 530-538, (Mar 1970)

1970 Amsden, A. and Harlow, F. H., "A Simplified MAC Technique for Incompressible Fluid Flow Calculations," Journ. Comput. Phys., 6, pp 322-325

1970 Roache, P. J., "Sufficiency Conditions for a Commonly Used Downstream Boundary Condition on Stream Function," Journ. Comput. Phys., 6, pp 317-321

1970 Putre, H. A., "Computer Solutions of the Unsteady Navier-Stokes Equations for an Infinite Hydrodynamic Step Bearing," NASA TN D-5682 (April 1970)

1970 Masliyah, J. H., Ph.D. Thesis, U. of British Columbia

1970 Amsden, A. A. and Harlow, F. H., "The SMAC Method: A Numerical Technique for Calculating Incompressible Fluid Flows," Los Alamos Lab Rept LA 4370, (May 1970)

1970 Pao, H. P., "A Numerical Computation of a Confined Rotating Flow," Trans. ASME Journ. Appl. Mech., pp 480-487 (June 1970)

1970 Masliyah, J. H. and Epstein, N., "Numerical Study of Steady Flow Past Spheroids," Journ. Fluid Mech., VOL 44, Part 3 pp 493-512

1970 Second International Conference on Numerical Methods in Fluid Dynamics, held at U. of California, Berkeley, Sept 1970, Holt, M. Chair., Abstracts of papers presented available from Clearinghouse AD-714156
Relevant Abstracts:
Gosman, A. D. and Spalding, D. B., "Computation of Laminar Flow Between Shrouded Rotating Disks"
Lugt, H. J. and Haussling, H. J., "Laminar Flows Past a Flat Plate at Various Angles of Attack"
Orszag, S. A., "Accuracy of Numerical Simulation of Incompressible Flows"
Koryavov, P. P. and Pavlovskii, Y., "Circular Cylinder Rotation in a Viscous Fluid Flow"
Ross, B. B. and Cheng, S. I., A Numerical Study of the Planar Laminar Near-Wake in a Supersonic Flow"
Fortin, M., Teman, R. and Peyret, R., "Calcul des Ecoulements D'un Fluide Visquex Incompressible"
Nichols, B. D., Recent Extensions to the Marker-and-Cell Method for Incompressible Fluid Flows"
Briley, W. R. and Walls, H. A., "A Numerical Study of Time-dependent Rotating Flow in a Cylindrical Container at Low and Moderate Reynolds Numbers"
Pritchett, J. W., "Incompressible Calculations of Underwater Explosion Phenomena"
Pracht, W. E., "Implicit Solution of Creeping Flows, with Application to Continental Drift"

1970 Proceedings of the 23rd Annual Conference on Engineering in Medicine and Biology, Washington, D. C. Nov 1970

Relevant papers:
Schuessler, G. B. and Hung, T. K., "Blood Flow Past a Stenotic Aortic Valve: A Computer Simulation," pg 23
Cheng, L., Clark, M. E. and Robertson, J. M., "Numerical Analysis of Oscillating Flow in the Vicinity of an Obstacle," pg 108

1970 Truesdell, Jr., L. C. and Adler, R. J., "Numerical Treatment of Fully Developed Laminar Flow in Helically Coiled Tubes," A.I.Ch.E. Journ. VOL 16, No. 6, pp 1010-1015 (Nov 1970)

1970 Cheng, S. I., "Numerical Integration of Navier-Stokes Equations," AIAA Journ., VOL 8, No. 12, pp 2115-2122, (Dec 1970)

1970 Korst, H. H. and Mueller, T. J., discussion of, "Laminar Separation, Reattachment and Transition of the Flow over a Downstream-facing Step," by Goldstein, R., et al, ASME Trans. Journ. Basic Eng., pp 732-741, (Dec 1970)

1970 Hurd, A. C. and Peters, A. R., "Analysis of Flow Separation in a Confined Two-dimensional Channel," ASME Trans. Journ. Basic Eng., pp 908-914, (Dec 1970)

APPENDIX C

DEVELOPMENT OF WALL BOUNDARY CONDITION FOR VORTICITY

Of several papers concerned with the specification of the vorticity on the solid boundaries of a flow field, that of Lugt and Rimon (22) is outstanding because they present the most general discussion of the method of imposing this boundary condition given to date. Their work is therefore used as the basis for the following analysis.

The continuity equation for axial symmetric flow, where x_1 and x_3 are the coordinates in the meridan plane and x_2 the azimuthal angle is (Rouse ([16])):

$$\frac{\partial}{\partial x_1}(h_2 h_3 V_1) + \frac{\partial}{\partial x_3}(h_1 h_2 V_3) = 0 \qquad \ldots\ldots[C\text{-}1]$$

where the quantities h_1, h_2 and h_3 are scale factors that relate the differential element of distance along an arc to an incremental distance along a coordinate axis:

$$dS_{x_i} = h_i \, dX_i \,, \qquad i = 1, 2, 3$$

and:

$$(dS)^2 = \sum_{i=1}^{3} (dS_{x_i})^2$$

Equation (C-1) can be exactly satisfied by introducing a stream function ψ such that:

$$V_1 = \frac{1}{h_3 h_2}\left(\frac{\partial \psi}{\partial x_3}\right)$$

$$V_3 = \frac{-1}{h_1 h_2}\left(\frac{\partial \psi}{\partial x_1}\right) \qquad \text{.....[C-2]}$$

If it is assumed that there is no flow in the azimuthal direction ($V_2 = 0$), then the non-zero component of vorticity, ζ, is given by:

$$\zeta = \frac{D^2\psi}{h_2} \equiv \frac{\zeta^*}{h_2} \qquad \text{.....[C-3]}$$

where the following definitions have been used:

$$D^2 \equiv G_1 \frac{\partial^2}{\partial x_1^2} + G_3 \frac{\partial^2}{\partial x_3^2} + H_2\left(\frac{\partial H_3}{\partial x_1}\frac{\partial}{\partial x_1} + \frac{\partial H_1}{\partial x_3}\frac{\partial}{\partial x_3}\right)$$

$$G_1 \equiv \frac{1}{h_1^2}, \quad G_2 \equiv \frac{1}{h_2^2}, \quad G_3 \equiv \frac{1}{h_3^2}$$

$$H_1 \equiv \frac{h_1}{h_2 h_3}, \quad H_2 \equiv \frac{h_2}{h_3 h_1}, \quad H_3 \equiv \frac{h_3}{h_1 h_2} \qquad \text{.....[C-4]}$$

The vorticity transport equation in the x_2 direction may be written as (16):

$$D^2(\zeta^*) = G_2 H_2 Re\left[\frac{2}{h_2}\frac{\partial(\psi, h_2)}{\partial(x_1, x_3)}\zeta^* - \frac{\partial(\psi, \zeta^*)}{\partial(x_1, x_3)}\right] \qquad \text{.....[C-5]}$$

Figure C-1 shows the configuration under consideration. Along the

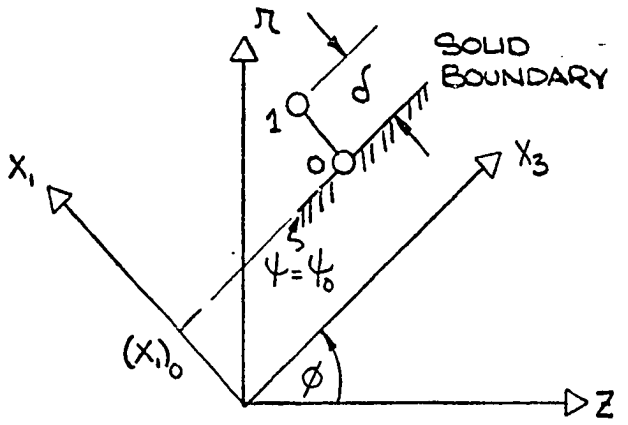

Figure (C-1)

Coordinate System of Surface Vorticity Evaluation

surface $(x_1)_o$ there is no slip, so from equation (C-3):

$$(V_1)_o = \left(\frac{1}{h_3 h_2}\frac{\partial \psi}{\partial X_3}\right)_o = 0$$

$$(V_3)_o = \left(\frac{-1}{h_1 h_2}\frac{\partial \psi}{\partial X_1}\right)_o = 0$$

which are generalized to read:

$$\left(\frac{\partial^n \psi}{\partial X_3^n}\right)_o = \left(\frac{\partial^n \psi}{\partial X_1 \partial X_3^{n-1}}\right)_o = 0 \quad , \; n \geq 1$$

Using these conditions in differentiations of equation (C-3):

$$(\zeta^*)_o = \left[G_1 \frac{\partial^2 \psi}{\partial X_1^2}\right]_o \qquad \text{.....[C-6]}$$

$$\left(\frac{\partial \zeta^*}{\partial X_1}\right)_o = \left[\left(\frac{\partial G_1}{\partial X_1} + H_2 \frac{\partial H_3}{\partial X_1}\right)\left(\frac{\partial^2 \psi}{\partial X_1^2}\right) + G_1 \frac{\partial^3 \psi}{\partial X_1^3}\right]_o \qquad \text{.....[C-7]}$$

$$\left(\frac{\partial^2 \zeta^*}{\partial x_1^2}\right)_o = \left[G_1\frac{\partial^4\psi}{\partial x_1^4} + \left(2\frac{\partial G_1}{\partial x_1} + H_2\frac{\partial H_3}{\partial x_1}\right)\left(\frac{\partial^3\psi}{\partial x_1^3}\right) + \left(\frac{\partial^2 G_1}{\partial x_1^2} + 2\frac{\partial H_2}{\partial x_1}\frac{\partial H_3}{\partial x_1} + 2H_2\frac{\partial^2 H_3}{\partial x_1^2}\right)\left(\frac{\partial^2\psi}{\partial x_1^2}\right) + G_3\frac{\partial^4\psi}{\partial x_1^2\partial x_3^2} + H_2\frac{\partial H_1}{\partial x_3}\left(\frac{\partial^3\psi}{\partial x_1^2\partial x_3}\right)\right]_o \quad \ldots\ldots[C\text{-}8]$$

$$\left(\frac{\partial \zeta^*}{\partial x_3}\right)_o = \left[\frac{\partial G_1}{\partial x_3}\frac{\partial^2\psi}{\partial x_1^2} + G_1\frac{\partial^3\psi}{\partial x_3\partial x_1^2}\right]_o \quad \ldots\ldots[C\text{-}9]$$

$$\left(\frac{\partial^2 \zeta^*}{\partial x_3^2}\right)_o = \left[\frac{\partial^2 G_1}{\partial x_3^2}\frac{\partial^2\psi}{\partial x_1^2} + 2\frac{\partial G_1}{\partial x_3}\frac{\partial^3\psi}{\partial x_1^2\partial x_3} + G_1\frac{\partial^4\psi}{\partial x_3^2\partial x_1^2}\right]_o \quad \ldots\ldots[C\text{-}10]$$

In addition, from equation (C-5):-

$$\left[G_1\frac{\partial^2 \zeta^*}{\partial x_1^2} + G_3\frac{\partial^2 \zeta^*}{\partial x_3^2} + H_3\left(\frac{\partial H_3}{\partial x_1}\frac{\partial \zeta^*}{\partial x_1} + \frac{\partial H_1}{\partial x_3}\frac{\partial \zeta^*}{\partial x_3}\right)\right]_o = 0 \quad \ldots\ldots[C\text{-}11]$$

Substituting equations (C-7) through (C-10) into (C-11) and solving for $(\partial^4\psi/\partial x_1^2\partial x_3^2)_o$ produces:

$$\left(\frac{\partial^4\psi}{\partial x_1^2\partial x_3^2}\right)_o = \left\{-\frac{G_1}{2G_3}\frac{\partial^4\psi}{\partial x_1^4} - \frac{1}{G_3}\left(\frac{\partial G_1}{\partial x_1} + H_2\frac{\partial H_3}{\partial x_1}\right)\frac{\partial^3\psi}{\partial x_1^3} - \left(\frac{H_2}{G_3}\frac{\partial H_1}{\partial x_3} + \frac{1}{G_1}\frac{\partial G_1}{\partial x_1}\right)\frac{\partial^3\psi}{\partial x_1^2\partial x_3} - \left[\frac{G_1\left(\frac{\partial^2 G_1}{\partial x_1^2} + 2\frac{\partial H_1}{\partial x_1}\frac{\partial H_3}{\partial x_1} + 2H_2\frac{\partial^2 H_3}{\partial x_1^2}\right) + G_3\frac{\partial^2 G_1}{\partial x_1^2} + H_2\frac{\partial H_3}{\partial x_1}\left(\frac{\partial G_1}{\partial x_1} + H_2\frac{\partial H_3}{\partial x_1}\right) + H_2\frac{\partial H_1}{\partial x_3}\frac{\partial G_1}{\partial x_3}}{2G_1G_3}\right]\frac{\partial^2\psi}{\partial x_1^2}\right\} \quad \ldots\ldots[C\text{-}12]$$

Combining equations (C-8) and (C-12) yields:

$$\left(\frac{\partial^2 \zeta^*}{\partial x_1^2}\right)_0 = \left\{\frac{G_1}{2}\frac{\partial^4 \psi}{\partial x_1^4} + \frac{\partial G_1}{\partial x_1}\frac{\partial^3 \psi}{\partial x_1^3} + \left[\frac{1}{2}\frac{\partial^2 G_1}{\partial x_1^2} + \frac{\partial H_2}{\partial x_1}\frac{\partial H_3}{\partial x_1} + H_2\frac{\partial^2 H_3}{\partial x_1^2} - \frac{G_3}{2G_1}\frac{\partial^2 G_1}{\partial x_1^2}\right.\right.$$

$$\left.\left. - \frac{H_2}{2G_1}\frac{\partial H_3}{\partial x_1}\left(\frac{\partial G_1}{\partial x_1} + H_2\frac{\partial H_3}{\partial x_1}\right) - \frac{H_2}{2G_1}\frac{\partial H_1}{\partial x_3}\frac{\partial G_1}{\partial x_3}\right]\frac{\partial^2 \psi}{\partial x_1^2} - \frac{G_3}{G_1}\frac{\partial G_1}{\partial x_1}\frac{\partial^3 \psi}{\partial x_1^2 \partial x_3}\right\}_0$$

.....[C-13]

Since x_1 is normal to the boundary surface, h_1 = constant. Under this condition equations (C-7) and (C-13) simplify to:

$$\left(\frac{\partial \zeta^*}{\partial x_1}\right)_0 = \left[G_1\frac{\partial^3 \psi}{\partial x_1^3} + H_2\frac{\partial H_3}{\partial x_1}\frac{\partial^2 \psi}{\partial x_1^2}\right]_0$$

.....[C-14]

$$\left(\frac{\partial^2 \zeta^*}{\partial x_1^2}\right)_0 = \left\{\frac{G_1}{2}\frac{\partial^4 \psi}{\partial x_1^4} + \left[\frac{\partial H_2}{\partial x_1}\frac{\partial H_3}{\partial x_1} + H_2\frac{\partial^2 H_3}{\partial x_1^2} - \frac{H_2}{2G_1}\left(\frac{\partial H_3}{\partial x_1}\right)^2\right]\frac{\partial^2 \psi}{\partial x_1^2}\right\}$$

.....[C-15]

Expanding ζ^* in a Tavlor's series in the direction normal to $(x_1)_0$:

$$\zeta_1^* = \zeta_0^* + \left(\frac{\partial \zeta^*}{\partial x_1}\right)_0 \delta + \left(\frac{\partial^2 \zeta^*}{\partial x_1^2}\right)_0 \frac{\delta^2}{2!} + O[\delta^3]$$

where: $\delta \equiv (x_1)_1 - (x_1)_0$

Inserting the expressions obtained for the derivatives i.e., equations (C-6), (C-14) and (C-15) into the expansion gives:

$$\zeta_1^* = \zeta_0^* + \frac{6(G_1)_0}{\delta^2}\left[\left(\frac{\partial^3 \psi}{\partial x_1^3}\right)_0 \frac{\delta^3}{3!} + \left(\frac{\partial^4 \psi}{\partial x_1^4}\right)_0 \frac{\delta^4}{4!}\right] +$$

$$\left\{\left(H_2\frac{\partial H_3}{\partial x_1}\right)_0 \delta + \left[\left(\frac{\partial H_3}{\partial x_1}\right)_0\left(\frac{\partial H_2}{\partial x_1}\right)_0 + \left(H_2\frac{\partial^2 H_3}{\partial x_1^2}\right)_0 - \frac{1}{2(G_1)_0}\left(H_1\frac{\partial H_2}{\partial x_1}\right)_0^2\right]\frac{\delta^2}{2}\right\}\frac{\zeta_0^*}{(G_1)_0} + O[\delta^3]$$

Similarly, a Taylor expansion for ψ normal to the boundary can be written as:

$$\psi_1 = \psi_0 + \frac{\zeta_0^*}{(G_1)_0}\frac{\delta^2}{2!} + \left[\left(\frac{\partial^3\psi}{\partial x_1^3}\right)_0\frac{\delta^3}{3!} + \left(\frac{\partial^4\psi}{\partial x_1^4}\right)_0\frac{\delta^4}{4!}\right] + O[\delta^5]$$

Uniting the last two equations and solving for ζ_0^*:

$$\zeta_0^* = \frac{\frac{6}{\delta^2}(G_1)_0(\psi_1-\psi_0) - \zeta_1^*}{2-\left(\frac{H_2}{G_1}\frac{\partial H_3}{\partial x_1}\right)_0\delta - \left(\frac{G_1}{2}\right)_0\left[\frac{\partial H_2}{\partial x_1}\frac{\partial H_3}{\partial x_1} + H_2\frac{\partial^2 H_3}{\partial x_1^2} - \frac{H_2^2}{2G_1}\left(\frac{\partial H_3}{\partial x_1}\right)^2\right]_0\delta^2}$$

or with the definitions of (C-4) inserted:

$$\zeta_0^* = \frac{\frac{6}{(h_1^2)_0}\frac{(\psi_1-\psi_0)}{\delta} - \zeta_1^*}{2-\left[\frac{h_2}{h_3}\frac{\partial(h_3/h_2)}{\partial x_1}\right]_0\delta - \left\{2\frac{\partial(h_2/h_3)}{\partial x_1}\frac{\partial(h_3/h_2)}{\partial x_1} + 2\frac{h_2}{h_3}\frac{\partial^2(h_3/h_2)}{\partial x_1^2} - \left(\frac{h_2}{h_3}\right)^2\left[\frac{\partial^2(h_2/h_3)}{\partial x_1^2}\right]^2\right\}\frac{\delta^2}{4}} + O[\delta^3]$$

For axisymmetric flow:

$$h_1 = h_3 = 1\,, \quad h_2 = r = x_1\cos\phi + x_3\sin\phi$$

so that:

$$\left[\frac{\partial(h_3/h_2)}{\partial x_1}\right]_0 = -\frac{\cos\phi}{r_0^2}\,, \quad \left[\frac{\partial^2(h_3/h_2)}{\partial x_1^2}\right]_0 = \frac{2\cos\phi}{r_0^3}\,, \quad \left[\frac{\partial(h_2/h_3)}{\partial x_1}\right]_0 = \cos\phi$$

Therefore:

$$\zeta_0 = \frac{\frac{6}{r_0\delta^2}(\psi_1-\psi_0) - \frac{r_1}{r_0}\zeta_1}{2 + \cos\phi\frac{\delta}{r_0} - \left(\frac{\cos\phi}{2}\frac{\delta}{r_0}\right)^2} + O[\delta^3] \qquad \text{.....[C-16]}$$

APPENDIX D

PREVIOUS TREATMENT OF INTRUDING CORNERS

Intruding corners are especially troublesome in the calculations because they are such large sources of vorticity generation. They have therefore received extensive attention in the literature. Some of the methods of dealing with the corners are individually detailed in the following. There is no particular order of presentation intended. Note that some of the studies cited were carried out in plane flow but are included for completeness.

1. Hung and Macagno (18) and (35) considered flow through a sudden pipe expansion, Figure (D-1A). They tried to force separation to occur at the corner by determining ζ_0 from a horizontal pipe wall equation, which is almost identical to equation (3-24) presented earlier and is written as:

$$\zeta_0 = \frac{\frac{6}{h^2 r_0}(\psi_1 - \psi_0) - \frac{r_2}{r_0}\zeta_1 - \frac{h}{2r_0}\zeta_2}{2 - \frac{h}{2r_0} + \frac{h^4}{4r_0^2}} + O[h^3] \qquad \text{.....[D-1]}$$

2. Kawaguti (40) analyzed plane flow through a contraction and expansion of a channel, Figure (D-1B). He let $\psi_1 = \psi_3$ and $\psi_2 = \psi_4$ and then used a finite difference form of equation (3-7) i.e.,:

$$\zeta_0 = -(\nabla^2\psi)_0 = -\frac{\psi_1 + \psi_2 + \psi_3 + \psi_4 - 4\psi_0}{h^2} = -\frac{2(\psi_1 + \psi_2)}{h^2}, \psi_0 = 0 \qquad \text{.....[D-2]}$$

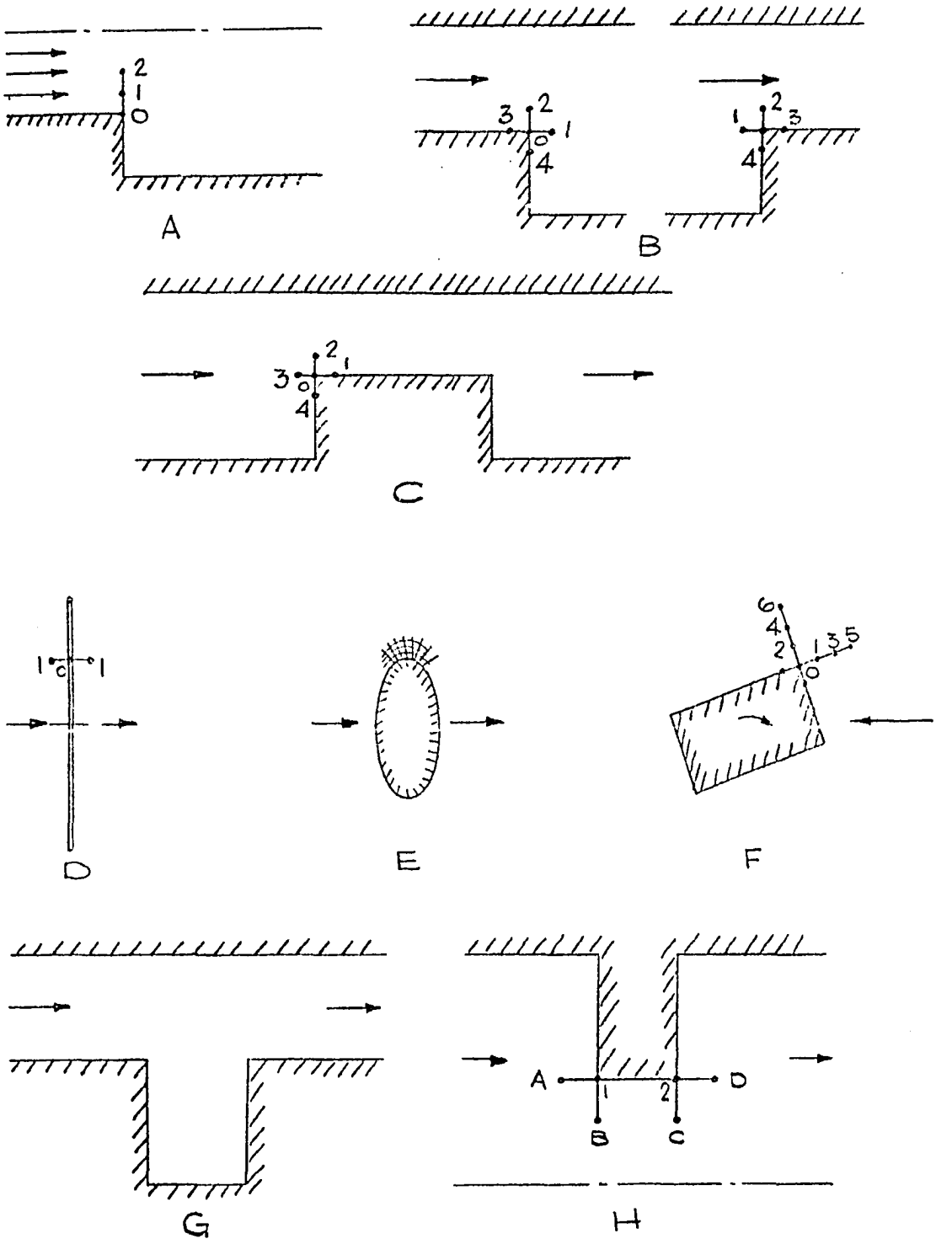

Figure D-1

Various Problems Involving Sharp Intruding Corners or Edges

Hung in (18) claims to have used this form but discarded it because it is only of O(h) accuracy.

3. Greenspan (19) treated the problem of plane flow over a rectangular obstacle on a channel wall, Figure (D-1C). Like Kawaguti, above, a four point star was placed on the corner node point and the corner vorticity was determined from the following since ψ_1, ψ_4, and ψ_0 were set equal to zero i.e., their wall boundary value:

$$\zeta_0 = -\frac{\psi_1+\psi_2+\psi_3+\psi_4-4\psi_0}{h^2} = -\frac{(\psi_3+\psi_2)}{h^2} \qquad \text{.....[D-3]}$$

4. Michael (8) worked on the axisymmetric flow around a circular disk, Figure (D-1D). The standard two-point form of equations (3-23) and (3-26):

$$\zeta_0 = \frac{3}{h^2 r_0}(\psi_1-\psi_0) - \frac{\zeta_1}{2} \qquad \text{.....[D-4]}$$

was used on both faces of the disk to within one grid point of the corner. A 4-point extrapolation formula was then used to determine the corner value of vorticity. This technique has been criticized by Rimon and Lugt in (9). These authors considered axisymmetric flow past an oblate spheroid for various thickness ratios, Figure (D-1E). In as much, the situation of an infinitely thin disk treated by Michael corresponds to the limiting zero thickness solution of Rimon and Lugt. These authors used a very fine mesh near the sharp corner and determined the surface vorticity by a second-order, one-sided differencing in double

precision arithmetic. In particular, the separation point prediction disagreed noticeably with that predicted by Michael. The difference between the two was attributed to Michael's technique of determining ζ_o at the sharp edge.

5. Thompson (41) investigated two dimensional unsteady flow past a body which is oscillating in pitch, Figure (D-1F). Three forms of corner vorticity calculation were tried. The first form was the same as that used by Greenspan above. This method was abandoned however because it produced irregularities in ψ ahead of the body. In the second method, Thompson started with:

$$\zeta_o = \left(\frac{\partial v}{\partial x} - \frac{\partial u}{\partial y}\right) \qquad \ldots\ldots [D\text{-}5]$$

Then a one sided difference, e.g.:

$$\left(\frac{\partial v}{\partial x}\right)_{ij} = \frac{-3v_{ij} + 4v_{i+1,j} - v_{i+2,j}}{2h} \qquad \ldots\ldots [D\text{-}6]$$

$$v_{ij} = -\left(\frac{\partial \psi}{\partial x}\right)_{ij} = \frac{\psi_{i-1,j} - \psi_{i+1,j}}{2h} \qquad \ldots\ldots [D\text{-}7]$$

are used along with similar forms for $(\partial u/\partial y)_{ij}$ in equation (D-5) to produce:

$$\zeta_o = \frac{2\psi_o - \frac{1}{4}(\psi_1 + \psi_2) - (\psi_3 + \psi_4) + \frac{1}{4}(\psi_5 + \psi_6)}{h^2} \qquad \ldots\ldots [D\text{-}8]$$

where the fact that u and v vanish at the surface of the body is taken into account. This form also produces some stream function irregular-

ities and was also discarded. However, it was preferred compared to the first technique. In the last method tried, a 5-point difference for the velocity gradients were used and for the corner shown in Figure (D-1F), the corner vorticity is calculated from:

$$\zeta_0 = \frac{\frac{2}{3}\psi_6 - \frac{1}{24}(\psi_1 + \psi_2 - 8\psi_3 - 8\psi_4 - \psi_5 - \psi_6)}{h^2} \quad \text{.....[D-9]}$$

Thompson claimed that this form produced no irregularities, but in a preliminary phase of the present study, this method tended to give a rather small wake region.

6. Mehta and Lavan (42) studied the flow in a rectangular cavity located in the lower wall of a two dimensional channel, Figure (D-1G). The corner value of vorticity was calculated using the same form as that used by Greenspan in the above. However, after convergence was assured, the solution near the corner was improved by subdividing the region near each corner into finer meshes and iterating further. The success of this method is obviously dependent upon the accuracy of the boundary values on the faces of the cutaway region surrounding the corners. These improved corner results are next used to reiterate the main flow and then the entire cycle is repeated until a desired convergence is obtained.

7. Mills (1) studied steady flow through a circular pipe orifice, Figure (D-1H). The corner vorticity was determined by a technique suggested by Thom many years ago in (24). In this method, the corner ζ_0 is presumed to be double valued. One value comes from a calculation in the

axial direction using equation (3-23), and the other from an expansion in the radial direction, equation (3-24). During the main flow calculation the appropriate value is then used, i.e., at points like A and D of Figure (D-1H) the axial ζ_0 is used while at points like B and C, the radial ζ_0 is employed. The same technique had been previously used by Lester in (20) for flow past both open and closed end Pitot tubes symmetrically located in a pipe.

8. Jarski (43) considered oscillating zero Reynolds number flow through a circular pipe orifice, Figure (D-1H). The corner vorticity was obtained by summing the vorticity secured from Taylor series expansions in both the axial and the radial directions i.e., equations (3-23) and (3-24). The technique was not altogether successful as it produced a slight hump in ψ near the corner.

A notable treatment of the entruding corner has been given by Roache, who treated flow over a backward facing step, in (44). Unfortunately, at the time of this writing that work was unavailable. A shorter version of this work was presented by Roache and Mueller in (36). In that study, it was mentioned that seven different methods for calculating the corner ζ_0 had been tried. Some involved rounding the sharp corner. The method finally agreed upon was the double valued, discontinuous treatment originated by Thom and used in Mills' paper. Even though the equation for calculating the particular corner ζ_0 differs from the equation used by Mills and Lester, the way in which the corner ζ_0 values were utilized is the same.

APPENDIX E

COMPUTER PROGRAM LISTING

```
C
C.....
C
C     NAME: ORIFIC
C
C     PURPOSE: TO NUMERICALLY SOLVE FOR STEADY, AXISYMMETRIC,
C              INCOMPRESSIBLE, VISCOUS FLOW THROUGH A PIPE ORIFICE
C              USING A GRADED MESH AND A 5-POINT FINITE DIFFERENCE
C              OPERATOR
C
C     PARAMETER DEFINITIONS:
C       MAJOR FIELD VARIABLES
C       ---------------------
C       S-STREAM FUNCTION
C       V-VORTICITY
C       Z-AXIAL DIMENSION
C       R-RADIAL DIMENSION
C       PDROP-PRESSURE DROP
C       VU-RADIAL VELOCITY COMPONENT
C       VV-AXIAL VELOCITY COMPONENT
C       BETA-RELAXATION PARAMETER
C       RE-REYNOLDS NUMBER
C       V1-ORIFICE CORNER VORTICITY-FRONT-AXIAL
C       V2-ORIFICE CORNER VORTICITY-FRONT-RADIAL
C       V12-ORIFICE CORNER VORTICITY-FOR SHARPE EDGE
C       V3-ORIFICE CORNER VORTICITY-REAR-RADIAL
C       V4-ORIFICE CORNER VORTICITY-REAR-AXIAL
C       L-ITERATION SWEEP NUMBER
C       KN-NO. OF STREAMLINES TO BE FOLLOWED IN THE INTERPOLATION
C       KV-NO. OF VORTICITIES TO BE FOLLOWED IN THE INTERPOLATION
C       ES-VALUE OF S OR V TO BE USED IN THE INTERPOLATION
C       GRID PARAMETERS
C       --------------
C       J-RADIAL NODE POINT INTEGER
C       I-AXIAL NODE POINT INTEGER
C       N-TOTAL NO. OF RADIAL NODE POINTS
C       M-TOTAL NO. OF AXIAL NODE POINTS
C       IF-INTEGER LOCATION OF UPSTREAM FACE OF ORIFICE
C       IR-INTEGER LOCATION OF DOWNSTREAM FACE OF ORIFICE
C       JT-INTEGER LOCATION OF TOP OF ORIFICE FROM PIPE WALL
C       I1-AXAIAL INTEGER FLAG SIGNALLING A MESH SIZE CHANGE  (ONE
C          UNIT AHEAD OF ACTUAL CHANGE)
C       I12-SAME AS I1
C       I2-AXIAL INTEGER FLAG SIGNALLING A MESH SIZE CHANGE IS PAST
C       I3-SAME AS I1
C       I34-SAME AS I1
C       I4-SAME AS I2
C       J1-RADIAL COUNTERPART OF I1
C       J2-RADIAL COUNTERPART OF I2
C       J3-SAME AS J1
C       J4-SAME AS J2
C       ------------------------------------------
C       NOTE: MORE FLAGS SHOULD BE DEFINED AS NECESSARY
C       ------------------------------------------
C       KEDGE-INTEGER USED TO INDICATE ORIFICE EDGE TYPE:
C            = 0 -SQUARE EDGE
C            = 1 -SHARPE EDGE
```

```
C       H-SIZE OF FIRST AXIAL GRID SPACE
C       G-RATIO OF FIRST GRID SPACE AXIAL TO FIRST GRID SPACE RADIAL
C       HT-GRID WIDTH AT TOP OF RADIAL LEG OF STAR
C       HR-GRID WIDTH AT RIGHT OF AXIAL LEG OF STAR
C       KR-INTEGER INDICATOR FOR DISTRIBUTION OF GRID SIZES (RADIAL)
C       LR-INTEGER INDICATOR FOR RATIO OF GRID SIZES (RADIAL)
C       KZ-AXIAL COUNTERPART OF KR
C       LZ-AXIAL COUNTERPART OF LR
C       OPERATOR PARAMETERS
C       ------------------
C       CFD(I,J,K)-COEFFICIENTS FOR FIRST DIFFERENCES
C                  I INDEX-RATIO OF GRID SIZES
C                  J INDEX-DISTRIBUTION OF GRID SIZES
C                  K INDEX-COEFFICIENT NO. K=1 FOR A5, K=2 FOR A4, ETC
C       CSD(I,J,K)-COEFFICIENTS FOR SECOND DIFFERENCES
C       A1,,,A5-COEFFICIENTS OF FIRST DIFFERENCES - RADIAL
C       B1,,,B5-COEFFICIENTS OF SECOND DIFFERENCES - RADIAL
C       C1,,,C5-COEFFICIENTS OF FIRST DIFFERENCES - AXIAL
C       D1,,,D5-COEFFICIENTS OF SECOND DIFFERENCES - AXIAL
C       MISCELLANEOUS PROGRAM PARAMETERS
C       -------------------------------
C       INPUT-TYPE OF GRID INITIALIZATION TO BE USED
C       LIMIT-TOTAL NUMBER OF FIELD SWEEPS ALLOWED FOR THE RUN
C       NUMB-NO. OF DATA SETS READ FROM TAPE UNIT 8
C       KANDO-INDICATES IF LAST TAPE DATA SET READ FROM UNIT 8 SHOULD
C            BE STORED ON UNIT 9
C            = 0 - NO DO NOT STORE, ITERATE FURTHER
C            = 1 - YES STORE DATA
C       MORE-= 0 (NO MORE DATA LEFT ON TAPE UNIT 8)
C            = INTEGER (INDICATE THE NO. OF DATA SETS STILL TO BE READ)
C       KPR-PRINT INTERVAL
C       KPRINT-PRINT INTEGER
C       MNEW-NEW TOTAL NO. OF AXIAL NODE POINTS
C
C.....
C
      IMPLICIT DOUBLE PRECISION (A-H,O-Z)
      DIMENSION S(125,27),V(125,27),CFD(3,3,5),CSD(3,3,5),R(27),HT(27)
     1,HR(125),KZ(125),KR(27),LZ(125),LR(27),ES(13),XS(125),YS(5,13),
     2KY(13),FUN(4),JR(27),JTYPE(27),VU(27),VV(27),Q(27)
      DATA V/3375*0.0/,S/3375*0.0/,R/27*1.0/
      F(T)=(T*T*T*T-2.*T*T)*.5
      KPROB=0
C     ----------------
C     INPUT CARD DATA
C     ---------------
      READ(5,1)NPROB
      READ(5,3)CFD
      READ(5,3)CSD
   24 READ(5,1)N,M,H,RE,BETA,G
      READ(5,2)IF,IR,JT
      READ(5,2)I1,I12,I2,I3,I34,I4
      READ(5,2)J1,J2,J3,J4
      READ(5,2)INPUT,LIMIT,KEDGE,KPR
      READ(5,2)NUMB,KANDO,MNEW,MORE
      WRITE(6,14)N,M,H,RE,BETA,G
      WRITE(6,15)IF,IR,JT,I1,I12,I2,I3,I34,I4,J1,J2,J3,J4,INPUT,LIMIT,
```

```
115*          1KEDGE,KPR
116*           KPROB=KPROB+1
117*     C     ------------------
118*     C     FORMAT STATEMENTS
119*     C     ------------------
120*          1 FORMAT(2I5,4D10.0)
121*          2 FORMAT(6I5)
122*          3 FORMAT(9D8.0)
123*          4 FORMAT(3I5,6F15.7)
124*          5 FORMAT(35H  ----------------------------  )
125*          6 FORMAT(10F10.5)
126*          7 FORMAT(5F12.5)
127*          8 FORMAT(1H1 9X,'FLOW FIELD :'I4,'X'I3,/ 9X,'ORIFICE LOC :'3X,
128*           1'FRONT I='I3,/ 25X,'REAR  I='I3,/25X,'TOP   J='I3,/11X,
129*           2'GRID SYS. :'3X,'R DIRECTION' /
130*           327X,I3,'H'/27X,I3,'H/2'/27X,I3,'H/4'/27X,I3,'H/2'/27X,I3,'H'/
131*           425X,'Z DIRECTION' /
132*           527X,I3,'H'/27X,I3,'H/2'/27X,I3,'H/4'/27X,I3,'H/2'/27X,I3,'H'/
133*           69X, 'FLOW PARAM. :'3X,'RE=' F5.1 //)
134*          9 FORMAT(6F10.0)
135*         10 FORMAT(1H1,6X,'Z',2X,13F9.4)
136*         11 FORMAT(14F9.4)
137*         12 FORMAT(9X,13F9.4)
138*         13 FORMAT(90X,9I3)
139*         14 FORMAT(1H1,9X,'N=',I3,/,10X,'M=',I3,/,10X,'H=',F5.3,/,10X,'RE=',
140*           1F5.1,/,10X,'BETA=',F5.3,/,10X,'G=',F5.3,//)
141*         15 FORMAT(2016)
142*         16 FORMAT(1H1,3X,'I',4X,'J TYPE',4X,'P(Z2)-P(Z1)',6X,'P(Z)-P(0)')
143*         17 FORMAT(1H1,9X,'ITERATION LIMIT REACHED')
144*         18 FORMAT(1H0,5X,'INITIALIZATION POSITION NO. ',I5)
145*         19 FORMAT(1H1,25X,'FLOW FIELD EXTENDED TO MNEW =',I3)
146*     C    ----------------------------
147*     C     INITIALIZE INTEGER CONSTANTS
148*     C    ----------------------------
149*          KPRINT=KPR
150*          L=0
151*          MM1=M-1
152*          MM2=M-2
153*          MM3=M-3
154*          NM1=N-1
155*          NM2=N-2
156*          IFM4=IF-4
157*          IFM3=IF-3
158*          IFM2=IF-2
159*          IFM1=IF-1
160*          IRP1=IR+1
161*          IRP2=IR+2
162*          IRP3=IR+3
163*          IRP4=IR+4
164*          JTP1=JT+1
165*          JTP2=JT+2
166*          JTP3=JT+3
167*          JTP4=JT+4
168*          JA=0
169*          JB=J1
170*          JC=J3-J1
171*          JD=NM2-J3
```

```
172*            JE=0
173*            IA=I1
174*            IB=I12-I1
175*            IC=I3-I12
176*            ID=I34-I3
177*            IE=MM1-I34
178*     C      ----------------------
179*     C      SET UP GRID STRUCTURE
180*     C      ----------------------
181*            G1=H/G
182*            H1=6./(G1*G1)
183*            H2=1.-G1
184*            H3=2.-G1-G1*G1/4.
185*            G2=G1/G
186*            H5=6./(G2*G2)
187*         25 HT(1)=G1
188*            DO 65 J=2,N
189*            IF(J-J1)30,35,40
190*         30 KR(J)=2
191*            LR(J)=2
192*            HT(J)=HT(J-1)
193*            GO TO 65
194*         35 KR(J)=1
195*            LR(J)=3
196*            HT(J)=HT(J-1)*.5
197*            GO TO 65
198*         40 IF(J-J2)45,30,50
199*         45 KR(J)=KR(J-1)+1
200*            LR(J)=LR(J-1)
201*            HT(J)=HT(J-1)
202*            GO TO 65
203*         50 IF(J-J3)30,55,60
204*         55 KR(J)=1
205*            LR(J)=1
206*            HT(J)=HT(J-1)*2.
207*            GO TO 65
208*         60 IF(J-J4)45,30,30
209*         65 CONTINUE
210*            R(1)=1.
211*            R(2)=H2
212*            DO 70 J=3,N
213*         70 R(J)=R(J-1)-HT(J-2)
214*            HR(1)=H
215*            HR(2)=H
216*            HR(MM1)=H
217*            HR(M)=H
218*            NP1=N+1
219*            DO 71 J=NP1,27
220*         71 R(J)=1.D0
221*            H4=(2.-G2/R(JT)-G2*G2/(4.*R(JT)*R(JT)))*R(JT)
222*            DO 120 I=3,MM1
223*            IF(I-I1)75,80,85
224*         75 KZ(I)=2
225*            LZ(I)=2
226*            HR(I)=HR(I-1)
227*            GO TO 120
228*         80 KZ(I)=1
```

```
229*            LZ(I)=3
230*            HR(I)=HR(I-1)*.5
231*            GO TO 120
232*         85 IF(I-I12)90,80,95
233*         90 KZ(I)=KZ(I-1)+1
234*            LZ(I)=LZ(I-1)
235*            HR(I)=HR(I-1)
236*            GO TO 120
237*         95 IF(I-I2)90,75,100
238*        100 IF(I-I3)75,105,110
239*        105 HR(I)=HR(I-1)*2.
240*            KZ(I)=1
241*            LZ(I)=1
242*            GO TO 120
243*        110 IF(I-I34)90,105,115
244*        115 IF(I-I4)90,75,75
245*        120 CONTINUE
246*  C     ------------------------
247*  C     INITIALIZE STREAM FUNCTION
248*  C     AND VORTICITY ARRAYS
249*  C     ------------------------
250*            DO 125 J=2,N
251*            T=R(J)
252*            S(1,J)=F(T)
253*            S(2,J)=S(1,J)
254*            S(M,J)=S(1,J)
255*            S(MM1,J)=S(1,J)
256*            V(1,J)=4.*T
257*            V(2,J)=V(1,J)
258*            V(M,J)=V(1,J)
259*            V(MM1,J)=V(1,J)
260*        125 CONTINUE
261*            GO TO (130,1404,1400,139),INPUT
262*  C     ------------------------------
263*  C     TYPE 1 INPUT: POISEUILLE FLOW
264*  C     ------------------------------
265*        130 DO 135 I=3,MM2
266*            DO 135 J=2,NM2
267*            S(I,J)=S(1,J)
268*        135 V(I,J)=V(1,J)
269*            DO 136 I=IFM2,IRP2
270*            DO 136 J=1,JTP2
271*            V(I,J)=0.0
272*        136 S(I,J)=-.5
273*            GO TO 140
274*  C     ------------------------------
275*  C     TYPE 4 INPUT: READ ARRAY FROM
276*  C                   TAPE UNIT NO. 8
277*  C     ------------------------------
278*        139 READ(8)S
279*            READ(8)V
280*            GO TO 1434
281*  C     ------------------------------------------------
282*  C     TYPE 3 INPUT: READ N+1 ARRAYS FROM TAPE UNIT 8
283*  C                   AND WRITE FIRST N OF THESE ON TO
284*  C                   TAPE UNIT 9
285*  C     ------------------------------------------------
```

```
286*     1400 IF(NUMB)  1402,1402,14000
287*    14000 DO 1401 I=1,NUMB
288*          READ(8)S
289*          READ(8)V
290*          WRITE(9)S
291*     1401 WRITE(9)V
292*     1402 READ(8)S
293*          READ(8)V
294*          IF(KANDO)1404,1404,1403
295*     1403 WRITE(9)S
296*          WRITE(9)V
297*     C    ------------------------------------
298*     C    TYPE 2 INPUT: ZERO AT ALL NODE POINTS
299*     C    ------------------------------------
300*     1404 IF(M-MNEW)1405,140,140
301*     C    ----------------
302*     C    EXTEND FLOW FIELD
303*     C    ----------------
304*     1405 DO 1406 I=M,MNEW
305*          DO 1406 J=1,N
306*          S(I,J)=S(M,J)
307*          V(I,J)=V(M,J)
308*          HR(I)=HR(MM1)
309*          KZ(I)=KZ(MM1)
310*     1406 LZ(I)=LZ(MM1)
311*          M=MNEW
312*          MM1=M-1
313*          MM2=M-2
314*          MM3=M-3
315*          IE=MM1-I34
316*     C    ----------------------------
317*     C    BOUNDARY CONDITION CALCULATIONS
318*     C    ----------------------------
319*     C    ----------------
320*     C    CENTER LINE B.C.
321*     C    ----------------
322*      140 DO 145 I=1,M
323*          S(I,NM1)=0.
324*          V(I,NM1)=0.0
325*          S(I,N)=S(I,NM2)
326*      145 V(I,N)=V(I,NM2)
327*          DIFFV=0.D0
328*          DIFFS=0.D0
329*          DO 146 J=1,N
330*          T=R(J)
331*          S(1,J)=F(T)
332*          S(2,J)=S(1,J)
333*          V(1,J)=4.*T
334*      146 V(2,J)=V(1,J)
335*     C    ----------
336*     C    EXIT B.C.
337*     C    ----------
338*          DO 154 J=2,N
339*          IF(KEDGE)151,151,153
340*      151 IF(RE)152,152,153
341*      152 IF(INPUT-3)1520,153,153
342*     1520 S(M,J)=S(MM3,J)
```

```
343*            S(MM1,J)=S(MM2,J)
344*            V(M,J)=V(MM3,J)
345*            V(MM1,J)=V(MM2,J)
346*            GO TO 154
347*        153 V(M,J)=V(1,J)
348*            V(MM1,J)=V(1,J)
349*            S(M,J)=S(1,J)
350*            S(MM1,J)=S(1,J)
351*        154 CONTINUE
352*      C     ------------------------------------
353*      C     INLET B.C. (SET IN INITIALIZATION)
354*      C     ------------------------------------
355*      C     ----------------
356*      C     PIPE WALL B.C.
357*      C     ----------------
358*            IF(L)157,157,159
359*        157 IF(INPUT-2)1570,159,159
360*       1570 DO 158 I=1,M
361*            S(I,1)=-.5
362*        158 V(I,1)=4.
363*            GO TO 189
364*        159 DO 165 I=1,IF
365*        160 V(I,1)=(H1*(S(I,2)-S(I,1))-H2*V(I,2))/H3
366*            S(I,1)=-.5
367*        165 CONTINUE
368*            DO 1650 I=IR,M
369*       1600 V(I,1)=(H1*(S(I,2)-S(I,1))-H2*V(I,2))/H3
370*            S(I,1)=-.5
371*       1650 CONTINUE
372*      C     ----------------------
373*      C     FRONT OF ORIFICE PLATE
374*      C     ----------------------
375*        169 DO 170 J=1,JT
376*            S(IF,J)=-.5
377*        170 V(IF,J)=(H5*(S(IFM1,J)+.5)/R(J)-V(IFM1,J))*.5
378*            V(IF,1)=0.0
379*            V1=V(IF,JT)
380*      C     ----------------------
381*      C     TOP OF ORIFICE PLATE
382*      C     ----------------------
383*            IF(KEDGE)171,171,175
384*        171 DO 172 I=IF,IR
385*            S(I,JT)=-.5
386*        172 V(I,JT)=(  H5*(S(I,JTP1)+.5)-R(JTP1)*V(I,JTP1))/H4
387*            V(IF,1)=0.0
388*            V(IR,1)=0.0
389*            V2=V(IF,JT)
390*            V3=V(IR,JT)
391*            V12=V2
392*            JREAR=JT
393*            GO TO 180
394*        175 V(IF,JT)=(H5*(S(IF,JTP1)+.5)-R(JTP1)*V(IF,JTP1))/H4
395*            V2=V(IF,JT)
396*            J=JTP1
397*            DO 176 I=IF,IR
398*            IP1=I+1
399*            J=J-1
```

```
400*            JP1=J+1
401*          S(I,J)=-.5
402*            H6=R(J)*(2.-G2/R(J)-G2*G2/(4.*R(J)*R(J)))
403*      176 V(I,J)=(.5*H5*(S(IP1,JP1)+.5)-R(JP1)*V(IP1,JP1))/H6
404*            V12=V(IF,JT)
405*          JREAR=JT-(IR-IE)*KEDGE
406*            V3=V(IR,JREAR)
407*     C    ----------------------
408*     C    REAR OF ORIFICE PLATE
409*     C    ----------------------
410*      180 DO 185 J=1,JREAR
411*          S(IR,J)=-.5
412*      185 V(IR,J)=(H5*(S(IRP1,J)+.5)/R(J)-V(IRP1,J))*.5
413*          V(IR,1)=0.0
414*            V4=V(IR,JREAR)
415*          V(IF,JT)=V1
416*            IF(L)189,189,200
417*      189 WRITE(6,8)M,N,IF,IR,JT,JA,JB,JC,JD,JE,IA,IB,IC,ID,IE,RE
418*          WRITE(6,2)I1,I12,I3,I34,I4
419*          WRITE(6,2)J1,J2,J3,J4
420*            DO 191 I=1,M
421*          DO 190 J=1,N
422*      190 WRITE(6,4)L,I,J,R(J),S(I,J),V(I,J)
423*          WRITE(6,5)
424*      191 CONTINUE
425*     C    -------------------------
426*     C    BEGIN FIELD CALCULATIONS
427*     C    -------------------------
428*      200 KIT=1
429*          DO 230 I=3,MM2
430*            IP1=I+1
431*          IP2=I+2
432*            IM1=I-1
433*          IM2=I-2
434*            IK=KZ(I)
435*          IL=LZ(I)
436*            HU=HR(I)
437*          IF(I-IFM1)2005,2015,2020
438*     2005 JS=2
439*     C    -------------------------
440*     C    SET OPERATOR COEFFICIENTS
441*     C    -------------------------
442*     2010 C1=CFD(IL,IK,5)
443*          C2=CFD(IL,IK,4)
444*            C3=CFD(IL,IK,3)
445*          C4=CFD(IL,IK,2)
446*            C5=CFD(IL,IK,1)
447*          D1=CSD(IL,IK,5)
448*            D2=CSD(IL,IK,4)
449*          D3=CSD(IL,IK,3)
450*            D4=CSD(IL,IK,2)
451*          D5=CSD(IL,IK,1)
452*            KD=1
453*          GO TO 2035
454*     2015 JS=2
455*          V(IF,JT)=V1
456*            C1=15.
```

```
457*            C2=-90.
458*            C3=50.
459*            C4=30.
460*            C5=-5.
461*            D1=55.
462*            D2=30.
463*            D3=-100.
464*            D4=20.
465*            D5=-5.
466*            KD=2
467*            GO TO 2035
468*    2020  IF(I-IRP1)2025,2030,2005
469*    2025  IF(I-IF)2026,2026,2027
470*    2026  JS=JTP1
471*            V(IF,JT)=V2
472*            V(IR,JREAR)=V3
473*            GO TO 2010
474*    2027  IF(I-IRP1)2028,2030,2005
475*    2028  JS=JS-KEDGE
476*            V(IF,JT)=V12
477*            V(IR,JREAR)=V3
478*            IF(KEDGE)2010,2010,2031
479*    2030  JS=2
480*            V(IR,JREAR)=V4
481*    2031  C1=-15.
482*            C2=90.
483*            C3=-50.
484*            C4=-30.
485*            C5=5.
486*            D1=55.
487*            D2=30.
488*            D3=-100.
489*            D4=20.
490*            D5=-5.
491*            KD=3
492*    2035  DO 230 J=JS,NM2
493*            JP1=J+1
494*            JP2=J+2
495*            JM1=J-1
496*            JM2=J-2
497*            JK=KR(J)
498*            JL=LR(J)
499*            HV=HT(J)
500*            GO TO (2050,2100,2115),KD
501*    2050  IF(RE)210,210,205
502*     205  ZV1=(C1*V(IP2,J)+7.*(C2*V(IP1,J)+C4*V(IM1,J))+C5*V(IM2,J))/7.
503*          ZS1=(C1*S(IP2,J)+7.*(C2*S(IP1,J)+C4*S(IM1,J))+C5*S(IM2,J))/7.+
504*         1C3*S(I,J)
505*     210  ZV2=(D1*V(IP2,J)+7.*(D2*V(IP1,J)+D4*V(IM1,J))+D5*V(IM2,J))/7.
506*          ZS2=(D1*S(IP2,J)+7.*(D2*S(IP1,J)+D4*S(IM1,J))+D5*S(IM2,J))/7.+
507*         1D3*S(I,J)
508*            GO TO 2140
509*    2100  IF(RE)2110,2110,2105
510*    2105  ZV1=C1*V(IF,J)+C2*V(IFM2,J)+C4*V(IFM3,J)+C5*V(IFM4,J)
511*          ZS1=C1*S(IF,J)+C2*S(IFM2,J)+C4*S(IFM3,J)+C5*S(IFM4,J)+C3*S(I,J)
512*    2110  ZV2=D1*V(IF,J)+D2*V(IFM2,J)+D4*V(IFM3,J)+D5*V(IFM4,J)
513*          ZS2=D1*S(IF,J)+D2*S(IFM2,J)+D4*S(IFM3,J)+D5*S(IFM4,J)+D3*S(I,J)
```

```
514*            GO TO 2140
515*    2115    IF(I-IRP1)2116,2120,2120
516*    2116    IM1=I-1
517*            IP1=I+1
518*            IP2=I+2
519*            IP3=I+3
520*            IF(RE)2118,2118,2117
521*    2117    ZV1=C1*V(IM1,J)+C2*V(IP1,J)+C4*V(IP2,J)+C5*V(IP3,J)
522*            ZS1=C1*S(IM1,J)+C2*S(IP1,J)+C4*S(IP2,J)+C5*S(IP3,J)+C3*S(I,J)
523*    2118    ZV2=D1*V(IM1,J)+D2*V(IP1,J)+D4*V(IP2,J)+D5*V(IP3,J)
524*            ZS2=D1*S(IM1,J)+D2*S(IP1,J)+D4*S(IP2,J)+D5*S(IP3,J)+D3*S(I,J)
525*            GO TO 2140
526*    2120    IF(RE)2130,2130,2125
527*    2125    ZV1=C1*V(IR,J)+C2*V(IRP2,J)+C4*V(IRP3,J)+C5*V(IRP4,J)
528*            ZS1=C1*S(IR,J)+C2*S(IRP2,J)+C4*S(IRP3,J)+C5*S(IRP4,J)+C3*S(I,J)
529*    2130    ZV2=D1*V(IR,J)+D2*V(IRP2,J)+D4*V(IRP3,J)+D5*V(IRP4,J)
530*            ZS2=D1*S(IR,J)+D2*S(IRP2,J)+D4*S(IRP3,J)+D5*S(IRP4,J)+D3*S(I,J)
531*    2140    IF(J-JS)2205,215,2205
532*    C       ---------------------------------
533*    C       SET RADIAL OPERATOR COEFFICIENTS
534*    C       ---------------------------------
535*     215    A1=-5.
536*            A2=30.
537*            A3=50.
538*            A4=-90.
539*            A5=15.
540*            B1=-5.
541*            B2=20.
542*            B3=-100.
543*            B4=30.
544*            B5=55.
545*            IF(J-NM2)216,217,217
546*     216    JP3=J+3
547*            RV1=A1*V(I,JP3)+A2*V(I,JP2)+A4*V(I,JP1)+A5*V(I,JM1)
548*            RV2=B1*V(I,JP3)+B2*V(I,JP2)+B4*V(I,JP1)+B5*V(I,JM1)
549*            RS1=A1*S(I,JP3)+A2*S(I,JP2)+A4*S(I,JP1)+A5*S(I,JM1)+A3*S(I,J)
550*            RS2=B1*S(I,JP3)+B2*S(I,JP2)+B4*S(I,JP1)+B5*S(I,JM1)+B3*S(I,J)
551*            GO TO 225
552*     217    JM3=J-3
553*            A1=-A1
554*            A2=-A2
555*            A3=-A3
556*            A4=-A4
557*            A5=-A5
558*            RV1= (A1*V(I,JM3)+A2*V(I,JM2)+A4*V(I,JM1)+A5*V(I,JP1))
559*            RV2= (B1*V(I,JM3)+B2*V(I,JM2)+B4*V(I,JM1)+B5*V(I,JP1))
560*            RS1= (A1*S(I,JM3)+A2*S(I,JM2)+A4*S(I,JM1)+A5*S(I,JP1)+A3*S(I,J))
561*            RS2= (B1*S(I,JM3)+B2*S(I,JM2)+B4*S(I,JM1)+B5*S(I,JP1)+B3*S(I,J))
562*            GO TO 225
563*    2205    IF(J-NM2)2206,215,215
564*    2206    A1=-CFD(JL,JK,5)
565*            A2=-CFD(JL,JK,4)
566*            A3=-CFD(JL,JK,3)
567*            A4=-CFD(JL,JK,2)
568*            A5=-CFD(JL,JK,1)
569*            B1=CSD(JL,JK,5)
570*            B2=CSD(JL,JK,4)
```

```
571*            B3=CSD(JL,JK,3)
572*            B4=CSD(JL,JK,2)
573*            B5=CSD(JL,JK,1)
574*            RV1=(A1*V(I,JP2)+7.*(A2*V(I,JP1)+A4*V(I,JM1))+A5*V(I,JM2))/7.
575*            RV2=(B1*V(I,JP2)+7.*(B2*V(I,JP1)+B4*V(I,JM1))+B5*V(I,JM2))/7.
576*            RS1=(A1*S(I,JP2)+7.*(A2*S(I,JP1)+A4*S(I,JM1))+A5*S(I,JM2))/7.+
577*           1A3*S(I,J)
578*            RS2=(B1*S(I,JP2)+7.*(B2*S(I,JP1)+B4*S(I,JM1))+B5*S(I,JM2))/7.+
579*           1B3*S(I,J)
580*       225 A=HU/HV
581*            B=HU/R(J)
582*            C=RE/R(J)
583*            D=R(J)*HU*HU*60.
584*            AA=A*A
585*            AB=A*B
586*            AC=A*C/60.
587*            BB=B*B*60.
588*            BC=B*C
589*     C      --------------------
590*     C      CALCULATE VORTICITY
591*     C      --------------------
592*      2260  OV=V(I,J)
593*            IF(RE)226,226,227
594*       226  VN=AA*RV2+ZV2+AB*RV1
595*            VD=BB-AB*A3-AA*B3-D3
596*            GO TO 228
597*       227  VN=AA*RV2+ZV2+AB*RV1+AC*(RS1*ZV1-ZS1*RV1)
598*            VD=BB-AB*A3-AA*B3-D3+AC*(ZS1*A3-RS1*C3)-BC*ZS1
599*       228  V(I,J)=OV+BETA*(VN/VD-OV)
600*     C      ------------------------
601*     C      CALCULATE STREAM FUNCTION
602*     C      ------------------------
603*      2280  OS=S(I,J)
604*            SN=AA*RS2+ZS2-AB*RS1-D*V(I,J)
605*            SD= AB*A3-AA*B3-D3
606*            S(I,J)=OS+BETA*SN/SD
607*            SUBS=DABS(S(I,J)-OS)
608*            SUBV=DABS(V(I,J)-OV)
609*            IF(DIFFS-SUBS)2281,2282,2282
610*       2281 DIFFS=SUBS
611*       2282 IF(DIFFV-SUBV)2283,2284,2284
612*       2283 DIFFV=SUBV
613*       2284 IF(L)229,230,230
614*        229 WRITE(6,2)I,J,IK,IL,JK,JL
615*            WRITE(6,6)A1,A2,A3,A4,A5,B1,B2,B3,B4,B5
616*            WRITE(6,6)C1,C2,C3,C4,C5,D1,D2,D3,D4,D5
617*            WRITE(6,7)RV1,RV2,RS1,RS2
618*            WRITE(6,7)ZV1,ZV2,ZS1,ZS2
619*            WRITE(6,7)HU,HV,R(J),OS,OV
620*            WRITE(6,7)VN,VD,SN,SD
621*            WRITE(6,5)
622*       230  CONTINUE
623*            WRITE(6,6)V1,V2,V12,V3,V4,DIFFS,DIFFV
624*     C      ---------------------
625*     C      CHECK FOR CONVERGENCE
626*     C      ---------------------
627*            IF(DIFFS-2.D-5)2300,2300,2301
```

```
628*     2300 IF(DIFFV-5.D-4)250,250,2301
629*     C    ------------------------------
630*     C      CONVERGENCE CRITERIA NOT MET
631*     C    ------------------------------
632*     2301 L=L+1
633*          IF(L-KPRINT)244,231,244
634*      231 DO 240 I=2,MM2
635*          DO 235 J=1,NM1
636*      235 WRITE(6,4)L,I,J,R(J),S(I,J),V(I,J)
637*          WRITE(6,5)
638*      240 CONTINUE
639*          KPRINT=KPRINT+KPR
640*     C    ------------------------------------
641*     C    IF ITERATION LIMIT NOT EXCEEDED = REPEAT
642*     C    ------------------------------------
643*      244 IF(L-LIMIT)140,245,245
644*      245 WRITE(6,17)
645*          IF(L-KPRINT-KPR)250,261,250
646*      250 DO 260 I=2,MM2
647*          DO 255 J=1,NM1
648*      255 WRITE(6,4)L,I,J,R(J),S(I,J),V(I,J)
649*          WRITE(6,5)
650*      260 CONTINUE
651*      261 IF(RE)265,265,300
652*      265 IF(INPUT-3)2650,300,300
653*     2650 DO 270 I=1,MM2
654*          IDOWN=MM1-I
655*          IUP=MM2+I
656*          HR(IUP)=HR(IDOWN)
657*          KZ(IUP)=KZ(IDOWN)
658*          LZ(IUP)=LZ(IDOWN)
659*          DO 270 J=1,N
660*          S(IUP,J)=S(IDOWN,J)
661*      270 V(IUP,J)=V(IDOWN,J)
662*          M=2*M-4
663*          MM2=M-2
664*      300 VFD1=(V(M-3,6)-8.*V(M-2,6)+8.*V(M-1,6)-V(M,6))/(12.*H)
665*          SFD1=(S(M-3,6)-8.*S(M-2,6)+8.*S(M-1,6)-S(M,6))/(12.*H)
666*      310 VFD2=(V(M-3,14)-8.*V(M-2,14)+8.*V(M-1,14)-V(M,14))/(12.*H)
667*          SFD2=(S(M-3,14)-8.*S(M-2,14)+8.*S(M-1,14)-S(M,14))/(12.*H)
668*      320 VFD3=(V(M-3,21)-8.*V(M-2,21)+8.*V(M-1,21)-V(M,21))/(12.*H)
669*          SFD3=(S(M-3,21)-8.*S(M-2,21)+8.*S(M-1,21)-S(M,21))/(12.*H)
670*          WRITE(6,6)VFD1,SFD1,VFD2,SFD2,VFD3,SFD3
671*      400 WRITE(9)S
672*          WRITE(9)V
673*          IF(INPUT-4)500,999,999
674*     C    -------------------------
675*     C
676*     C
677*     C    STREAMLINE AND VORTICITY
678*     C    CONTOUR INTERPOLATION
679*     C    -------------------------
680*      500 READ(5,2)KN,KV
681*          READ(5,9)(ES(K),K=1,KN)
682*          WRITE(6,10)(ES(K),K=1,KN)
683*          DO 510 I=1,M
684*      510 XS(I)=0.
```

```
685*            DO 520 K=1,KN
686*            DO 520 J=1,5
687*      520 YS(J,K)=0.
688*            L=1
689*            DO 630 I=1,M
690*            IF(I-1)525,525,530
691*      525 XS(1)=0.
692*            GO TO 535
693*      530 IF(I-2)531,531,532
694*      531 XS(2)=H
695*            GO TO 535
696*      532 XS(I)=XS(I-1)+HR(I-2)
697*      535 IF(I-IF)550,545,540
698*      540 IF(I-IR)545,545,550
699*      545 L=JT-(I-IF)*KEDGE
700*            GO TO 555
701*      550 L=1
702*      555 DO 600 K=1,KN
703*            LL=1
704*            SS=ES(K)
705*            KY(K)=0
706*            DO 595 J=L,NM2
707*            IF(KV)560,560,565
708*      560 DA=S(I,J+1)-SS
709*            DB=S(I,J)-SS
710*            GO TO 570
711*      565 DA=V(I,J+1)-SS
712*            DB=V(I,J)-SS
713*      570 DD=DA-DB
714*            AB=DA*DB
715*            IF(AB)575,575,595
716*      575 IF(DD)585,580,585
717*      580 YS(LL,K)=R(J)
718*            GO TO 586
719*      585 YS(LL,K)=R(J)-DB*(R(J+1)-R(J))/DD
720*      586 KY(K)=LL
721*            LL=LL+1
722*      595 CONTINUE
723*      600 CONTINUE
724*            DO 604 K=1,KN
725*            IF(K-1)601,601,602
726*      601 NLL=KY(1)
727*            GO TO 604
728*      602 IF(KY(K)-NLL)604,604,603
729*      603 NLL=KY(K)
730*      604 CONTINUE
731*            DO 615 K=1,KN
732*            IF(NLL-KY(K))615,615,605
733*      605 LL=KY(K)+1
734*            DO 610 J=LL,NLL
735*      610 YS(J,K)=111.1111
736*      615 CONTINUE
737*            WRITE(6,13)NLL,(KY(K),K=1,KN)
738*            DO 630 LL=1,NLL
739*            IF(LL-1)620,620,625
740*      620 WRITE(6,11)XS(I),(YS(1,K),K=1,KN)
741*            GO TO 630
```

```
  625 WRITE(6,12)(YS(LL,K),K=1,KN)
  630 CONTINUE
      IF(KV)500,500,700
C     ---------------------------
C
C     PRESSURE DROP INTEGRATIONS
C
C     ---------------------------
  700 READ(5,2)KJ
      READ(5,2)(JR(K),K=1,KJ)
      READ(5,2)(JTYPE(K),K=1,KJ)
      WRITE(6,16)
  750 DO 845 K=1,KJ
      J=JR(K)
      SUM=0.
      PSUM=0.
      KEITH=JTYPE(K)
      IF(KEITH-1)760,760,800
  760 I=1
  761 L=0
  762 L=L+1
      FUN(L)=(.5*V(I,5)-8.*V(I,4)/3.+6.*V(I,3)-8.*V(I,2)+(H+25./6.)*
     1 V(I,1))/H
      IF(L-3)763,764,764
  763 I=I+1
      GO TO 762
  764 DELP=-H*(FUN(1)+4.*FUN(2)+FUN(3))/3.
      SUM=SUM+DELP
      WRITE(6,4)I,J,K,DELP,SUM
      IF(I-19)761,765,765
  765 L=0
  766 L=L+1
      FUN(L)=(.5*V(I,5)-8.*V(I,4)/3.+6.*V(I,3)-8.*V(I,2)+(H+25./6.)*
     1 V(I,1))/H
      IF(L-4)767,768,768
  767 I=I+1
      GO TO 766
  768 DELP=-3.*H*(FUN(1)+3.*FUN(2)+3.*FUN(3)+FUN(4))/16.
      SUM=SUM+DELP
      WRITE(6,4)I,J,K,DELP,SUM
  769 L=0
  770 L=L+1
      FUN(L)=(.5*V(I,5)-8.*V(I,4)/3.+6.*V(I,3)-8.*V(I,2)+(H+25./6.)*
     1 V(I,1))/H
      IF(L-3)771,772,772
  771 I=I+1
      GO TO 770
  772 DELP=-H*(FUN(1)+4.*FUN(2)+FUN(3))/12.
      SUM=SUM+DELP
      WRITE(6,4)I,J,K,DELP,SUM
      IF(I-26)769,775,775
  775 SUM=0.0
      INN=1
      I=IR
  780 GO TO (781,782,783),INN
  781 INS=IR
      INF=I3+1
```

```
799*            FACT=.25
800*            GO TO 785
801*       782  INS=I3+1
802*            INF=I34+1
803*            FACT=.5
804*            GO TO 785
805*       783  INS=I34+1
806*            INF=M-2
807*            FACT=1.
808*       785. INK=INF-INS
809*            KODD=2*(INK/2)-INK
810*            IF(KODD)787,786,787
811*       786  KTIMES=INK/2
812*            GO TO 788
813*       787  KTIMES=(INK-3)/2
814*       788  IF(KTIMES)794,794,789
815*       789  DO 793 INT=1,KTIMES
816*            L=0
817*       790  L=L+1
818*            FUN(L)=(.5*V(I,5)-8.*V(I,4)/3.+6.*V(I,3)-8.*V(I,2)+(H+25./6.)*
819*           1 V(I,1))/H
820*            IF(L-3)791,792,792
821*       791  I=I+1
822*            GO TO 790
823*       792  DELP=-H*(FUN(1)+4.*FUN(2)+FUN(3))/3.*FACT
824*            SUM=SUM+DELP
825*       793  WRITE(6,4)I,J,K,DELP,SUM
826*            IF(I-INF)794,798,798
827*       794  L=0
828*       795  L=L+1
829*            FUN(L)=(.5*V(I,5)-8.*V(I,4)/3.+6.*V(I,3)-8.*V(I,2)+(H+25./6.)*
830*           1 V(I,1))/H
831*            IF(L-4)796,797,797
832*       796  I=I+1
833*            GO TO 795
834*       797  DELP=-3.*H*(FUN(1)+3.*FUN(2)+3.*FUN(3)+FUN(4))/8.*FACT
835*            SUM=SUM+DELP
836*            WRITE(6,4)I,J,K,DELP,SUM
837*       798  INN=INN+1
838*            IF(INN-4)780,845,845
839*       800  INN=1
840*            I=3
841*            WRITE(6,16)
842*       805  GO TO (810,811,812,813,814),INN
843*       810  INS=3
844*            INF=I1+1
845*            FACT=1.
846*            GO TO 815
847*       811  INS=I1+1
848*            INF=I12+1
849*            FACT=.5
850*            GO TO 815
851*       812  INS=I12+1
852*            INF=I3+1
853*            FACT=.25
854*            GO TO 815
855*       813  INS=I3+1
```

```
      INF=I34+1
      FACT=.5
      GO TO 815
  814 INS=I34+1
      INF=M-2
      FACT=1.
  815 INK=INF-INS
      KODD=2*(INK/2)-INK
      IF(KODD)822,821,822
  821 KTIMES=INK/2
      GO TO 823
  822 KTIMES=(INK-3)/2
  823 IF(KTIMES)828,828,8230
 8230 DO 827 INT=1,KTIMES
      L=0
      VU(1)  =(104.*S(I,NM2)-114.*S(I,N-3)+56.*S(I,N-4)-11.*S(I,N-5))/
     1(3.*H*H)
  824 L=L+1
      FUN(L)=-2.*(.5*V(I,N-5)-8.*V(I,N-4)/3.+6.*V(I,N-3)-8.*V(I,NM2))/H
      IF(L-3)825,826,826
  825 I=I+1
      GO TO 824
  826 DELP=-H*(FUN(1)+4.*FUN(2)+FUN(3))/3.*FACT
      VU(2)  =(104.*S(I,NM2)-114.*S(I,N-3)+56.*S(I,N-4)-11.*S(I,N-5))/
     1(3.*H*H)
      DELKE=(VU(2)*VU(2)-VU(1)*VU(1))*.5
      PDROP=DELP-RE*DELKE
      PSUM=PSUM+PDROP
      SUM=SUM+DELP
  827 WRITE(6,4)I,J,K,DELP,SUM,VU(1),VU(2),PDROP,PSUM
      IF(I-INF)828,835,835
  828 L=0
      VU(1)  =(104.*S(I,NM2)-114.*S(I,N-3)+56.*S(I,N-4)-11.*S(I,N-5))/
     1(3.*H*H)
  829 L=L+1
      FUN(L)=-2.*(.5*V(I,N-5)-8.*V(I,N-4)/3.+6.*V(I,N-3)-8.*V(I,NM2))/H
      IF(L-4)830,831,831
  830 I=I+1
      GO TO 829
  831 DELP=-3.*H*(FUN(1)+3.*FUN(2)+3.*FUN(3)+FUN(4))/8.*FACT
      VU(2)  =(104.*S(I,NM2)-114.*S(I,N-3)+56.*S(I,N-4)-11.*S(I,N-5))/
     1(3.*H*H)
      DELKE=(VU(2)*VU(2)-VU(1)*VU(1))*.5
      PDROP=DELP-RE*DELKE
      PSUM=PSUM+PDROP
      SUM=SUM+DELP
      WRITE(6,4)I,J,K,DELP,SUM,VU(1),VU(2),PDROP,PSUM
  835 INN=IINN+1
      IF(INN-6)805,840,840
  840 WRITE(6,5)
  845 CONTINUE
C     ----------------------
C
C     VELOCITY CALCULATIONS
C
C     ----------------------
      DO 980 I=3,MM2
```

```
913*            IP1=I+1
914*            IP2=I+2
915*            IM1=I-1
916*            IM2=I-2
917*            IK=KZ(I)
918*            IL=LZ(I)
919*            HU=HR(I)
920*            IF(I-IFM1)905,910,915
921*      905   JS=2
922*      906   C1=CFD(IL,IK,5)
923*            C2=CFD(IL,IK,4)
924*            C3=CFD(IL,IK,3)
925*            C4=CFD(IL,IK,2)
926*            C5=CFD(IL,IK,1)
927*            KD=1
928*            GO TO 926
929*      910   JS=2
930*            C1=15.
931*            C2=-90.
932*            C3=50.
933*            C4=30.
934*            C5=-5.
935*            KD=2
936*            GO TO 926
937*      915   IF(I-IRP1)920,924,905
938*      920   IF(I-IF)921,921,922
939*      921   JS=JTP1
940*            GO TO 906
941*      922   IF(I-IRP1)923,924,906
942*      923   JS=JS-KEDGE
943*            IF(KEDGE)906,906,925
944*      924   JS=2
945*      925   C1=-15.
946*            C2=90.
947*            C3=-50.
948*            C4=-30.
949*            C5=5.
950*            KD=3
951*      926   JSM1=JS-1
952*            DO 927 J=1,JSM1
953*            VU(J)=0.0
954*      927   VV(J)=0.
955*            DO 970 J=JS,NM2
956*            JP1=J+1
957*            JP2=J+2
958*            JM1=J-1
959*            JM2=J-2
960*            JK=KR(J)
961*            JL=LR(J)
962*            HV=HT(J)
963*            GO TO (930,935,940),KD
964*      930   ZS1=(C1*S(IP2,J)+7.*(C2*S(IP1,J)+C4*S(IM1,J))+C5*S(IM2,J))/7.+
965*           1C3*S(I,J)
966*            GO TO 945
967*      935   ZS1=C1*S(IF,J)+C2*S(IFM2,J)+C4*S(IFM3,J)+C5*S(IFM4,J)+C3*S(I,J)
968*            GO TO 945
969*      940   ZS1=C1*S(IR,J)+C2*S(IRP2,J)+C4*S(IRP3,J)+C5*S(IRP4,J)+C3*S(I,J)
```

```
970*      945 IF(J-JS)950,950,955
971*      950 A1=-5.
972*          A2=30.
973*          A3=50.
974*          A4=-90.
975*          A5=15.
976*          IF(J-NM2)951,952,952
977*      951 JP3=J+3
978*          RS1=A1*S(I,JP3)+A2*S(I,JP2)+A4*S(I,JP1)+A5*S(I,JM1)+A3*S(I,J)
979*          GO TO 960
980*      952 JM3=J-3
981*          A1=-A1
982*          A2=-A2
983*          A3=-A3
984*          A4=-A4
985*          A5=-A5
986*          RS1= (A1*S(I,JM3)+A2*S(I,JM2)+A4*S(I,JM1)+A5*S(I,JP1)+A3*S(I,J))
987*          GO TO 960
988*      955 IF(J-NM2)956,950,950
989*      956 A1=-CFD(JL,JK,5)
990*          A2=-CFD(JL,JK,4)
991*          A3=-CFD(JL,JK,3)
992*          A4=-CFD(JL,JK,2)
993*          A5=-CFD(JL,JK,1)
994*          RS1=(A1*S(I,JP2)+7.*(A2*S(I,JP1)+A4*S(I,JM1))+A5*S(I,JM2))/7.+
995*         1A3*S(I,J)
996*      960 VU(J)=-RS1/(R(J)*HV*60.)
997*          VV(J)= ZS1/(R(J)*HU*60.)
998*          VSQ=VU(J)*VU(J)+VV(J)*VV(J)
999*      970 Q(J)=DSQRT(VSQ)
1000*         VV(NM1)=0.
1001*         VU(NM1)=(104.*S(I,NM2)-114.*S(I,N-3)+56.*S(I,N-4)-11.*S(I,N-5))/
1002*        1(3.*H*H)
1003*         Q(NM1)=VU(NM1)
1004*         DO 975 J=1,NM1
1005*     975 WRITE(6,4)L,I,J,R(J),VU(J),VV(J),Q(J)
1006*         WRITE(6,5)
1007*     980 CONTINUE
1008*         IF(MORE)999,999,985
1009*     985 DO 990 I=1,MORE
1010*         READ(8)S
1011*         READ(8)V
1012*         WRITE(9)S
1013*     990 WRITE(9)V
1014*     999  IF(NPROB-KPROB)635,635,24
1015*     635 STOP
1016*         END
```

SELECTED BIBLIOGRAPHY

1. Mills, R. D., "Numerical Solutions of Viscous Flow Through a Pipe Orifice at Low Reynolds Numbers," Journal Mech. Eng. Sci., pp 133-140, VOL 10, No. 2, 1968

2. Johansen, F. C., "Flow Through Pipe Orifices at Low Reynolds Numbers," Proc. Roy. Soc., pp 231-245, 126(A) 1930

3. Donovan, L. F., "A Numerical Solution of Unsteady Flow in a Two Dimensional Square Cavity," AIAA Journal pp 524-529, VOL 8, No. 3, March 1970

4. Putre, H. A., "Computer Solution of Unsteady Navier-Stokes Equations for an Infinite Hydrodynamic Step Bearing," NASA TN D-5682, April 1970

5. Gillis, J. and Brandt, D., "Numerical Integration of Equations of Motion of a Viscous Fluid," Weizmann Inst. of Sci., SR No. 1, (Clearinghouse order No. AD-614915), Oct 1964

6. Truesdell, Jr., L. C. and Adler, R. J., "Numerical Treatment of Fully Developed Laminar Flow in Helically Coiled Tubes," AIChE Journal, pp 1010-1015, VOL 16, No. 6, Nov 1970

7. Thom, A., "An Arithmetical Solution of Certain Problems in Steady Viscous Flow," Aero. Res. Comm. Rep. and Memo No. 1475, May 1932

8. Michael, P., "Steady Motion of a Disk in a Viscous Fluid," Physics of Fluids, pp 466-471, VOL 9, No. 3, March 1966

9. Rimon, Y. and Lugt, H. J., "Laminar Flows Past Oblate Spheroids of Various Thicknesses," Physics of Fluids, pp 2465-2472, VOL 12, No. 12, Dec 1969; Also, NSPDL Washington Applied Math. Lab. Note, AML-16-69, March 1969

10. Rimon, Y., "Numerical Solution of the Incompressible Time-Dependent Viscous Flow Past a Thin Oblate Spheroid," Physics of Fluids Supplement II, High-Speed Computing in Fluid Dynamics, pp II-65 to II-75, Dec 1969

11. Thoman, D. C. and Szewczyk, A. A., "Time-Dependent Viscous Flow Over a Circular Cylinder," Physics of Fluids Supplement II, High-Speed Computing in Fluid Dynamics, pp II-76 to II-86, Dec 1969; Also, "Numerical Solutions of the Time-Dependent Flow of a Viscous, Incompressible Fluid over Stationary and Rotating Cylinders," Heat Transfer and Fluid Lab., Dept of M.E., Univ. of Notre Dame, T.R. 66-14, July 1966

12. Lee, J. and Fung, Y., "Flow in Locally Constricted Tubes at Low Reynolds Numbers," Journ. of Appl. Mech. Trans. ASME, pp 9-16, March 1970

13. Friedman, M. and Gillis, J., "Viscous Flow in a Pipe with Absorbing Walls," Journ. of Appl. Mech., Trans ASME, pp 819-822, Dec 1967

14. Friedman, M., "Flow in a Circular Pipe with Recessed Walls," Journ. of Appl. Mech., Trans. ASME, pp 5-8, March 1970

15. Tuve, G. L. and Sprenkle, R. E., "Orifice Discharge Coefficients for Viscous Liquids," Instruments, pp 201-206 VOL 6, 1933

16. Rouse, H., Advanced Mechanics of Fluids, Wiley, New York, 1959

17. Wang, Y. L. and Longwell, P. A., "Laminar Flow in the Inlet Section of Parallel Plates," AIChE Journ., pp 323-329, VOL 10, No. 3, May 1964

18. Hung, T. K., Laminar Flow in Conduit Expansions, Ph.D. Thesis, U. of Iowa, August 1966

19. Greenspan, D., "Numerical Studies of Steady, Viscous, Incompressible Flow in a Channel with a Step," Journ. of Engineering Math., pp 21-28, VOL 3, No. 1, Jan 1969

20. Lester, W. G. S., "The Flow Past a Pitot Tube at Low Reynolds Numbers; Part I - The Numerical Solution of the Navier-Stokes Equations for Steady Viscous Axi-symmetric Flow; Part II - The Effects of Viscosity and Orifice Size on a Pitot Tube at Low Reynolds Numbers," Aero. Res. Coun. R&M No. 3240, 1961

21. Taylor, D. J., "The Stability of Boundary Conditions in the Numerical Solution of the Time-dependent Navier-Stokes Equations," Aero. Res. Council No. 30406, Aug 1968; Clearinghouse No. AD-679436

22. Lugt, H. J. and Rimon, Y., "Finite-Difference Approximation of the Vorticity of Laminar Flows at Solid Surfaces," NSRDC, Washington App. Math Lab. Tech. Note AML-67-69 Sept 1969

23. Jarski, E. J., Haberman, W. and John, J., "Oscillating Viscous Flow Through Pipe Orifices at Vanishing Reynolds Number," (To be published)

24. Thom, A., "Arithmetical Solution of Equations of the Type $\nabla^4 \psi$ = const.," Aero. Res. Coun. R&M 1604, March 1933

25. Jenson, V. G., "Viscous Flow Round a Sphere at Low Reynolds Numbers (<40)," Proc. Roy. Soc. (London), pp 346-366, 249A, 1959

26. Son, J. S. and Hanratty, T. J., "Numerical Solution for Flow Around a Cylinder at Reynolds Numbers of 40, 200 and 500," Journ. of Fluid Mech., VOL 35, Part 2, pp 369-386, 1969

27. Thom, A. and Apelt, J. C., Field Computations in Engineering and Physics, D. Van Nostrand, 1961

28. Milne, W. E., Numerical Calculus, Princeton University Press, 1949

29. Thom, A. and Apelt, C. J., "A Note on the Convergence of Numerical Solutions of the Navier-Stokes Equations," Aero. Res. Coun. R&M 3061, June 1956

30. Lester, W. G. S., "Some Convergence Problems in the Numerical Solution of the Navier-Stokes Equations," Aero. Res. Coun. R&M 3239, July 1960

31. Underwood, R. L., "Calculation of Incompressible Flow Past a Circular Cylinder at Moderate Reynolds Numbers," Journ. of Fluid Mech., VOL 37, Pt. 1, pp 95-114, 1969

32. Rimon, Y. and Cheng, S., "Numerical Solution of a Uniform Flow Over a Sphere at Intermediate Reynolds Numbers," Phys. of Fluids, VOL 12, No. 5, pp 949-959, May 1969

33. Weinbaum, S., "On the Singular Points in the Laminar Two-Dimensional Near Wake Flowfield," Journ. of Fluid Mech., VOL 33, Part 1, pp 38-63, 1968.

34. Schubert, G., "Viscous Incompressible Flow Over Wall Projections and Depressions," AIAA Journal, Tech. Note, pp 373-375, VOL 5, No. 2, Feb 1967

35. Macagno, E. O. and Hung, T. K., "Computational and Experimental Study of a Captive Annular Eddy," Journ. Fluid Mech., pp 43-64, Part 1, 1967

36. Roache, P. J. and Mueller, T. J., "Numerical Solutions of Laminar Separated Flows," AIAA Journal, pp 530-538, VOL 8, No. 3, March 1970

37. Hama, F. R., "Experimental Studies on the Lip Shock," AIAA Journal, pp 212-219, VOL 6, No. 2, Feb 1968

38. Donaldson, I. S., "On the Separation of a Supersonic Flow at a Sharp Corner," AIAA Journal, pp 1086-1088, VOL 5, No. 6, June 1967

39. Hall, N. A., Thermodynamics of Fluid Flow, Prentice-Hall, 1957

40. Kawaguti, M., "Numerical Solutions of the Navier-Stokes Equations for the Flow in a Channel with a Step," Math. Res. Center, Univ. of Wisconsin, MRC Tech. Summary Rep. No. 574, May 1965: Clearinghouse No. AD-620108

41. Thompson, Jr., J. F., "Numerical Solution of the Incompressible, Two-Dimensional, Time-Dependent, Navier-Stokes Equations for a Body Oscillating in Pitch in a Moving Fluid," Dept. of Aerophysics and Aerospace Eng., Mississippi State Univ., Rept No. 86, Oct 1968; Clearinghouse No. AD-678611

42. Mehta, U. B. and Lavan, Z., "Flow in a Two-Dimensional Channel with a Rectangular Cavity," Journ. of Appl. Mech. ASME Trans., pp 897-901, Dec 1969

43. Jarski, E. J., Dynamics of Viscous Fluid Oscillations in Hydraulic Lines, Ph.D. Thesis, University of Maryland, Jan 1970; also issued as NSRDL Annapolis Rept 3201, Jan 1970

44. Roache, P. J., Numerical Solutions of Compressible and Incompressible Laminar Separated Flows, Ph.D. dissertation, Univ. of Notre Dame, Nov 1968

VITA

Name: Theo Gordon Keith, Jr.

Permanent address: 12609 Chanler Lane, Bowie, Maryland.

Degree and date to be conferred: Ph.D., 1971.

Date of birth: July 2, 1939.

Place of birth: Cleveland, Ohio.

Secondary education: West Technical High School
1957.

Collegiate institutions attended		Degree	Date of Degree
Cleveland State University (Formerly Fenn College)	1960-1964	B.M.E.	June 1964
University of Maryland	1964-1968	M.S.	June 1968
University of Maryland	1968-1971	Ph.D.	August 1971

Major: Mechanical Engineering.

Minor: Mathematics.

Position held: Mechanical Engineer, GS-12
Naval Ship Research and Development Laboratory
Annapolis, Maryland